Peptide Mediated siRNA Delivery: Physicochemical and *in vitro* Characterizations

by

Maggie Man Kei Law

A thesis
presented to the University of Waterloo
in fulfillment of the
thesis requirement for the degree of
Master of Applied Science
in
Chemical Engineering

Waterloo, Ontario, Canada, 2007

Author's Declaration

I hereby declare that I am the sole author of this thesis. This is a true copy of the thesis, including any required final revisions, as accepted by my examiners.

I understand that my thesis may be made electronically available to the public.

Maggie Law

2007

Abstract

Short interfering RNAs (siRNAs) trigger RNA interference (RNAi) both in vitro and in vivo, where the expression of the encoded protein is silenced. Its potential use as a therapeutic agent is limited by its rapid enzymatic degradation and low cellular uptake. Therefore, a delivery carrier is desired to increase its solution stability and improve cellular uptake. In this study, Arginine-9 (R9), a cell penetrating peptide derived from the HIV 1 Tat protein, was investigated as a potential carrier for siRNAs at pH 7.3. The optical activity of siRNA decreased with increasing R9 concentration, with only 7.8±3.8% of the initial absorbance at 260nm remained at siRNA saturation. The highest binding ratio of R9 to siRNA determined from the UV/Vis spectra was 10.3:1 (corresponds to a charge ratio of 2.2:1 (+/-)). The measured hydrodynamic diameter increased with increasing R9, with a maximum value of ~1μm at siRNA saturation. At R9 to siRNA charge ratios below 5.74:1, the surface charge of the complexes increased rapidly with the addition of R9. However, the rate of increase of Zeta potential decreased significantly with subsequent addition of R9. At charge ratio above 1.43:1, the complexes expressed low surface charge which led to the formation of aggregates in solution. A new peptide library was designed which utilized several properties of known cell penetrating peptides. *In vitro* siRNA transfection of eGFP siRNA with C166-GFP cells was used to determine the transfection efficiency of the new peptides. Preliminary results of the newly designed peptides showed that some of them are not as effective when compared to Lipofectamine 2000 (Invitrogen). However, this experimental protocol can be extended to study transfection efficiency of the remaining peptides in the library.

Acknowledgements

First, I would like to thank my supervisor Professor Pu Chen for giving me the opportunity of participating in this innovative, multi-disciplinary research, and also for his guidance and feedback over my Master's study.

Special thanks have to be given to Professor Jean Duhamel for his stimulating discussions and Professor Eric Jervis for his constructive suggestions and experimental training. I would also like to thank various personnel in the Chemical Engineering Department for provide me with such an excellent learning environment.

I would also like to thank the members of the Nano-Bio Interfacial Engineering Group, especially Mei Wang, Shane Fung, and Hong Yang for their constructive technical discussions and for training me on various experimental methods. I would also like to thank Joyce Cheng for her assistance in data collection and discussions.

Last but not least, I am grateful to my loving parents, relatives and friends who have been supporting me through various ups and down all these years.

Table of Contents

Author's Declaration ii
Abstract iii
Acknowledgements iv
Table of Contents v
List of Figures vii
List of Tables xiii
Chapter 1 Introduction 1
1.1 RNAi and siRNA 2
1.2 Mechanisms of RNAi 3
1.3 Carrier Mediated siRNA Delivery 5
1.4 Objectives 8
Chapter 2 Literature Review 9
2.1 Existing Nucleic Acid Delivery Technologies 9
2.1.1 Viral Carriers 9
2.1.2 Liposomes 10
2.1.3 Polymeric Carrier 11
2.2 Peptide Mediated Drug Delivery 13
2.2.1 Cell Penetrating Peptides Derived from Proteins 17
2.2.2 Cationic Peptides 20
2.2.3 Designed Amphiphilic Cell Penetrating Peptides 21
2.3 Preparation of peptide-NA nanoparticles 28
Chapter 3 Physicochemical Characterization of siRNA-Peptide Complexes 30
3.1 Materials and Methods 30
3.2 Results 33
Chapter 4 Design of Peptide Carriers and Preliminary *in vitro* Evaluation 48
4.1 New Peptide Sequences 50
4.2 Materials and Methods 52
4.3 Results and Discussion 55
4.3.1 Optimization of siRNA Dosage by Fluorescence Microscopy 56
4.3.2 Transfection Efficiencies of Peptides Candidates 59
Chapter 5 Conclusions 75

Chapter 6 Future Work and Recommendations 77
References 81
Appendix A Equilibrium Binding Isotherm Determination 88
Appendix B Auxiliary Data/Graphs 95

List of Figures

Figure 1-1. An illustration of a siRNA with 21 base pairs and a two nucleotide overhang at the 3' end. 3

Figure 1-2. Gene silencing by siRNA. Long double-stranded RNA is cleaved by Dicer. The resulting siRNAs is then incorporated to the RNA induced silencing complex (RISC). Upon separation and cleavage of the sense strand, the anti-sense strand then guides the RISC to the complementary mRNA. The target mRNA is then cleaved and degraded. 4

Figure 1-3 Nucleic acid-carrier complexes internalized through endocytosis. The complexes are first associated to the surface of the cell membrane (1), and they are then internalized by endocytosis (2). The carrier then mediates the escape from the endosome into the cytoplasm. Endosomal escape of the complexes is initiated by the intrinsic membrane permeability of the carrier or acquired membrane permeability due to pH sensitivity (3, 4). For complexes that fail to escape the endosome are degraded in the lysosome (5). Depending on the type of genetic material, the nucleic acids are then translocated to the nucleus for transcription (6), or remain in the cytoplasm for translational arrest and RNA interference (7). 7

Figure 2-1 Schematic of Polymer Structures: Linear (Top left), branched (top right), cross-linked (bottom left), and dendritic (bottom right). 13

Figure 2-2: Structure of peptide derivatives bearing a guanidino group [113]. 16

Figure 2-3: Schematic representing possible cellular uptake mechanisms: inverted micelle (A); barrel stave (B); toroidal pore (C); carpet mechanism (D). Adapted from Herbig et al [112]. 16

Figure 2-4 Schematic of a Primary Amphiphilic Peptide. The hydrophobic and hydrophilic domains are represented by the blue and yellow sections in the figure respectively. 24

Figure 2-5 Schematics of secondary amphiphilic peptides. (left) Hel 9-9 forms an α-helix with a hydrophilic side (grey circles) and hydrophobic side (white circles) consisting of lysine and leucine, respectively [97]. (right) EAK16-II adopts a β-sheet conformation consisting of hydrophobic alanines (patterned rectangles) and hydrophilic lysine (+) and glutamic acid (-) [171]. 26

Figure 2-6: This figure outlines a proposed hypothetical model of interaction between an amphipathic peptide in two equilibrium states (micelles and single molecules) and a membrane model. The circles represent a frontal view of molecules of an amphipathic peptide (the yellow parts correspond to the hydrophobic part of the molecules and the blue parts correspond to hydrophilic parts. The polar heads of the phosphatidylcholine bilayer are represented by light blue circles whereas the hydrophobic tails are black). Single molecules of peptide insert into the outer layer of the bilayer by mean of hydrophobic interactions (a), while in (b) the hydrophilic outer parts of the micelles interact with the hydrophilic macromolecules or phospholipids heads [116]. 27

Figure 3-1. Absorption spectra of siRNA in pH 7.3 HEPES buffer with increasing peptide concentration (from 0 to 40 μM). (From top to bottom) 34

Figure 3-2. Hypochromicity of siRNA at 260 nm as a function of R9 concentration for siRNA concentrations of 1.5 μM (○), 3.0 μM (■), and 4.5 μM (✳). Solid lines are the line of best fit generated by Prism. Error bars represent the largest standard deviation from 3 replicates at each siRNA concentration. 35

Figure 3-3. Hypochromicity of siRNA at 260 nm as a function of +/- charge ratio for siRNA concentrations of 1.5 μM (○), 3.0 μM (■), and 4.5 μM (✳). Solid lines are the line of best fit generated by Prism. 36

Figure 3-4. Circular dichroic spectra of siRNA in pH 7.3 HEPES buffer with increasing peptide concentration (from 0 to 40 μM). (from top to bottom) 39

Figure 3-5. Relative change in ellipticity of siRNA at 260 nm as a function of R9 concentration for siRNA concentrations of 1.5 μM (○) and 3.0 μM (■). Solid lines are the line of best fit generated by Prism. 40

Figure 3-6. Relative change in ellipticity of siRNA at 260 nm as a function of +/- charge ratio for siRNA concentrations of 1.5 μM (○) and 3.0 μM (■). Solid lines are the line of best fit generated by Prism. 41

Figure 3-7. Hydrodynamic diameter and Zeta potential of CTGF siRNA-R9 complexes at 1.5 μM siRNA. Zeta potential of siRNA and siRNA-R9 complexes is expressed in solid bars; Zeta potential of R9 is represented by diagonal bar; and size is represented by a solid line. 43

Figure 3-8 In solution atomic force microscopy image of CTGF siRNA (3.0 μM) and R9 (35 μM) complexes on mica. 45

Figure 3-9. Absorbance at 260 nm of siRNA (1.5 μM) and siRNA-R9 (1.5 μM / 150 μM) complex solution upon 2 M salt addition. The absorbance of siRNA only and siRNA-R9 complex solutions are monitored prior to salt addition (white), 2 hours after salt addition (diagonal), and one day after salt addition (black). 47

Figure 4-1. C166-GFP cells at 48 hours after eGFP siRNA transfection, using Lipofectamine 2000 as transfection agent. Fluorescence and corresponding bright field images are shown. 58

Figure 4-2. C166-GFP cells at 24 hours after eGFP siRNA transfection at specified +/- charge ratios, using R9 as transfection agent. Fluorescence and the corresponding bright field images are shown. Fluorescence images of the peptide controls are shown in the Appendix. 60

Figure 4-3. C166-GFP cells at 24 hours after eGFP siRNA transfection at specified +/- charge ratios, using EAK 16 II as transfection agent. Bottom panel shows the peptide only controls for the corresponding peptide concentration used for siRNA transfection in the top panel. Fluorescence and the corresponding bright field images are shown. 61

Figure 4-4. C166-GFP cells at 24 hours after eGFP siRNA transfection at specified +/- charge ratios, using EAK 16 IV as transfection agent. Fluorescence and the corresponding bright field images are shown. Fluorescence images of the peptide controls are shown in the Appendix. 62

Figure 4-5. C166-GFP cells at 24 hours after eGFP siRNA transfection at specified +/- charge ratios, using ACS as transfection agent. Bottom panel shows the peptide only controls for the corresponding peptide concentration used for siRNA transfection in the top panel. Fluorescence and the corresponding bright field images are shown. 63

Figure 4-6. C166-GFP cells at 24 hours after eGFP siRNA transfection at specified +/- charge ratios, using ACS-R9 as transfection agent. Bottom panel shows the peptide only controls for the corresponding peptide concentration used for siRNA transfection in the top panel. Fluorescence and the corresponding bright field images are shown. 64

Figure 4-7. C166-GFP cells at 48 hours after eGFP siRNA transfection at specified +/- charge ratios, using R9 as transfection agent. Fluorescence and the corresponding bright field images are shown. Fluorescence images of the peptide controls are shown in the Appendix. 65

Figure 4-8. C166-GFP cells at 48 hours after eGFP siRNA transfection at specified +/- charge ratios, using EAK 16 II as transfection agent. Fluorescence and the corresponding bright field images are shown. 66

Figure 4-9. C166-GFP cells at 48 hours after eGFP siRNA transfection at specified +/- charge ratios, using EAK 16 IV as transfection agent. Fluorescence and the corresponding bright field images are shown. Fluorescence images of the peptide controls are shown in the Appendix. 67

Figure 4-10. C166-GFP cells at 48 hours after eGFP siRNA transfection at specified +/- charge ratios, using ACS as transfection agent. Fluorescence and the corresponding bright field images are shown. 68

Figure 4-11. C166-GFP cells at 48 hours after eGFP siRNA transfection at specified +/- charge ratios, using ACS-R9 as transfection agent. Fluorescence and the corresponding bright field images are shown. 69

Figure 4-12. FACS results for the negative, positive, and normal controls (from left to right), which corresponds to non-treated cells, siRNA-Lipofactamine 2000 treated cells, and naked siRNA treated cells, respectively. 70

Figure 4-13. FACS results for siRNA-R9 transfected cells in 24 hours at charge ratio (+/-) of 2:1, 5:1, and 10:1 (from left to right). 71

Figure 4-14. FACS results for siRNA-EAK 16 II transfected cells in 24 hours at charge ratio (+/-) of 2:1, 5:1, and 10:1 (from left to right). 71

Figure 4-15. FACS results for siRNA-EAK 16 IV transfected cells in 24 hours at charge ratio (+/-) of 2:1, 5:1, and 10:1 (from left to right). 71

Figure 4-16. FACS results for siRNA-ACS transfected cells in 24 hours at charge ratio (+/-) of 2:1, 5:1, and 10:1 (from left to right). 72

Figure 4-17. FACS results for siRNA-ACS-R9 transfected cells in 24 hours at charge ratio (+/-) of 2:1, 5:1, and 10:1 (from left to right). 72

Figure 4-18. FACS results for siRNA-R9 transfected cells in 48 hours at charge ratio (+/-) of 2:1, 5:1, and 10:1 (from left to right). 72

Figure 4-19. FACS results for siRNA-EAK 16 II transfected cells in 48 hours at charge ratio (+/-) of 2:1, 5:1, and 10:1 (from left to right). 73

Figure 4-20. FACS results for siRNA-EAK 16 IV transfected cells in 48 hours at charge ratio (+/-) of 1:1, 5:1, and 10:1 (from left to right). 73

Figure 4-21. FACS results for siRNA-ACS transfected cells in 48 hours at charge ratio (+/-) of 2:1, 5:1, and 10:1 (from left to right). 73

Figure 4-22. FACS results for siRNA-ACS-R9 transfected cells in 48 hours at charge ratio (+/-) of 2:1, 5:1, and 10:1 (from left to right). 74

List of Tables

Table 2-1 Sequences of naturally occurring cell penetrating peptides (CPPs) 18

Table 2-2 Sequences of synthetic cell penetrating peptides 23

Table 4-1 Designed peptides sequences investigated in preliminary *in vitro* experiment. 52

Chapter 1

Introduction

Short interfering RNA (siRNA) and various types of nucleic acid (NA) based drugs, such as plasmid DNAs and oligonucleotides, have shown promising therapeutic potential with several ongoing clinical trials [1] but lacked a suitable formulation to achieve high delivery efficiency and potency. When administered, a significant portion of these NA based drugs are excreted through the reticuloendothelial system (RES) mainly due to their small size and hydrophilicity. Furthermore, they are subjected to enzymatic degradation during circulation and within the cell. As a result, the potency of these drugs is decreased, and in some cases an increase of drug dosage is required to compensate these effects. Since NA drugs function in the cytosol or the nucleus, the inability of hydrophilic drugs to effectively travel across the hydrophobic core of the plasma membrane, and sometimes the nuclear membrane, is another major obstacle for their therapeutic application. If the drug does not bear a cell-specific target moiety, it can potentially be taken up by all cells and may cause unwanted side effects when accumulated at non-targeted sites.

In order to overcome these challenges, several methods have been developed to increase the delivery of NAs. For instance, structural modification of the phosphodiester backbone of the NAs can be applied to increase the stability of the NAs against nucleases [2], thus to prolong the circulation half-life of the drug. In addition to various established delivery methods, the carrier mediated delivery of siRNA has received increasing attention recently. Peptides, due

to their biodegradability, biocompatibility, and versatility have a very promising potential to be used as a carrier for siRNA delivery.

1.1 RNAi and siRNA

Various enzymes and structural components in a cell are proteins, which are genetically encoded by the DNA. The first step of protein production is the transcription of DNA which yields messenger RNAs (mRNAs). Messenger RNAs are then being translated to proteins within the ribosome. The freshly produced protein will go through the cell's regulatory process, and fold to obtain its functional conformation, which can be assisted by molecular chaperones.

RNA interference (RNAi) is an evolutionary conserved mechanism that performs a sequence specific, post transcriptional gene silencing (PTGS) through the use of short RNAs. RNAi is first identified in *C. elegans* by Fire and Mello [3]. RNAi can be triggered by several sub-type of short RNAs, which include short interfering RNA (siRNA), micro RNA (miRNA), tiny non-coding RNA (tncRNA), small modulatory RNA (smRNA), and short hairpin RNA (shRNA) [4,5]. Double stranded RNA (dsRNA) can act as a precursor of RNAi in invertebrates to obtain siRNAs upon its cleavage by the Dicer. However, dsRNA triggers interferon response in vertebrates [5], which prevents its use in therapeutic applications.

Short interfering RNA is a double stranded RNA with 21-22 nucleotides in length. Two nucleotides on the 3' end on both the sense and anti-sense strands are overhanging (Figure

1-1). Short interfering RNA is either the product of the enzymatic cleavage of long dsRNA by the dicer, or can be produced synthetically [5].

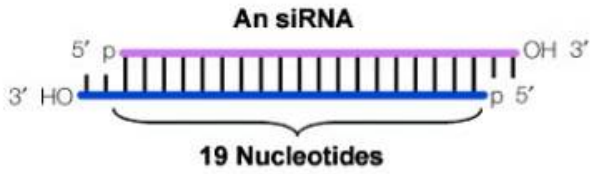

Figure 1-1. An illustration of a siRNA with 21 base pairs and a two nucleotide overhang at the 3' end.

(Reference: Dykxhoorn. 2003. Nature Revs. Mol. Cell. Biol.)

1.2 Mechanisms of RNAi

Once the siRNA is located in the cytosol, Ago2 cleaves the sense strand of the siRNA [6,7]. Further, since the 5'of the anti-sense strand is less thermodynamically stable then the 5' of the sense strand [8], the anti-sense strand will be thermodynamically favored to incorporate to the RNA induced silencing complex (RISC). The anti-sense sequence of the siRNA that is incorporated into the RISC would pair with its complementary mRNA sequence (Figure 1-2). The mRNA is then cleaved enzymatically by Ago2. Since the cleaved RNA fragments lack either the cap structure m7G or the polyA tail, which are essential to RNA stability, this leads to further degradation of the mRNA molecule. Since mRNA is the precursor to protein translation, the protein encoded by such mRNA thus cannot be synthesized. Gene silencing

by RNAi is also referred to as post-transcriptional gene silencing (PTGS) because the silencing takes place after transcription and before translation.

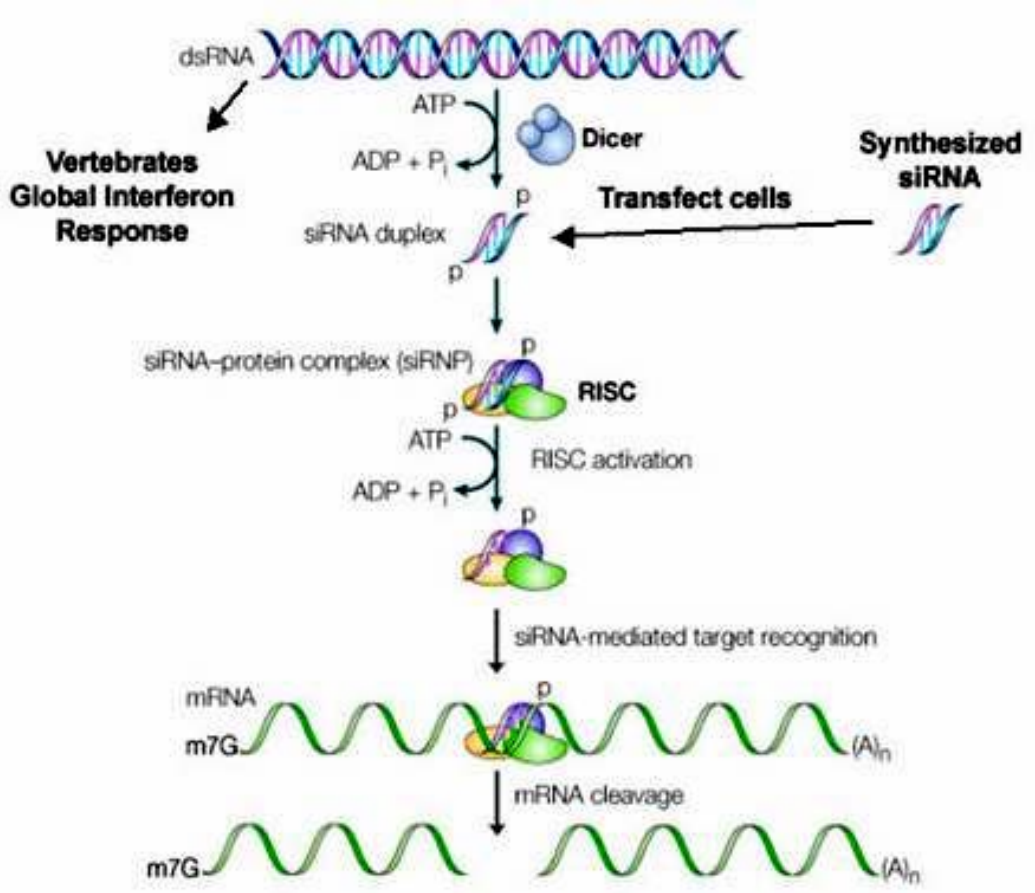

Figure 1-2. Gene silencing by siRNA. Long double-stranded RNA is cleaved by Dicer. The resulting siRNAs is then incorporated to the RNA induced silencing complex (RISC). Upon separation and cleavage of the sense strand, the anti-sense strand then guides the RISC to the complementary mRNA. The target mRNA is then cleaved and degraded.

(Reference: Dykxhoorn. 2003. Nature Revs. Mol. Cell. Biol.)

1.3 Carrier Mediated siRNA Delivery

Recently, the carrier-mediated delivery system has become a prevalent approach for improving the cellular delivery of nucleic acids (NAs). The carriers, self-associated or covalently conjugated with the NAs, are designed to prolong drug circulation time, to improve membrane permeation, and increase cell targeting capabilities, while being biocompatible and biodegradable. A safe drug delivery system should exert minimal side effects, that is, minimal cytotoxicity and inflammatory response, especially to non-targeted cells. Hydrophobic or highly charged particles can interact with opsonins, where the resulting complexes are removed from circulation by phagocytes and the reticuloendothelial system (RES) [9,10], which essentially decreases the effective drug concentration. Neutrally charged particles are found with a lower opsonization rate than charged particles due to decrease in electrostatic interactions with opsonins [9,11]. Complex size also has an effect on the rate of opsonization. In addition, smaller carrier-drug complexes, which have a smaller surface area, display slow opsonization and thus a longer bloodstream circulation time [10]. Since many carrier-drug complexes are mainly internalized through the temperature and energy dependent endocytosis pathways (Figure 1-3), small complexes with size 100-200 nm will facilitate cellular internalization [9,11]. Upon cellular internalization, the concentration of various enzymes within the vesicle increases and the pH is about 5.0 during the transition from early to late endosomes. The increase in enzymatic degradation and acute pH changes would decrease the drug potency if the carrier cannot escape from or withstand the harsh environment within the late endosome, or later in the lysosome. Recently, molecules such as the amino acid histidine, that has a pKa close to the range of 5 to 7, have been used as a

"proton sponge" to minimize the pH changes as well as induce leakage in the late endosome/lysosome [12,13].

In order to achieve cellular targeting, specific molecules, such as antibodies, that can interact with surfaces of the targeted cells, can be grafted onto the surface of the carrier-drug complexes [14,15]. For passive cellular targeting, the carrier-drug complex should exhibit physiochemical properties similar to the targeting site, such that it can easily diffuse to the targeted cells [16,17]. Release kinetics of the drug from the carrier-drug complexes is another essential aspect in the carrier design. It is desirable to have high drug packing density within the complex, where the drug can be released in a controllable manner that is below the toxic concentration but above the minimum therapeutic concentration. Thus, the determination of size, surface charge and surface chemistry is essential when characterizing the physicochemical properties of carrier-drug complexes [18,19].

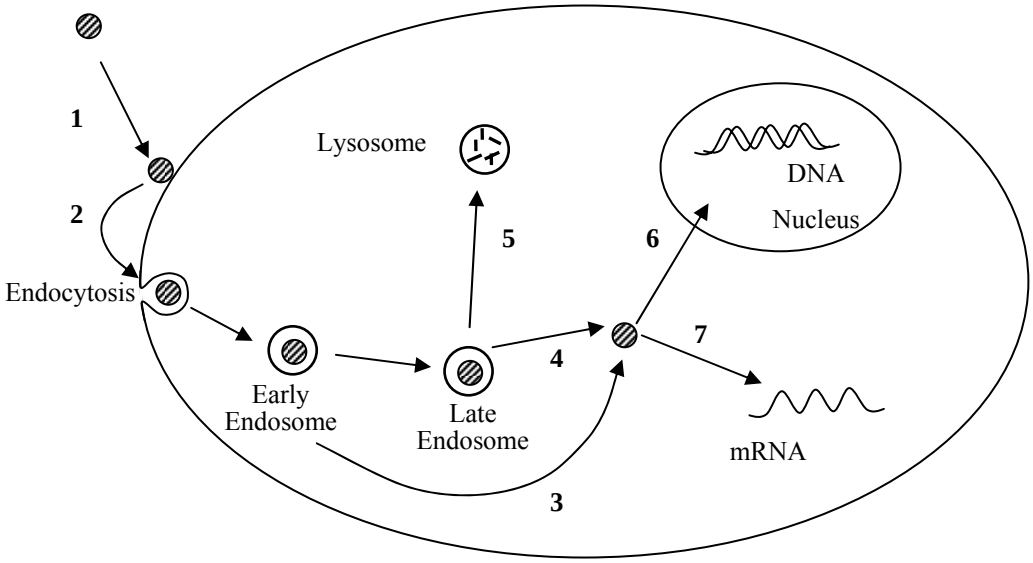

Figure 1-3 Nucleic acid-carrier complexes internalized through endocytosis. The complexes are first associated to the surface of the cell membrane (1), and they are then internalized by endocytosis (2). The carrier then mediates the escape from the endosome into the cytoplasm. Endosomal escape of the complexes is initiated by the intrinsic membrane permeability of the carrier or acquired membrane permeability due to pH sensitivity (3, 4). For complexes that fail to escape the endosome are degraded in the lysosome (5). Depending on the type of genetic material, the nucleic acids are then translocated to the nucleus for transcription (6), or remain in the cytoplasm for translational arrest and RNA interference (7).

1.4 Objectives

The objectives in this research were:

- To study the concentration effect on the complexation between a cell penetrating peptide R9 and a model siRNA.
- To characterize the siRNA-R9 complexes in terms of size and surface charge at various siRNA/R9 ratios.
- To elucidate the forces associated with the interaction between siRNA and R9.
- To design new peptides as carriers for effective siRNA delivery
- To investigate the effectiveness of the designed peptides using *in vitro*.

Chapter 2

Literature Review

2.1 Existing Nucleic Acid Delivery Technologies

Various types of carriers have been developed to improve the delivery of NAs. The carrier mediated approach is appealing since a vast variety of materials can be used and each can be engineered to obtain the desired properties. The materials used in the carrier-mediated delivery range from lipids [20-27], peptides [28-31], polysaccharides [32], synthetic [33-37] and natural polymers [38], gold [39,40], ceramics [41], to virus capsids [42]. They are mainly in the form of liposomes [20-27], micelles [43-47], dendrimers [48], emulsions [49], microemulsions [50-54], hydrogels [40], micro/nano-tubes [55,56], micro/nano-capsules [57-62], nanocrystals [21] and conjugates [63-65]. Furthermore, the various materials can be used in combination[40,66-68] with various biological constructs, such as antibodies and ligands, to further improve the biostability and targeting ability of the drug system [67,69,70].

2.1.1 Viral Carriers

To date, the viral delivery system can achieve the highest delivery efficiency. A virion is made up of genetic materials protected by a protein coating, which is referred to as capsid. Virus capsids or virus-like particles are made up of multiple copies of one or a few proteins. These materials have defined structures, are easy to produce and are homogeneous in size. Drug particles can be loaded within the capsid or grafted on the exterior. As well, various

molecules such as antibodies, fluorophores, and peptides can be conjugated to specific locations on the capsid surface for cell targeting, to act as probes, or to improve solution properties of carrier-drug complexes [71]. Various viral carriers have demonstrated high drug delivery efficiency *in vitro*, but were found to be cytotoxic in a number of *in vitro*, *in vivo* and clinical studies [72]. The new generation of adenoviral vectors, where all viral coding genes are removed, have shown high transfection efficiency with significantly reduced cytotoxicity [73].

2.1.2 Liposomes

With several formulations already approved by the FDA [74], the lipid-based carrier system represents a mature technology and is a relatively simple and reliable method for drug delivery *in vitro*. Each lipid molecule consists of a hydrophilic head and a hydrophobic tail, where the hydrophilic head can be positively, negatively, or neutrally charged. Some common lipids used as drug carriers are DOTAP, DOPC, and DOPE. When suspended in solution, the lipid based carrier can form liposomes, which are lipid bilayer vesicles. The liposome based delivery system is very efficient in entrapping hydrophobic drugs in the hydrophobic region in the bilayer [75]. Depending on the solubility of the drug in the hydrophobic region of the liposome, the entrapping efficiency [76] of the drug at a specific carrier concentration can be as high as 100% [75]. Hydrophilics drugs, such as NAs, are associated with liposomes mainly via electrostatic interaction with the charged head group. The entrapping efficiency of liposomes for hydrophilic drugs is lower when compared to hydrophobic drugs (~30%), but can be increased by various physical and chemical methods,

such as using freeze drying and pH gradient [75]. However, highly charged liposomes often interact with serum proteins and trigger complement activation; subsequently they are cleared out by phagocytes and the RES rapidly [77]. Complement activation can be reduced by lowering the liposome concentration. However, at a low and non-toxic liposome concentration, the effective drug concentration is often too low or the transfection efficiency is only slightly better than naked drugs [77]. In general, neutrally and negatively charged liposomes are less cytotoxic due to decreased interactions with serum proteins. However, cationic liposomes can express substantially higher transfection efficiency than the neutrally or negatively charged liposomes. Therefore, surface modifications of liposomes, such as PEGylation, are used to decrease complement activation. When grafted on liposomes, PEG increases the hydrodynamic volume that protects the liposome and the drug from clearance, complement activation, and enzymatic degradation [74,78-80]. When administered intravenously, liposomes have a tendency to be taken up by the lungs and liver. The limited biodistribution offers an opportunity to exploit the use of liposomes for targeted delivery to the lungs [81,82] and liver [78,83], however this also limits the bioavailability of liposome enclosed drugs in other areas. Although with numerous successes *in vitro*, due to its instability, cytotoxicity, and poor biodistribution, lipid based carriers have encountered difficulties in various *in vivo* and clinical studies [79,84].

2.1.3 Polymeric Carrier

Synthetic and natural polymers have been used as carriers for various drug molecules. Polymers are macromolecules made up of repeated units of covalently bonded monomers.

Some synthetic polymers are biodegradable, such as poly(ortho ester)s and poly(amino acid)s, and some are not, such as silicone elastomers, and poly(ethylene glycol) (PEG). Natural polymers such as chitosan, dextran and albumin can also be used as drug carriers. Polymers have a variety of three-dimensional structures which range from linear, branched, cross-linked, to dendritic. (Figure 2-1) The different types of monomers in a heterochain polymer can be arranged to give additional structural varieties such as blocks and grafts. The versatility in chemical structure provides excellent foundation for the design of the polymeric drug carrier. For example, polymeric micelles [37,44-46,85], di- or tri-block copolymers [34-37], and dendritic polymers [86,87] have been investigated. In particular, PEG is one of the most frequently used polymers for drug delivery. PEG has high water solubility, biocompatibility and chain flexibility. PEG has minimum interaction with serum proteins; thus it provides "stealth" from opsonins and phagocytes to the carrier it is associated with. Subsequently, PEG conjugated drugs and PEG coated carrier-drug complexes have shown longer circulation half-lives [67,88-91]. PEG has been approved by the FDA for use in various carrier mediated drug formulations, foods, and cosmetics [88]. Poly (L-Lysine) (PLL) has also been used as a carrier for genetic materials [48,92]. The positively charged lysine residues from PLL can electrostatically interact with the negatively charged phosphate groups in nucleic acids, forming PLL-NA complexes. PLL in various structures has been shown to interact with various NAs with negligible cytotoxicity [93-95].

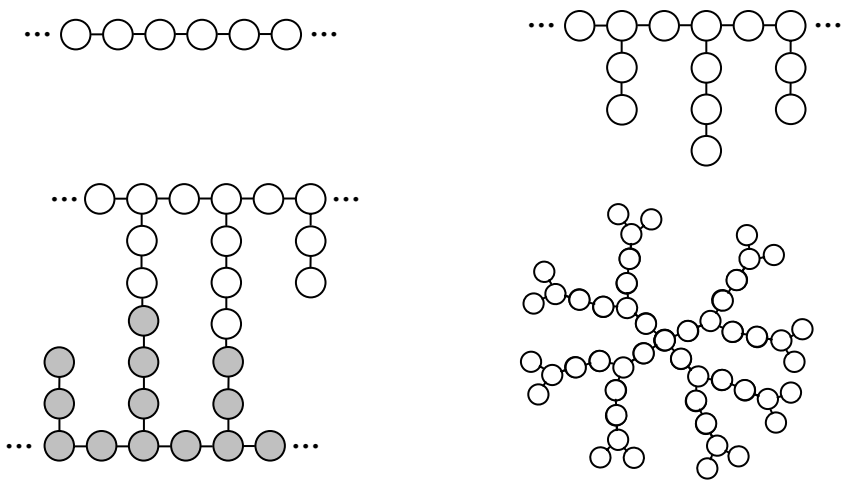

Figure 2-1 Schematic of Polymer Structures: Linear (Top left), branched (top right), cross-linked (bottom left), and dendritic (bottom right).

2.2 Peptide Mediated Drug Delivery

Peptides are short sequences of amino acids covalently linked through a peptide bond. Usually with 30 or less amino acids, peptides represent a very promising drug carrier material, which has received increasing attention since the 1990s. The rationale for peptide mediated NA delivery evolved from the biochemical knowledge that the active sites of enzymes, receptor ligands and antibodies involve about 5 to 20 amino acids. Thus, it should be possible to use small synthetic peptides to emulate the active sites of proteins and formulate synthetic DNA complexes that are, for example, as efficient as viruses, but do not have their limitations. Numerous peptides investigated as a NA carrier are of biological origin. For instance, cell penetrating peptides (CPPs), fusogenic peptides, nuclear uptake peptides, and receptor-based targeting peptides are derived from existing cellular or viral proteins. One advantage of using synthetic peptide is the readily and accurate determination

of its molecular structure and purity. Due to its biological origin, it is biodegradable and more likely to be biocompatible. Furthermore, through the use of the 20 naturally occurring amino acids, each with different hydrophobicity, size, and other solution properties, the chemical and structural design of peptide carriers is highly versatile. The versatility of peptide carrier design also provides an opportunity for the synthesis of multifunctional reagents that can improve stability, transfection, and targeting ability. This approach is necessary to provide a rational basis, rather than an empirical one, on which significant improvements can be made in the delivery systems.

Peptide based carriers have successfully delivered hydrophobic molecules, proteins, and genetic materials in various *in vitro* / *in vivo* studies [28,30,66,96-100]. Certain synthetic peptide derivatives, such as D-amino acids [101], β-amino acids [102], peptoid [101] and carbamate [103] have also been studied and have shown superior transfection abilities when compared to natural peptides. (Figure 2-2) Depending on the primary structure and the solvent, a peptide can attain secondary structures such as α-helix or β-pleated sheet, similar to those found in proteins. The importance of α-helical [97,104] and β-pleated sheet [105-107] structures to membrane translocation have been acknowledged in some studies. For example, the membrane translocation properties of two primary amphiphilic peptides [Pα] and [Pβ] were studied [108], where the former has an α-helical structure and the later has a β-sheet structure. It is found that both peptides are capable of membrane insertion; however in their preliminary studies, only the siRNA delivered by [Pβ] is capable of inducing silencing activity. The difference in the transfection ability among the two peptides is

possibly due to the higher availability of hydrogen bonding sites in the β-strand whilst most of the hydrogen-bonding sites are occupied within the α-helical peptide. Despite the importance of the peptide secondary structure in drug delivery, it is not the only factor that determines cellular uptake of drug molecules since some peptides in the random coil conformation, such as oligoarginine, can also deliver drugs across the cell membrane [109,110].

In general, cellular uptake can either be energy dependent or independent. Other than macrophages, the energy dependent pathways for cells generally include macropinocytosis, clathrin-mediated endocytosis, and caveolin-mediated endocytosis [111]. On the other hand, the possible energy independent cellular uptake mechanisms include the inverted micelle, barrel stave, toroidal pore, and carpet models [112]. (Figure 2-3) In the inverted micelle model, the peptide first associate with the bilayer surface through electrostatic interaction. The lipid bilayer reorganizes itself to minimize the exposure of the complex to the solvent, which eventually leads to the formation of an inverted micelle in the bilayer and is later released to the cytosol. (Figure 2-3A) It has been proposed that peptides can behave similar to membrane proteins, where pores are resulted when the amphiphilic peptides embed in the lipid bilayer as cylindrical pores. A barrel stave is resulted when the outer surface of the pore is hydrophobic, thus interacting with the hydrophobic core of the bilayer. (Figure 2-3B) In contrast, a toroidal pore is resulted when the surrounding of the pore is hydrophilic and interacts with the hydrophilic heads of the bilayer. (Figure 2-3C) In the carpet model, the peptide first associates with the membrane surface, then the basic residues trigger

reorganization of the membrane structure, which eventually leads to transfer of extracellular materials into the cytosol. (Figure 2-3D)

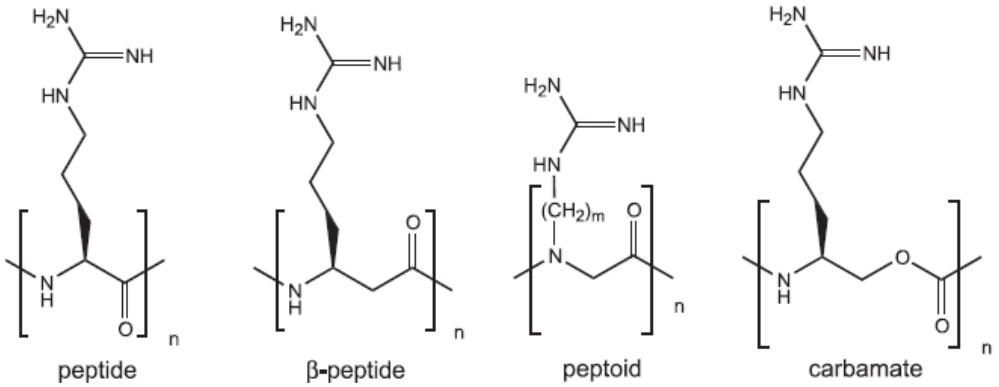

Figure 2-2: Structure of peptide derivatives bearing a guanidino group [113].

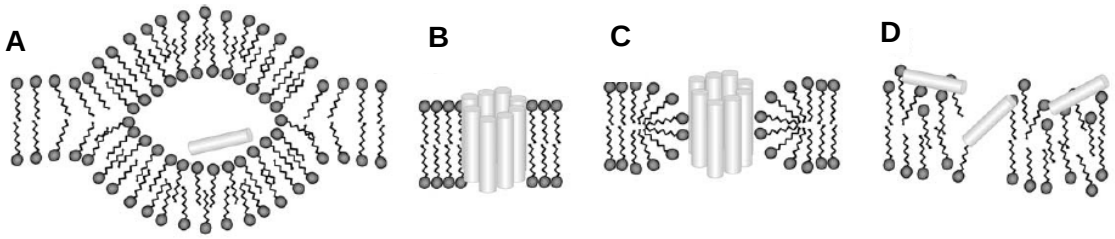

Figure 2-3: Schematic representing possible cellular uptake mechanisms: inverted micelle (A); barrel stave (B); toroidal pore (C); carpet mechanism (D). Adapted from Herbig et al [112].

2.2.1 Cell Penetrating Peptides Derived from Proteins

Although the cell membrane acts as a highly selective barrier to foreign materials, many viruses possess proteins that are able to perturb the cell membrane and release their contents into cells. A number of peptide carriers were derived from these viral proteins, where they are the shortest peptide sequences responsible for cell penetration (also referred to as the minimum effective peptide sequences). These peptides such as Tat and Penetratin are referred to as cell penetrating peptides (CPPs) or protein transduction domains (PTDs). They have shown high cell penetration ability in various *in vitro* / *in vivo* investigations [29,30,96,114,115]. Some protein-derived CPPs are given in Table 2-1. Although the internalization mechanisms are not well-defined for the majority of CPPs, recent research has shown that multiple internalization routes are available [112,116,117].

Table 2-1 Sequences of naturally occurring cell penetrating peptides (CPPs)

Peptide	Origin	Sequence	Ref.
adenoviral core peptide μ (mu)	Adeno virus	MRRAHHRRRRASHRRMRGG	[118]
Caiman crocodylus Ig(v) light chain		MGLGLHLLVLAAALQGA	[119]
E5	Influenza virus	GLFEAIAEFIEGGWEGLIEG	[120]
E5CA	Influenza virus	GLFEAIAEFIEGGWEGLIEGCA	[121]
E5WYG	Influenza virus	GLFEAIAEFIEGGWEGLIEGWYG	[122]
gp41 fusion sequence		GALFLGWLGAAGSTMGA	
H5WYG	Influenza virus	GLFHAIAAHFIHGGWHGLIHGWYG	[123]
HA	Influenza virus	GLFEAIAGFIENGWEGMIDG	[124]
		GLFEAIAGFIENGWEGMIDGWYG	[125]
HBV-PreS2/TLM		PLSSIFSRIGDP	[126]
hCT derived peptide		LGTYTQDFNKFHTFPQTAIGVGAP	[127]
Human b3 integrin signal sequence		VTVLALGALAGVGVG	
INF-1	Influenza virus	GLFEAIAGFIENGWEGMIDGGGC	[128]
INF-7	Influenza virus	GLFEAIEGFIENGWEGMIDGWYG	[128]
K5	Influenza virus	GLFKAIAKFIKGGWKGLIKG	[120]
Melittin	Venom of Apis mellifera	GIGAVLKVLTTGLPALISWIKRKRQQ	[121]
MPM (membrane permeable motif) IP/K-FGF	Kaposi fibroblast growth factor (K-FGF)	AAVALLPAVLLALLAP, AAVLLPVLLAAP	[129], [130]
PDX-1		RHIKIWFQNRRMKWKK	[131]
Penetratin (43-58)	Antennapedia	RQIKIWFQNRRMKWKK	[132]
Prion protein		N-terminal (1-28)	[133]
pVEC		LLIILRRRIRKQAHAHSK-amide	[134]
SynB1	Protegrins	RGGRLSYSRRRFSTSTGR	[135]
Tat (48-60)	HIV-1	GRKKKRRQRRRPPQ	[136]
VP22		DAATATRGRSAASRPTERPRAPARSASRPRRPVD	[106]

Tat, a trans-activating transcriptional activator of HIV-1, is one of the most studied among all protein derived CPPs. The Tat protein has 86 amino acids but only the cluster of basic amino acids RKKRRQRRR, starting from amino acid residue 49 to 57 is responsible for the cell penetrating property of the Tat peptide [136]. Each Tat peptide has eight positive charges, resulting from two lysines and six arginines. Due to charge repulsion, the Tat peptide remains as a random coil in solution [137]. The Tat peptide has successfully delivered fluorophores [96], peptides [30], proteins [28,138] and oligonucleotides [139] in various *in vitro* [115], *ex*

vivo [96], and *in vivo* [28,96] models. Recent research has shown that Tat enters the cell mainly through adsorptive endocytosis [140]. Due to the presence of cationic residues, the CPP is first adsorbed onto the negatively charged cell surface through electrostatic interaction, before being internalized through several types of endocytosis, such as clathrin-dependent endocytosis [140], caveolin-dependent endocytosis [141], and raft-dependent macropinocytosis [142].

The Antennapedia (Antp) protein is a membrane transduction protein that corresponds to the transcription factor of Drosophila. Penetratin, the minimal effective sequence for cell penetration, is the third α-helix from Antp (amino acid residues 43-58) [143]. Penetratin is α-helical in hydrophobic environment but it has no specific secondary structure in aqueous solution [143]. However, the α-helical structure is not essential to membrane translocation since point mutation with proline, which disturbs secondary structures, did not prevent the internalization of Penetratin [143]. Further experiments have shown that the basic amino acids and the tryptophan residue at position 6 of the peptide (48 of Antp) are essential to the uptake of Penetratin [132,144]. Recent confocal laser scanning microscopy and flow cytometry experiments have shown that the Penetratin has very low lipid vesicle permeability and that uptake *in vitro* is temperature and ATP dependent [114,145,146]. Based on these results, Penetratin was suggested to be taken up through the endocytic pathways but not the energy independent inverted micelles uptake mechanism [114,145,146].

2.2.2 Cationic Peptides

The oligomers of the four cationic amino acids, lysine, arginine, histidine, and ornithine can translocate through the cell membrane and be localized in the cytosol and the nucleus [147]. Basic amino acids, such as lysine and arginine, are positively charged in physiological pH; thus they can interact with negatively charged drug molecules or cell membrane through columbic interactions.

The transfection efficiency of therapeutic materials delivered by oligolysine is generally low [147], because highly charged oligolysine are rapidly removed from circulation in the RES. Various methods have been employed to increase its efficiency. For example, Adami and Rice [148] have used a cysteine containing, lysine-rich-peptide (CWK18), which allows the formation of disulfide bond between peptide molecules in an oxidation condition. Complex stability is improved upon disulfide bond formation induced by glutaraldehyde. Later, McKenzie, Kwok, and Rice [149] have shown that these disulfide-crosslinked complexes are smaller in size, and display slower opsonization rate, when compared with uncross-linked complexes. The *in vitro* transfection efficiency of such a complex is found to be higher since the release of DNA is only triggered by disulfide bond reduction in the cytosol. Highly charged oligolysine often interacts with serum proteins which decreases its efficiency. It is found that the transfection efficiency can be increased by conjugating oligolysine with PEG [94]. In addition, the transfection efficiency of oligolysine-complexes is limited by poor endosomal escape [92], which has been improved recently by facilitating endosomal escape or bypassing the endosomal pathway [150-152]. For example, histidine residues have been

used to enhance endosomal escape due to their protonation upon decreasing in pH. Histidine-containing oligolysine has shown higher transfection efficiency *in vitro* [153].

Six out of the 13 amino acids in the cell penetrating peptide HIV-1 Tat are arginines [136]. Oligoarginine is a derivative of the Tat peptide that has preserved the cell penetration property of the Tat peptide. The chain length effect of oligoarginine has been investigated by two research groups [101,154]. In general, the cell penetration capability of oligoarginine requires a minimum chain length of four to five arginine residues and that decaarginine gives the maximum translocation efficiency. The translocation efficiency decreases when the chain length is further increased. In another study, the authors have investigated the effect of spacing between arginine segments in a peptide with seven arginines and three non basic amino acid residues [155]. The sample peptides always perform better in cellular internalization when compared with the heptaarginine, which suggest that not only the number of arginines present is important, but also the spacing between arginine residues. It is believed that the spacing between arginine residues provide structural flexibility to the functional group, which eventually leads to an increase in translocation efficiency.

2.2.3 Designed Amphiphilic Cell Penetrating Peptides

Since the amphiphilic lipid bilayer is the major component of a cell membrane, it appears feasible to use an amphiphilic peptide to carry a drug across the cell membrane, where one can expect that the hydrophilic section of the peptide first interacts with the membrane

surface with subsequent translocation to the cytosol assisted by the hydrophobic section of the peptide. A list of amphiphilic cell penetrating peptides is given in Table 2-2.

Table 2-2 Sequences of synthetic cell penetrating peptides

Names	Sequence	Type of Amphiphilicity	Reference
6	MGLGLHLLVLAAALQGAKSKRKV	Primary	[156]
[1], A, SP, 3	MGLGLHLLVLAAALQGAWSQPKKKRKV	Primary	[156-159]
[2], *X,* 4	MGLGLHLLVLAAALQGAKKKRKV	Primary	[156,159]
[3], FP, B, 1	GALFLGWLGAAGSTMGAWSQPKKKRKV	Primary	[156-159]
[4], 2	GALFLGWLGAAGSTMGARKKKRKV	Primary	[156,159]
[5], MPG_NLS	GALFLGFLGAAGSTMGAWSQPKSKRKV	Primary	[159,160]
5, SP-NLS	MGLGLHLLLAAALQGAKKKRKV	Primary	[156,161]
Bc	GALALGALGAAGSTMGAWSQPKKKRKV	Primary	[157]
FP1, Ba, MPG	GALFLGFLGAAGSTMGAWSQPKKKRKV	Primary	[160]
FP2, Bb	GALFLGFLGAAGAAMGAWSQPKKKRKV	Primary	[157,158,160]
FP3	GALALGLLGAAGSTMGAWSQPKKKRKV	Primary	[157,158]
FP4, Bd	GALFLAFLAAALSLMGLWSQPKKKRKV	Primary	[158]
GALA	WEAALAEALAEALAEHLAEALAEAEALEALAA	Secondary	[157,158]
gp41 fusion sequence	GALFLGWLGAAGSTMGA	Primary	[162]
JTS-1	GLFEALLELLESLWELLLEA	Secondary	[163]
KALA	WEAKLAKALAKALAKHLAKALAKALKACEA	Secondary	[163]
Model amphiphilic peptide (MAP)	KLALKLALKALKAALKLA	Secondary	[164]
MPS (human integrin β3 signal sequence)	VTVLALGALAGVGVG		[165]
MPS (kaposi FGF signal sequence)	AAVALLPAVLLALLAP		[129]
MPS (kaposi FGF signal sequence)	AAVLLPVLLAAP		[166]
P3	VAYISRGGVSTYYSDTVKGRFTRQKYNKRA		[167]
Pep-1	KETWWETWWTEWSQPKKKRKV	Primary	[167]
PreS2-TLM	PLSSIFSRIGDP		[105]
SPM	MGLGLWLLVLAAALQGAKKKRKV	Primary	[168]
SV40 (T-antigen NLS)	PKKKRKV		[134]
Transportan	GWTLNSAGYLLGKINLKALAALAKKIL	Primary	[169]
4_3	LARLLARLLARL	Secondary	[97]
4_3S	LARSLARSLSRL	Secondary	[97]
4_6	LARLLARLLARLLRALLRALLRAL	Secondary	[97]
4_6S	LARSLARSLSRLLRSLSRALSRAL	Secondary	[97]
4_6P	LARLLARLLARPPRALLRALLRAL		[97]
[Pa]	GALFLAFLAAALSLMGLWSQPKKKRKV	Primary	[108]
[Pb]	GALFLGFLGAAGSTMGAWSQPKKKRKV	Primary	[108]
Hel 13-5	KLLKLLLKLWLKLLKLLL	Secondary	[170]
Hel 11-7	KLLKLLLKLWKKLLKLLK	Secondary	[170]
Hel 9-9	KLLKKLLKLWKKLLKKLK	Secondary	[170]

There are two major types of amphiphilic cell penetrating peptides, namely primary and secondary amphiphilic peptides. Primary amphiphilic peptides have specific hydrophobic and hydrophilic domains joint by a linker in the primary sequence (Figure 2-4). The hydrophobic region can interact with hydrophobic drugs and anchor itself in the cell membrane. The hydrophilic region, on the other hand, interacts with hydrophilic drugs and the cell membrane surface through electrostatic interactions. In general, the primary amphiphilic peptides adopt a random coil structure at neutral pH but a defined secondary structure upon a change in pH or interaction with the cell membrane [105,116]. The high efficiency of primary amphiphilic peptides may be attributed to the change in secondary structure at low pH, which can induce leakage of the endosomal membrane and facilitate endosomal escape of carrier-drug complexes. One example of primary amphiphilic cell penetrating peptide is MPG [105]. It consists of a hydrophobic domain derived from a fusion sequence and a nuclear localization sequence, joint through a linker. MPG changes its conformation from random coil to β-sheet structure when interacting with the cell membrane. It is proposed that MPG achieves cell penetration through the formation of pores on the cell membrane.

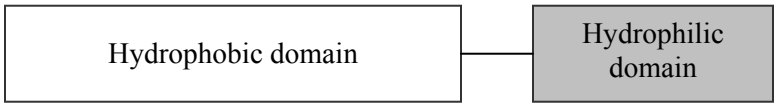

Figure 2-4 Schematic of a Primary Amphiphilic Peptide. The hydrophobic and hydrophilic domains are represented by the blue and yellow sections in the figure respectively.

On the other hand, when the amphiphilic nature of the molecule is originated from its secondary structure, that is α-helix or β-sheet structures, it is referred to as secondary amphiphilicity (Figure 2-5). Many peptide delivery carriers are designed based on α-helix amphiphilicity [97,108,170] while investigations based on amphiphilic β-sheet peptides are very limited [108,171]. For secondary amphiphilic peptides, two equilibrium states can exist for its interaction with cell membrane. (Figure 2-6) Secondary amphiphilic peptides can be embedded in the cell membrane so that the hydrophobic side is anchored in the hydrophobic core of the bilayer and the hydrophilic side interacts with the hydrophilic heads of the lipid bilayer. Alternatively, the peptides can first form micelles or aggregates to minimize the exposure of hydrophobic residues to the solvent, and then associate with the cell membrane [116].

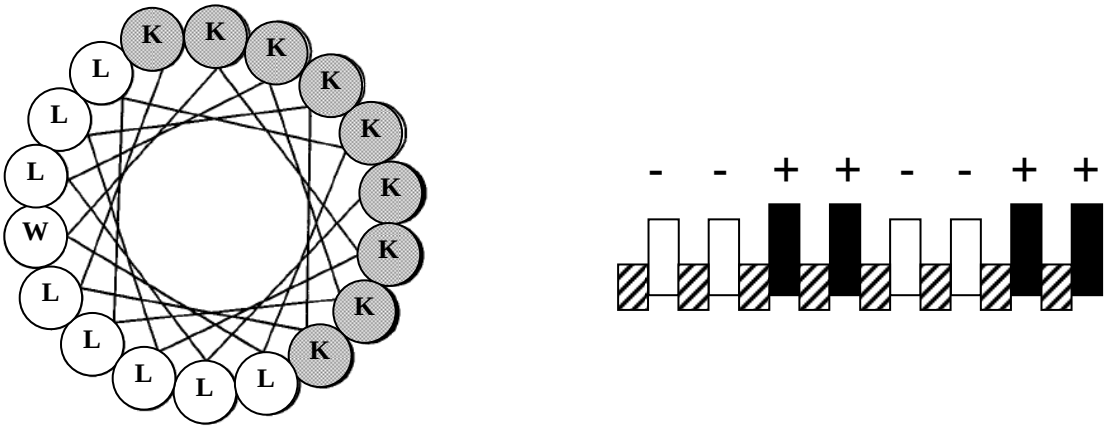

Figure 2-5 Schematics of secondary amphiphilic peptides. (left) Hel 9-9 forms an α-helix with a hydrophilic side (grey circles) and hydrophobic side (white circles) consisting of lysine and leucine, respectively [97]. (right) EAK16-II adopts a β-sheet conformation consisting of hydrophobic alanines (patterned rectangles) and hydrophilic lysine (+) and glutamic acid (-) [171].

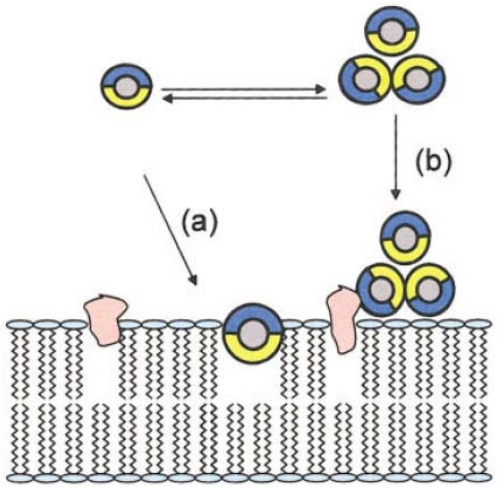

Figure 2-6: This figure outlines a proposed hypothetical model of interaction between an amphipathic peptide in two equilibrium states (micelles and single molecules) and a membrane model. The circles represent a frontal view of molecules of an amphipathic peptide (the yellow parts correspond to the hydrophobic part of the molecules and the blue parts correspond to hydrophilic parts. The polar heads of the phosphatidylcholine bilayer are represented by light blue circles whereas the hydrophobic tails are black). Single molecules of peptide insert into the outer layer of the bilayer by mean of hydrophobic interactions (a), while in (b) the hydrophilic outer parts of the micelles interact with the hydrophilic macromolecules or phospholipids heads [116].

The interaction between oligonucleotides and peptides from a group of amphiphilic α-helical peptides were being investigated and it was found that these peptides are able to bind to oligonucleotides and form aggregates [172]. These amphiphilic α-helical peptides display low cytotoxicity. However, the transfection efficiency of 4_6, which shows the best result among the group, is still 3-5 times lower than the liposome based carrier Lipofectin

(Invitrogen). GALA and KALA are two examples of α-helical amphiphilic peptides. In particular, GALA can form a helical structure corresponding to a decrease in pH, in which the glutamic acids (pKa~4.2) are protonated [173]. The transition to an α-helix enables the peptide to disrupt the endosomal membrane so that the drug cargo is released into the cytosol. However, GALA does not have any cationic residues to self-associate with NAs. KALA has a sequence similar to GALA, where some aniline residues are replaced with lysine and the number of glutamic acid residues is reduced [174]. KALA has preserved the cell penetration property of GALA and is able to translocate across the cell membrane when complexed with NAs [173].

2.3 Preparation of peptide-NA nanoparticles

In carrier mediated NA delivery, the carrier-NA nanoparticles can be formed by conjugation where the two molecules are covalently linked together. Several options are available for covalent conjugation of peptides to NAs, including the use of cross-linking agents, triple-helix-forming oligonucleotides, and attachment to the ends of linear NAs. The type and length of covalent linker should be considered carefully, as the appropriate spacer length and chemistry are critical to allow intracellular recognition and activity of the NAs. Normally conjugation of peptides to NAs involves formation of a disulfide bond, which can be rapidly cleaved in the reducing environment of the cell. It is not yet clear whether use of cleavable bonds offers advantages or maybe necessary for application [175].

Another common method to form carrier-drug nanoparticles is through molecular self-association, where it is usually driven by hydrogen bonding, electrostatic and/or hydrophobic interactions. In comparison to chemical modifications of the phosphodiester backbone, which is time-consuming and costly [176], carrier-drug complexes formed by the binding of peptides to the NAs may provide a simple and fast means to protect the NAs from degradation. Many positively charged peptides can interact with the negatively charged phosphate backbone of NAs through electrostatic interactions. In this case, the stoichiometry of complexation may affect cellular uptake. In the consideration of self-associated peptide-NA complexes, the incorporation of NAs with peptides is one of the most critical steps in the formulation procedures for peptide-based NA delivery systems.

Chapter 3

Physicochemical Characterization of siRNA-Peptide Complexes

In the search of a suitable formulation for peptide mediated siRNA delivery systems, it is of our interest to characterize a model siRNA-peptide complex using various physicochemical methods. A siRNA sequence that corresponds to the connective tissue growth factor (CTGF) was chosen as the model siRNA for its potential of breast cancer treatment. The TAT derived cell penetrating peptide Arginine-9 (R9) was chosen as the model peptide. In this study, we have utilized UV-Vis spectroscopy, circular dichroism, dynamic light scattering, Zeta potential measurements to investigate the physicochemical properties of CTGF siRNA-R9 complexes, including their equilibrium binding ratio, complex structure, size, and surface charge. The driving force for the complexation reaction was also verified by a salt addition experiment.

3.1 Materials and Methods

siRNA and R9 Peptide. The connective tissue growth factor (CTGF) siRNA was chosen as the model siRNA for this study. It had a sense sequence of 5'CGGUGUACCGAGCCCAGAUdTdT 3' and an antisense sequence of 5'AUCUCCGCUCGGUACACCGdTdT 3'. It was purchased from Dharmacon (processing option A4; Lafayette, CO). The molar concentrations of siRNA, were determined by absorption spectroscopy, using an extinction coefficient of 355021 L/mol•cm. Crude R9

peptide with N-terminal acetylation and C-termination amidation (AcN-RRRRRRRRR-CNH2) was purchased from the Sheldon Biotechnology Center at McGill University (Montreal, QC). Peptide identity was confirmed by mass spectroscopy and HPLC. Other reagents were all commercially available and were of analytical grade.

Preparation of siRNA-R9 complexes. Prior to use, siRNA and R9 peptides were first dissolved in Milli-Q water separately (Millipore, USA), divided in aliquots in microcentrifuge tubes, and stored in -20 ^{o}C after drying in Eppendorf Vacufuge Concentrator 5301. SiRNA at concentrations 1.5 μM, 3.0 μM, and 4.5 μM was first suspended in HEPES buffer (6 mM HEPES-NaOH, 20 mM NaCl, 0.2 mM MgCl2, pH 7.3), then added to the dried peptide vials to achieve a final peptide concentration ranging from 0-60 uL. The resulting complex solutions were stirred vigorously for 10 s with a vortex mixer and incubated for 3 hours at room temperature.

UV-Vis Absorbance. UV-Vis absorption spectra of each sample was obtained on a Hewlett-Packard 8452A diode array spectrophotometer (California, USA) at wavelengths between 190 nm and 364 nm, using a 75 μL quartz cuvette. Background absorbances were subtracted from the acquired signal.

Circular Dichroism. Circular dichroism (CD) measurements were preformed with a J-810 Spectropolarimeter (Jasco, USA). Spectra were acquired from samples in a 55 μL, 3mm path length quartz cuvette at 25 ^{o}C. Spectra were scanned from 400 to 200 nm at 200 nm/min, with a response time of 2 s and pitch of 1 nm. Spectra shown are the average of 3 replicates.

Hydrodynamic Diameter and Zeta Potential Measurements. The hydrodynamic diameter of siRNA-R9 complexes was measured by dynamic light scattering (DLS) and Zeta potential by laser doppler velocimetry (LDV) at 25 ºC using a Zetasizer Nano ZS (Malvern, UK) equipped with a 4 mW He-Ne laser operating at 633 nm. All measurements were performed at 25 ºC at a measurement angle of 173º. SiRNA and R9 stock solutions were separately filtered through 0.2 μm non-protein binding syringe filters (Pall, USA) prior to complexation. The size and Zeta potential are presented as the mean value ± standard deviation from three measurements of at least 10 runs per measurement.

Atomic Force Microscopy (AFM). A Picoscan atomic force microscope (Molecular Imaging, Arizona, USA) was used to study the morphology of the siRNA-R9 complexes/aggregates in solution. It was operated in Acoustic AC mode in solution using silicon nitride cantilevers (DNP-S, Digital Instruments), with a spring constant of 0.58 N/m and a typical tip radius of 10 nm. Tapping frequency is controlled in the range of 16-18 kHz. 400 μL of sample solution was deposited on a freshly cleaved mica surface. To avoid evaporation, Teflon sealed liquid environmental chamber was used.

Salt effect on siRNA-R9 binding. High concentration of salt can destabilize non-covalent interactions, including electrostatic interactions and hydrogen bonds. Two solutions were first prepared, one with 1.5 μM siRNA only and the other with an addition of 150 μM of R9. One hour after peptide addition, 2 M sodium chloride was separately added to the two

solutions. UV-Vis absorbance spectra of the two solutions were monitored before salt addition, two hours after salt addition and one day after salt addition.

3.2 Results

UV-Vis Absorbance

The interaction between CTGF siRNA and a cell penetrating peptide R9 has been investigated with various spectroscopic methods. The UV-Vis absorbance spectra of 3.0 μM siRNA in the absence and presence of R9 at concentrations ranging from 0 – 40 μM are shown in Figure 3-1. The characteristic peaks of siRNA at 210 nm and 260 nm are due to the presence of phosphate groups and nucleotide base pairs, respectively [177]. The addition of R9 induced a decrease in the absorbance of the complex solution. The hypochromic effect on siRNA absorbance due to peptide addition is more pronounced with increasing peptide concentration, until reaching saturation at peptide concentrations above 32 μM. Hypochromicity of siRNA spectra was also observed upon peptide addition at siRNA concentrations of 1.5 μM and 4.5 μM. It is also noted that the red/blue shift at absorption maxima (210 nm and 260 nm) is negligible.

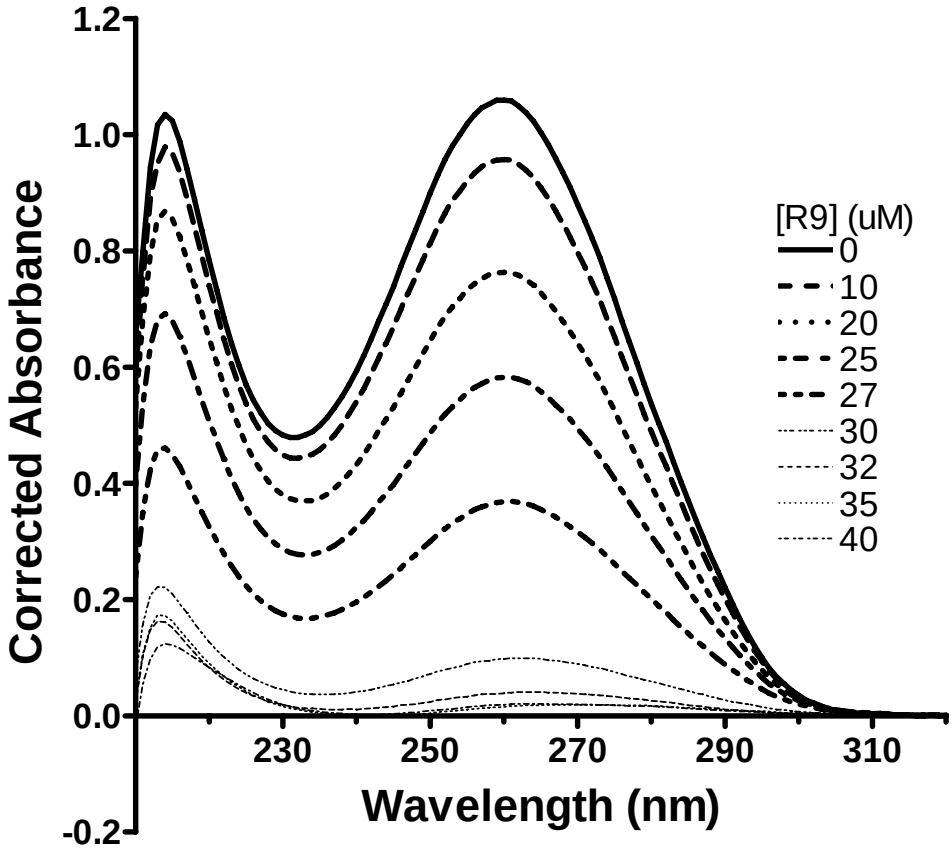

Figure 3-1. Absorption spectra of siRNA in pH 7.3 HEPES buffer with increasing peptide concentration (from 0 to 40 μM). (From top to bottom)

The hypochromic effect on siRNA due to the addition of R9 at a given wavelength can be quantified by the relative change in absorbance, ΔOD_r, defined as $\Delta OD_r=(OD_o-OD)/OD_o$ where OD_o is the initial absorbance of the free siRNA and OD is the observed absorbance of the sample containing siRNA-peptide complexes. The hypochromic effect at 260 nm upon peptide addition, expressed in terms of peptide concentration, is quantified for siRNA concentrations of 1.5 μM, 3.0 μM, and 4.5 μM. (Figure 3-2) A plot of hypochromicity can also be presented with respect to charge ratio, which is a normalization of R9 concentration

with respect to siRNA concentration, expressed in terms of the charge ratio of positively charged R9 to negatively charged siRNA. (Figure 3-3)

At 3.0 μM siRNA, the relative change in absorbance initially increases (UV absorbance at 260 nm initially decreases) with increasing peptide concentration and eventually reaches a plateau after reaching saturation at 32 μM of R9, where only 7.8% of initial absorbance remained upon saturation. When hypochromicity was plotted against +/- charge ratio for siRNA concentrations of 1.5 μM, 3.0 μM, and 4.5 μM, a significant portion of the curves overlapped. The relative change in absorbance reaches its maximum at a charge ratio (+/-) of 2.2, which corresponds to a molecular binding ratio of 10.3 peptides per siRNA.

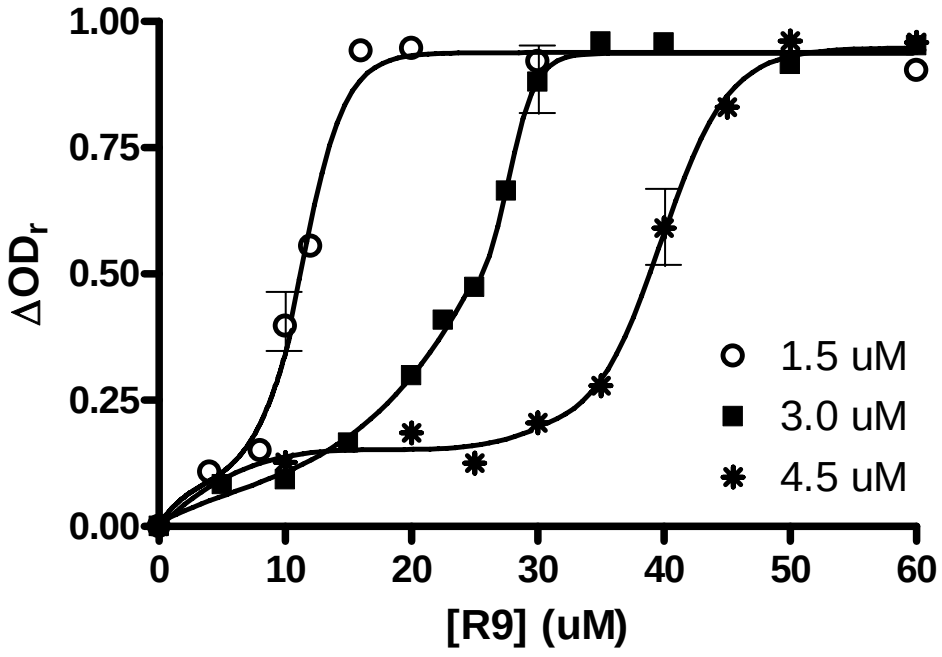

Figure 3-2. Hypochromicity of siRNA at 260 nm as a function of R9 concentration for siRNA concentrations of 1.5 μM (○), 3.0 μM (■), and 4.5 μM (✳). Solid lines are the line of

best fit generated by Prism. Error bars represent the largest standard deviation from 3 replicates at each siRNA concentration.

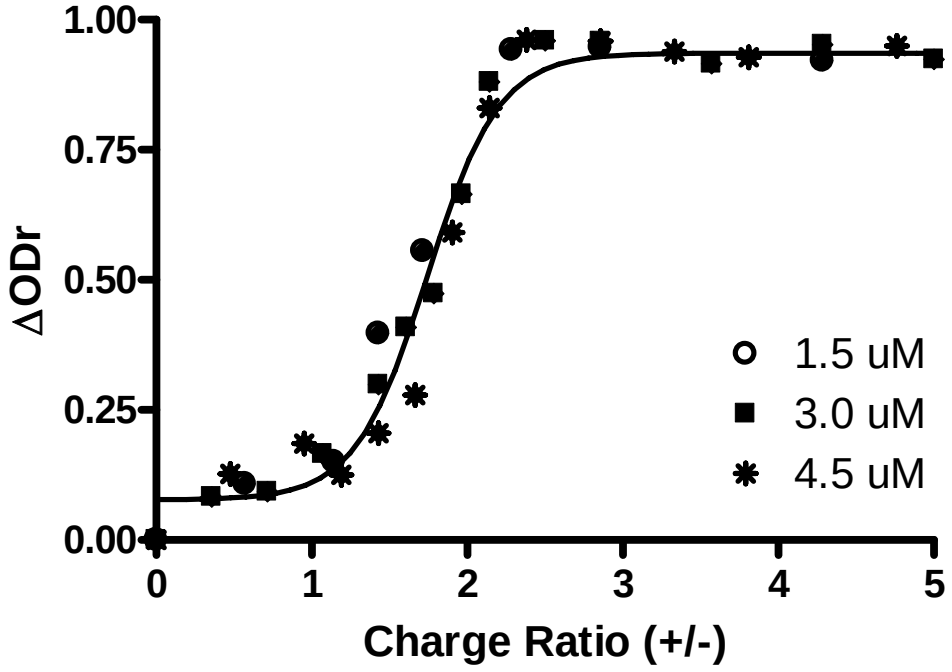

Figure 3-3. Hypochromicity of siRNA at 260 nm as a function of +/- charge ratio for siRNA concentrations of 1.5 μM (○), 3.0 μM (■), and 4.5 μM (✳). Solid lines are the line of best fit generated by Prism.

An important parameter for the determination of the optical properties of nucleic acids is the electric dipole transition moment (μ_{OA}), which represents the movement of charge density during the transition from the ground state to the excited state [177]. A larger dipole moment would result in a higher absorption band. In addition to contribution of absorbance from individual nucleic acid bases, interaction between nucleic acid bases or other species in solution also affect their absorption intensities. When the resultant transition dipole moment

is decreased, a decrease in absorbance occurs, and it is described as hypochromic. On the other hand, when the resultant transition dipole moment is increased, an increase in absorbance occurs and it is described as hyperchromic. When the guanidino groups from R9 interact with nucleoside bases via hydrogen bonding, electron density contributed by the nucleic acid bases will be delocalized which resulted in a decrease in the magnitude of the electric dipole transition moment, and thus hypochromicity in the UV-Vis spectra.

The analysis method developed by Bujalowski and Lohman [178] was applied to the absorbance data at 260 nm in attempt to obtain the equilibrium binding parameters between CTGF siRNA and R9 (see Supplementary information). However, the analysis method was found not to be applicable to this experimental system. The signal contributed by the siRNA at 260 nm is solely from the nucleoside bases and it is possible that the decrease in absorbance cannot reflect the interactions that underwent other modes of interaction, such as electrostatic interaction with the phosphate backbone. More likely, aggregation of complexes, which was not included in the derivation developed by Bujalowski and Lohman, also affects the applicability of this method [179].

Circular Dichroism

The circular dichroic (CD) spectra of siRNA-R9 complexes prepared at various R9 concentrations at 3.0 mM siRNA are shown in Figure 3-4. The siRNA has characteristic peaks around 210 nm and 265 nm (see Supplementary Information), which, when compared to the CD spectrum of established nucleic structures [177], confirms that the siRNA

possesses a right handed structure, similar to that of A-DNA. As the concentration of R9 increases, the ellipticity of complex solutions decreases progressively, until reaches a plateau at R9 concentrations above 35 μM.

Similarly, the relative change in ellipticity, $\Delta\theta_r$, is defined as $\Delta\theta_r=(\theta_o-\theta)/\theta_o$, where θ_o is the initial ellipticity of the free siRNA and θ is the observed ellipticity of the sample containing siRNA-peptide complexes. A plot of the relative change in ellipticity over increasing R9 concentration, expressed separately in terms of R9 concentration and +/- charge ratio, is given in Figure 3-5 and Figure 3-6 respectively. By monitoring the changes in the CD spectra upon titration of peptide, the stoichiometry was found to be 10.7 R9 peptides per siRNA at saturation (+/- charge ratio of 2.2), which agrees with the results given by UV absorbance. Previous study on the binding between poly-L-arg and nucleotides [180] has obtained a binding ratio of 2 arginine to one nucleotide, which corresponds to binding ratios between siRNA and R9 obtained by both UV and CD in this study.

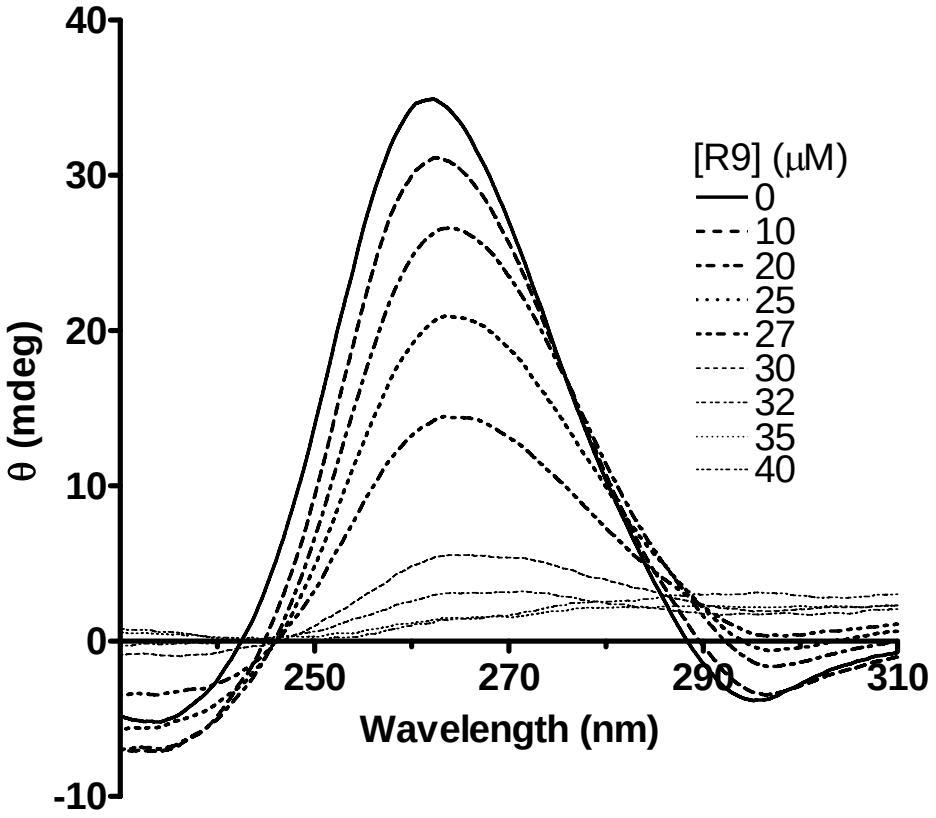

Figure 3-4. Circular dichroic spectra of siRNA in pH 7.3 HEPES buffer with increasing peptide concentration (from 0 to 40 μM). (from top to bottom)

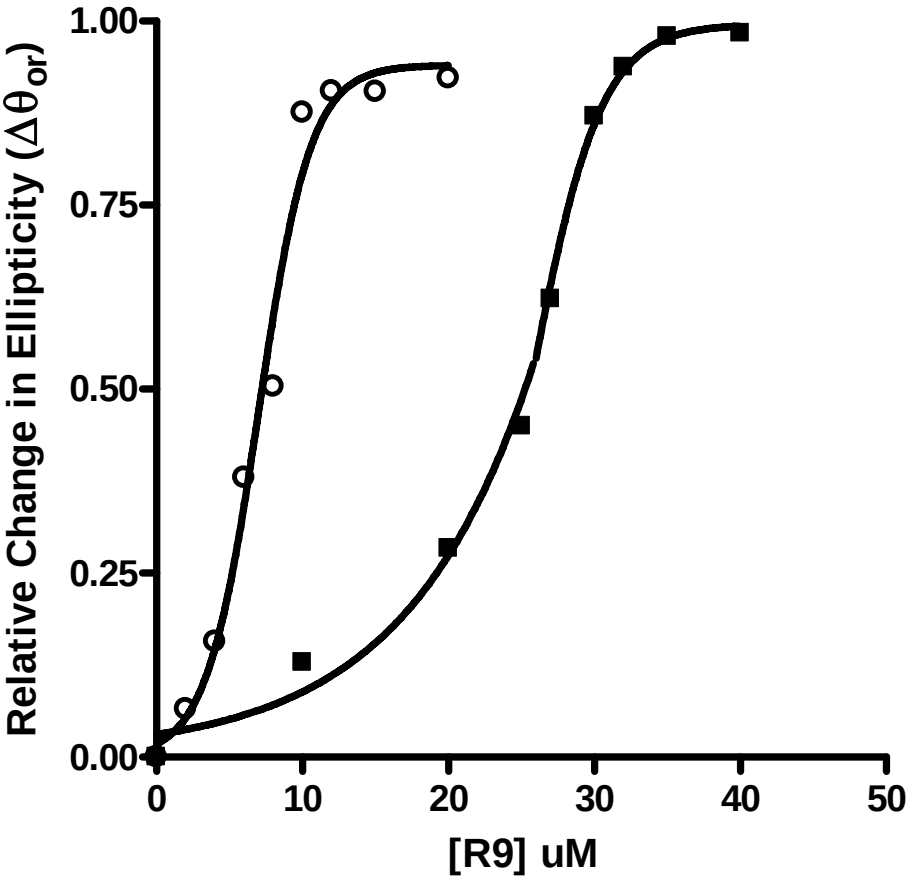

Figure 3-5. Relative change in ellipticity of siRNA at 260 nm as a function of R9 concentration for siRNA concentrations of 1.5 μM (○) and 3.0 μM (■). Solid lines are the line of best fit generated by Prism.

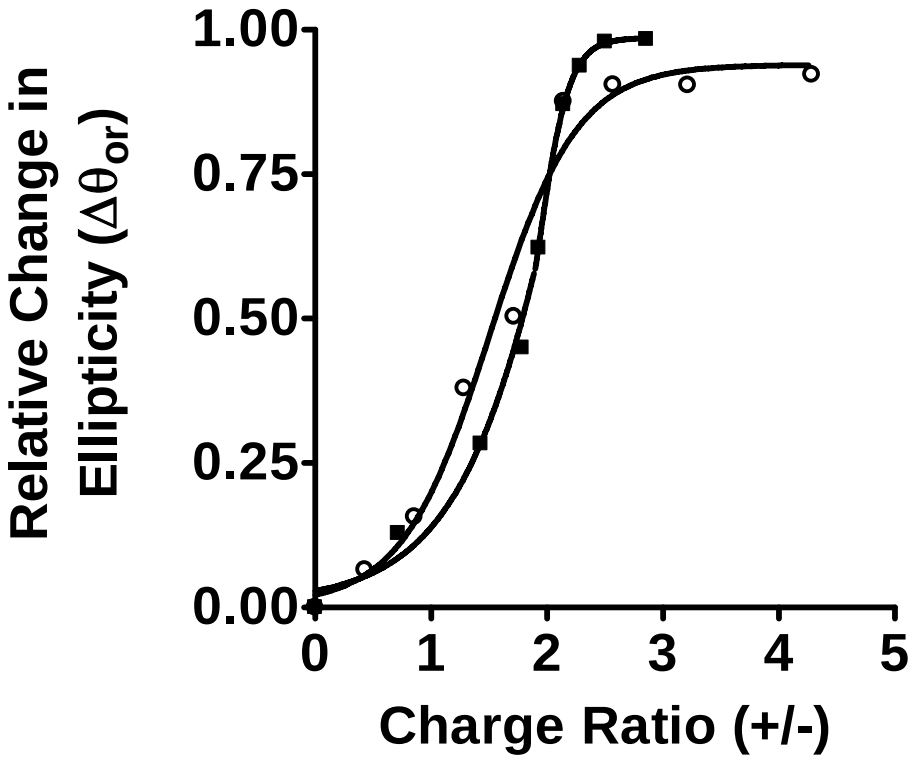

Figure 3-6. Relative change in ellipticity of siRNA at 260 nm as a function of +/- charge ratio for siRNA concentrations of 1.5 μM (○) and 3.0 μM (■). Solid lines are the line of best fit generated by Prism.

Circular dichroism measures the difference in absorption spectrum between left-handed and right handed polarized light. Therefore, CD provides sensitive and unique spectra for chiral molecules, and it has been widely used in structural determination of proteins and nucleic acids. With increasing R9 concentrations, the ellipticity of complex solution decreased, while the maximum and minimum peaks experience negligible shifting, which suggested that the structure of the siRNA experienced minimal structural changes upon interacting with R9. The decrease in ellipticity of siRNA due to increasing peptide concentration can be attributed

to the decrease in absorbance of the nucleosides in siRNA-R9 complexes, similar to the spectra obtained by UV-Vis spectroscopy.

Hydrodynamic Diameter and Zeta Potential Measurements

The size and surface charge of the siRNA-R9 complexes are characterized by measuring the hydrodynamic diameter and Zeta potential (Figure 3-7). CTGF siRNA adopts the structure of the right-handed A form of DNA in solution, with a measured hydrodynamic diameter of 5.21 nm, which is very close to the theoretical value of 5.46 nm for a 21 base pair siRNA [181]. R9 peptide adopts a random coil structure (also confirmed by CD), and its hydrodynamic diameter is found to be 6.81 nm. With increasing peptide concentration, both the hydrodynamic diameter and Zeta potential of the complex solution increased. The size of the complexes increases until its value reaches 1055.8 nm. The Zeta potential of CTGF siRNA in HEPES is -36.2 mV, which reflects the contribution from the 42 negative charges on the phosphate group at neutral pH; whereas the Zeta potential of R9 in HEPES is 28.1 mV, due to the positively charged guanidino group. The increase in Zeta potential is the most pronounced when the charge ratio is between 1.43 and 8.57 mV, while its value increased consistently upon additional peptide addition.

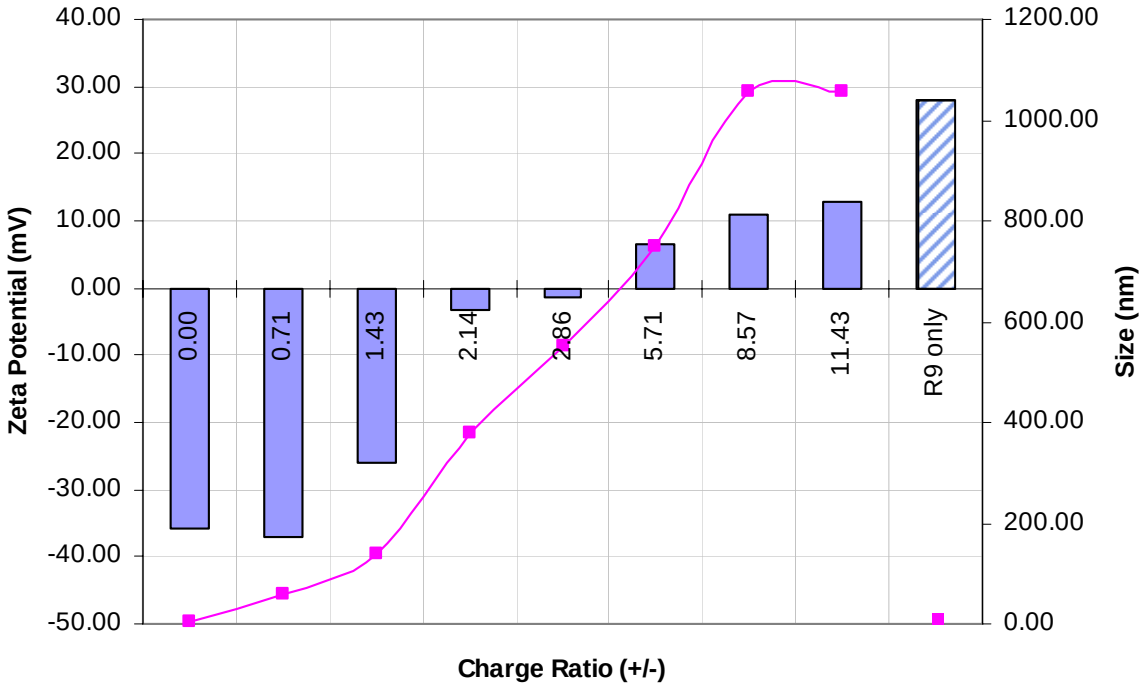

Figure 3-7. Hydrodynamic diameter and Zeta potential of CTGF siRNA-R9 complexes at 1.5 μM siRNA. Zeta potential of siRNA and siRNA-R9 complexes is expressed in solid bars; Zeta potential of R9 is represented by diagonal bar; and size is represented by a solid line.

The rate of increase in the hydrodynamic diameter is at maximum when the charge ratio is between 1.43 and 8.57, where the value of the surface charge is low. The increase in hydrodynamic diameter strongly demonstrated that the two species interact with each other. Further, since the hydrodynamic diameter increased by almost 200 fold, the results also indicate that siRNA and R9 forms large aggregates upon complexation.

According to the DVLO theory for colloidal systems [182], the energy barrier resulting from the repulsive force prevents two particles approaching one another and adhering together. However, when sufficient energy is given to overcome the barrier, the attractive forces will pull them into contact where they adhere strongly and/or irreversibly together. When the complexes have low Zeta potential, electrostatic repulsion is low thus the particles in solution can adhere to each other and result in large aggregates. The results from DLS and Zeta potential suggest that the complexation reaction is saturated when the charge ratio is above 8.57, which is higher than the values obtained by UV-Vis spectroscopy and CD. Thus, it is suggested that the hydrogen bonding sites between nucleosides and R9 is first depleted among the three. It can be seen that UV-Vis spectroscopy and CD can detect the complexation of siRNA and R9 only at charge ratio below 2.2.:1, further complexation and aggregation phenomena cannot be detected by these two methods. Furthermore, it is worth noting that UV-Vis absorbance and CD signal has reached saturation at a charge ratio of ~2.2:1, which is very close to the isoelectric point of the siRNA-R9 complexes.

Moreover, since size and surface charge are the essential parameters contributing to the activation of the complement system. As seen in Figure 3-7, peptide concentration can be used to control the size and surface charge of the siRNA-R9 complexes so that the interaction between the siRNA-peptide complexes and the immune system can be minimized during delivery.

Morphology of siRNA-R9 complexes

Atomic force microscopy has been used to determine the morphology of the siRNA-R9 complexes. As seen in Figure 3-8, the siRNA-R9 complexes are shown to have a poly-dispersed, globular structures on mica surfaces. Furthermore, these small globular structures tend to aggregate to form larger structures.

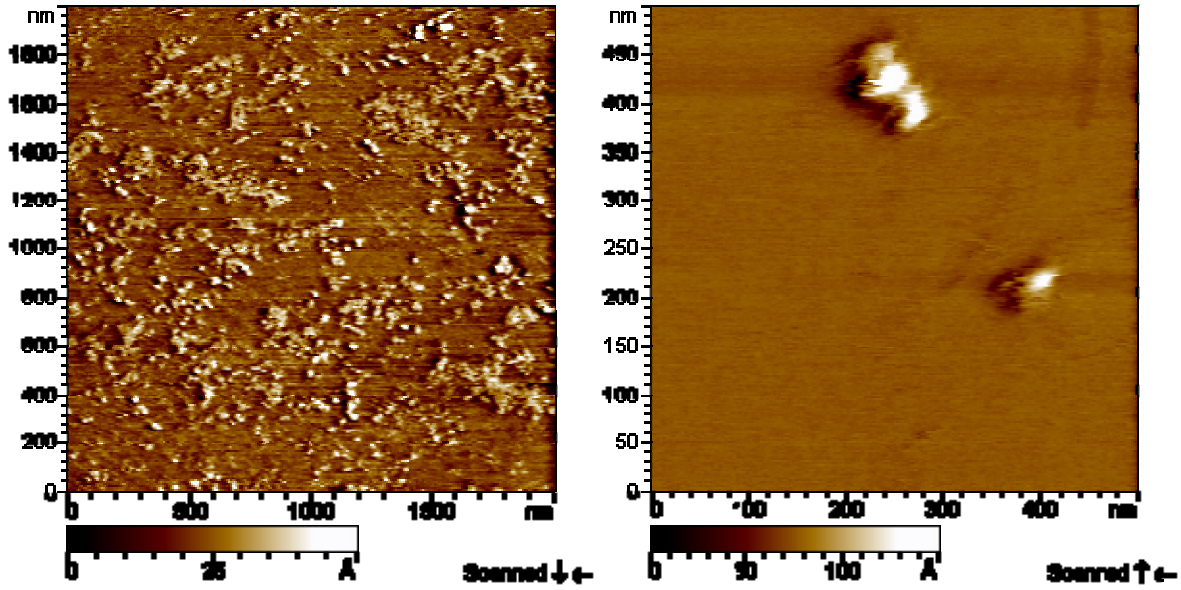

Figure 3-8 In solution atomic force microscopy image of CTGF siRNA (3.0 μM) and R9 (35 μM) complexes on mica.

Salt effect on siRNA-R9 binding

Ionic interaction contributed by salts can destabilize non-covalent interactions. In this study, a high concentration of sodium chloride (2 M) was added to the siRNA-R9 complex solution to investigate the driving force of the complexation reaction. Similar to the UV-Vis abosorbance results above, hypochromicity is seen when excess peptide is added to siRNA, where the absorbance dropped by 83.0% in one hour following peptide addition (Figure 3-9). Two hours after the addition of 2 M sodium chloride, the absorbance of the complex solution increased and its absorbance is 13.1% lower than the absorbance of siRNA under the same treatment. The absorbance of the complex solution was monitored after one day and the absorbance remained the same.

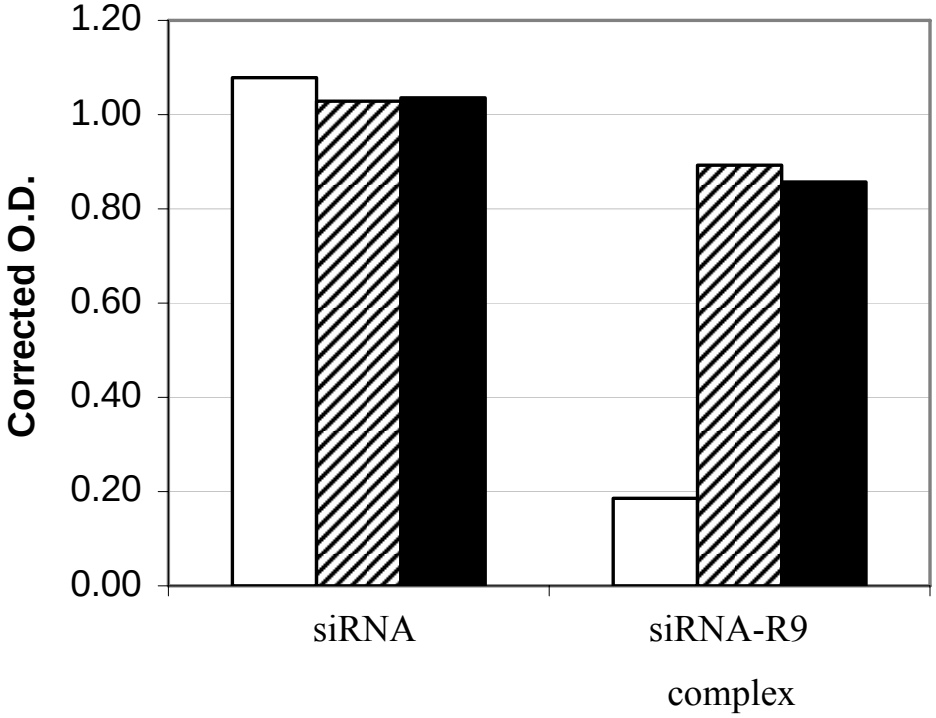

Figure 3-9. Absorbance at 260 nm of siRNA (1.5 μM) and siRNA-R9 (1.5 μM / 150 μM) complex solution upon 2 M salt addition. The absorbance of siRNA only and siRNA-R9 complex solutions are monitored prior to salt addition (white), 2 hours after salt addition (diagonal), and one day after salt addition (black).

Chapter 4

Design of Peptide Carriers and Preliminary *in vitro* Evaluation

Despite the versatility and biodegradability of the peptide delivery system, its use for nucleic acid delivery is limited by its low transfection efficiency when compared to lipid and virus based delivery systems. Since peptide carriers has promising potential in transfecting siRNA efficiently, it is the interest of our group to develop new peptide sequences that can promote siRNA transfection efficiency.

The desired properties of the new peptide carrier include:

- The peptide should interact with siRNA through non-covalent interactions such as Columbic forces and hydrogen bonding. In particular, basic amino acids such as lysine and arginine can interact with the negatively charged phosphate group on the sugar ring through electrostatic interaction. Covalent bonds between the carrier and siRNA such as conjugation, and the use of cross-linking agents, increase the complexity of the design and processing of the siRNA formulation.
- The carrier should have high siRNA loading capacity so that more siRNA can be delivered at low cost.
- The optimal size for cellular internalization through endocytosis is between 100 nm to 200 nm in diameter, whereas smaller complexes, depending on their surface properties, can directly penetrate the cell membrane. Cellular translocation of larger complexes

experiences increasing difficulties. Since endocytosis is one of the most common routes for cellular translocation, the siRNA-peptide complexes should be controlled to have a size below 200 nm.

- Surface charge of the siRNA-peptide complexes is an essential parameter towards complex aggregation and the triggering of immune response through complement activation. Therefore, the surface charge of siRNA-peptide complexes should be controlled within a narrow range so that the complexes are free from aggregation and are stealth from the immune system.

- Various exonucleases are able to degrade siRNA prior silencing of protein expression. Therefore one of the most important properties of siRNA-carrier complexes is to protect the siRNA from premature degradation and other harsh environments.

- Previously published sequences were analyzed and amino acids with specific functions were identified to be incorporated in new sequences. These amino acids include pH sensitive amino acids histidine and glutamic acid, as well as basic amino acids lysine and arginine.

- It is very important that the peptide carrier is biocompatible. Therefore, cytotoxicity evaluation of peptide carriers at various concentrations should be carried out.

4.1 New Peptide Sequences

Based on the above design criteria, 54 peptides (including controls) in 5 categories were designed:

The first group contains eight peptides that mainly consist of arginine and histidine. Two previous studies [155,183] have investigated the translocation efficiency of arginine peptides of various lengths. It is found that arginine peptides with seven to nine residues have the highest translocation efficiency, while at least five arginine residues are required for translocation to take place. Histidine is a pH sensitive amino acid as it will be protonated at low pH. When histidine containing peptide is taken in the endosome during endocytosis, it acts as a proton sponge which disrupts the endosomal pH; this results leakage of the endosomal content, which release the siRNA complexes to the cytosol. The two amino acids are utilized in this design to combine the cell penetration property and the endosome disruptive property. The chain length effect of each residue as well as the effect of charge distribution is investigated among this group of peptides.

The second group consists of peptides that are designed to have an α-helical secondary structure that have three distinct sections when viewed from the top, each contributed by the amino acids leucine, histidine and arginine. It is believed that hydrophobic residues such as leucine can assist in cell penetration through interacting with the hydrophobic tails in the lipid bilayer (ref), and also assist in pore formation in the cell membrane. A three factor

center composite design was incorporated in the primary sequences, for the investigation of the effect of peptide chain length, hydrophobicity, and face angle in the helical structure. The secondary structure of the designed peptides was predicted using NNPREDICT [184].

Since many peptide delivery carriers are designed based on α-helix amphiphilicity [97,108,170] while investigations based on amphiphilic β-sheet peptides are very limited [108,171]. Therefore, the third group consists of peptides was designed to investigate the possibility of using peptides with β-strand secondary structures as delivery vehicle. This group of peptide consists of ionic complementary peptides, which can self-assemble through complementarily of ionic residues and hydrophobic forces, and also peptides that are designed to be ionic complementary as well as having geometric matches between basic amino acid residues and phosphate backbone.

Wender *et al.* have shown that oligo-D-arginine has higher cell penetrating efficiency when compared to the natural occurring oligo-L-arginine [101]. This group of peptides has natural occurring L-arginine substituted with D-arginine.

The final group of peptide contains the derivatives of known peptide sequences, including various cell penetrating peptides, endosomal disruptive peptides, and self-assembly peptides. For example, amino acids lysine and alanine are substituted with arginine and leucine for KLA peptide.

These newly designed peptides are expected to enhance the transfection efficiency of siRNA upon complexation. The transfection efficiency of the siRNA-peptide complexes was monitored by the green fluorescence emitted by a green fluorescence protein (GFP) containing cell line C166-GFP through fluorescence microscopy and fluorescence detected flow cytometry. However, due to time constraints, the transfection efficiency was evaluated on peptides listed in Table 4-1 only.

Table 4-1 Designed peptides sequences investigated in preliminary *in vitro* experiment.

Name	# of a.a.	Sequence	Predicted Secondary Structure www.cmpharm.ucsf.edu/~nomi/nnpredict.html	# of Helical A.A.	Hydrophobicity	Charges pH 7.2		Charges pH 4.2	
						+	-	+	-
R9	9	n-RRRRRRRRR-c	- - - - - - - - -	0	0.0000	9	0	9	0
EAK 16 IV	16	n-AEAEAEAEAKAKAKAK-c	- - HHHHHHHHHHHH - -	12	0.3945	4	4	4	2
EAK 16 II	16	n-AEAEAKAKAEAEAKAK-c	- - HHHHHHHHHHHH - -	12	0.3945	4	4	4	2
ACS	11	n-ACSSSPSKHCG-c	- - - - - - - - - - -	0	0.4445	1	0	2	0
ACS-R9	23	n-ACSSSPSKHCGGGGRRRRRRRRR-c	- -	0	0.2720	10	0	11	0

4.2 Materials and Methods

Cell Culture. Mouse endothelial cells C166-GFP was purchased from American Type Cell Culture (ATCC CRL-2583; VA, USA). The cell line was transfected with pEGFP-N1 (Clontech, CA, USA) that encodes the enhanced green fluorescence protein (eGFP) by the depositor. C166-GFP cells were maintained in low glucose Dulbecco's modified Eagle's medium (DMEM; Invitrogen, ON, Canada), supplemented with 10% heat inactivated fetal

bovine serum (FBS; Invitrogen, ON, Canada) and 0.02mg/mL G418 (Sigma Aldrich, Canada).

SiRNA, Peptides, and Transfection Agent. The eGFP siRNA with target sequence 5'-GCG ACG TAA ACG GCC ACA AGT TC -3' was purchased from Dharmacon (Cat. No. P-002102-01-20; CO, USA). The molar concentrations of siRNA, were determined by absorption spectroscopy, using an extinction coefficient of 362,408 L/mol•cm. A peptide array consists of crude peptide swith N-terminal acetylation and C-termination amidation was purchased from Pepscan Systems (Leystad, Netherlands). Peptide identity was confirmed by mass spectroscopy. Other reagents were all commercially available and were of analytical grade. The transfection agent Lipofectamine 2000 (Invitrogen, ON, Canada) was used as a positive control for comparison. The dosage of Lipofectamine 2000 was controlled at a siRNA ratio of 20 pmol to 1 μL, as suggested by the manufacturer.

Preparation of siRNA-peptide complexes. Prior to use, siRNA was first dissolved in Milli-Q water (Millipore, USA), divided in aliquots in microcentrifuge tubes, and stored in -86 ^{o}C after drying in Eppendorf Vacufuge Concentrator 5301. Stock siRNA was prepared in HEPES buffer (6 mM HEPES-NaOH, 20 mM NaCl, 0.2 mM MgCl2, pH 7.3). Peptides were first dissolved in dimethyl sulfoxide (DMSO) one day prior to transfection. Stock siRNA and peptide solutions were then balanced with HEPES to obtain desired concentrations for complexation (10X final concentration at 50 μL per sample). The maximum siRNA concentration used was 160 nM and the highest peptide concentration used was at a +/-

charge ratio of 20:1. The resulting complex solutions were stirred vigorously for 10 s with a vortex mixer and incubated for 3 hours at room temperature.

Transfection Protocol. C166-GFP cells were seeded at 15000 cells/well on 24 well plates one day before transfection. Fifty microlitres of complex solution and 200 μL of DMEM were added to each well. After four hours, 250 μL of DMEM with 20% FBS was added to each well. Cells were harvested over two days for eGFP fluorescence monitoring.

Fluorescence Microscopy. The eGFP from the siRNA transfected cells were observed using an Axiovert 200 Fluorescence Microscope (Carl Zeiss, Jena, Germany) equipped with a 10x objective, directly on 24-well plates, without cell fixation. The excitation and emission filters for fluorescence imaging have band passes of 485±20 nm and 525±25 nm, respectively.

Cell Fixation. Upon siRNA transfection, C166-GFP cells were harvested over 2 days, fixed in 2% paraformaldehyde (PFA) for the detection of eGFP expression by flow cytometry. Each well on the 24-well plate was first rinsed with 500 μL phosphate buffered saline (PBS) once, trypsinized with 200 μL of 0.25% trypsin-EDTA, and the cells were resuspended by Mg^{2+} and Ca^{2+} containing PBS. The cells were centrifuged at 1000 rpm for 10 mins, and then the supernantant was removed. The cells were then resuspended in 2% PFA and stored at 4 ^{o}C until flow cytometry analysis.

Flow Cytometry. Fluorescence and light scattering intensity distributions of C166-GFP cells were obtained by flow cytometry (FACS Vantage SE, Becton Dickinson, USA) with a laser

excitation wavelength of 488 nm. Fluorescence emission of eGFP is obtained with a 530 ± 30 nm band pass filter. At least 5000 events were recorded. Data were analyzed by FCS Express software (Version 3). Gates were applied to exclude cell debris and unhealthy cells from analysis.

4.3 Results and Discussion

In this study, C166-GFP cells were transfected with eGFP siRNA, using peptides as a delivery carrier. The efficiency of siRNA silencing is monitored at the protein level where the eGFP fluorescence was monitored by fluorescence microscopy and flow cytometry. For effective eGFP silencing, the eGFP fluorescence intensity is expected to decrease upon siRNA transfection since the mRNA encoding for the eGFP is degraded. Upon reaching the cytosol, the successfully delivered siRNA would perform RNAi which prevents the downstream production of eGFP until the siRNA is eventually degraded by endonucleases. However, GFP that is already present in the cytosol prior to siRNA delivery would still give fluorescence before it is degraded by intracellular proteases. Therefore, it is very important to monitor the effect of silencing over time. The effect of siRNA silencing was monitored over 2 days at 24 hours and 48 hours. The base line of eGFP fluorescence is obtained from the fluorescence of untreated cells. The normal and positive controls were cells transfected with naked siRNA and siRNA-Lipofectamine 2000 complexes, respectively. Due to time constraints, only five peptides, R9, EAK 16 IV, ACS, ACS-R9, and EAK 16 II were investigated. (Table 4-1)

4.3.1 Optimization of siRNA Dosage by Fluorescence Microscopy

The dosage for siRNA transfection has to be controlled within a very specific range. The extent of siRNA silencing is limited when a low dosage is used; however, sequence non-specific silencing can be triggered when the siRNA dosage is too high [185]. In general, the siRNA dosage used for transfection is at a maximum of 100 nM [186]. Detectable transfections with siRNA concentration as low as 25 nM have been reported [187,188]. Optimization of siRNA dosage was performed with siRNA concentrations ranging from 0 to 160 nM, using Lipofectamine 2000 as transfection agent. The effect of eGFP silencing was monitored using Fluorescence microscopy. (Figure 4-1)

The brightness of GFP from the fluorescence images was used as an indicator of the siRNA silencing efficiency. As seen in Figure 4-1, when the dosage of siRNA increases, the brightness of the GFP in the fluorescence images decreases. Silencing effect of eGFP has become significant when siRNA concentration reaches 80 nM. Furthermore, at siRNA concentration of 120 and 160 nM, a decrease in confluency is observed, which indicates a decrease in cell viability. Cytotoxicty is also observed in the Lipofactamine 2000 only control (dosage used is equivalent to the volume required to tranafect siRNA at 100 nM). The decrease in cell viability is mainly due to the non-specific silencing effect happened at high siRNA concentration, or due to the increased cytotoxicity of the liposome based transfection agent [77,79,84]. From the siRNA dosage optimization results, it is found that 80 nM siRNA is able to provide a significant silencing effect while maintaining high cell viability. The

concentration of siRNA used in subsequent transfection would be 80 nM unless otherwise stated.

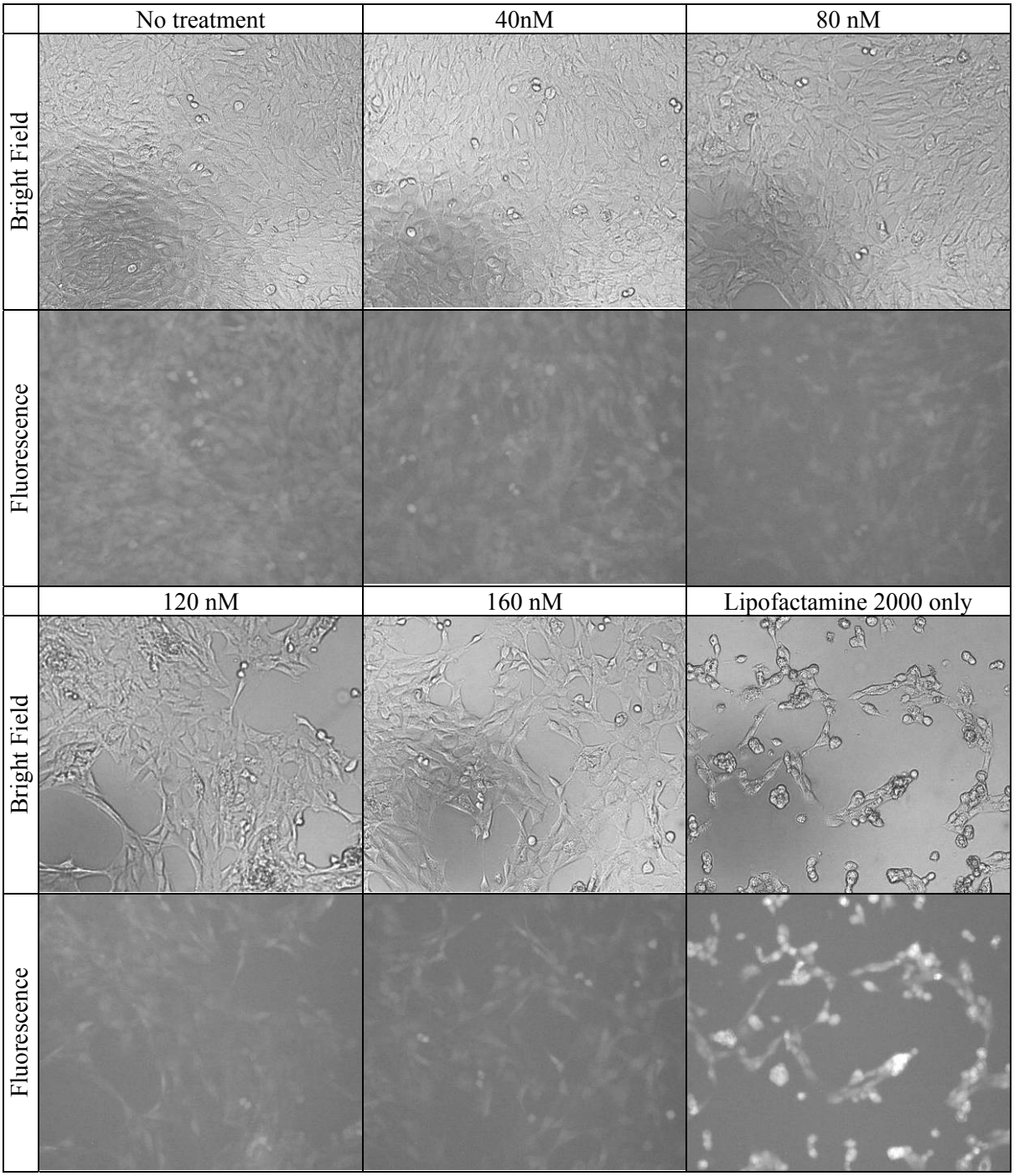

Figure 4-1. C166-GFP cells at 48 hours after eGFP siRNA transfection, using Lipofectamine 2000 as transfection agent. Fluorescence and corresponding bright field images are shown.

4.3.2 Transfection Efficiencies of Peptides Candidates

Five peptides from Table 4-1, R9, EAK 16 IV, ACS, ACS-R9, and EAK 16 II were used as carriers in siRNA transfection. The fluorescence intensities of transfected cells were monitored after 24 hours and 48 hours, using fluorescence microscopy (Figures 4-2 to 4-11) and fluorescence detected flow cytometry (Figures 4-12 to 4-19).

Both bight field images and fluorescence images of the C166-GFP cells treated with siRNA-peptide complexes at various charge ratios, together with the negative controls, are shown in Figure 4-2 to 4-11, where Figure 4-2 to 4-6 are the images taken at 24 hours whereas Figure 4-7 to 4-11 are the images taken at 48 hours. By comparing the GFP intensities between the non-treated cells and the siRNA-peptide complex treated cells at 24 and 48 hours, it can be seen that there is no significant decrease in fluorescence intensity from the siRNA-peptide complexes treated cells when compared to the siRNA-Lipofectamine 2000 treated cells (Figure 4-1).

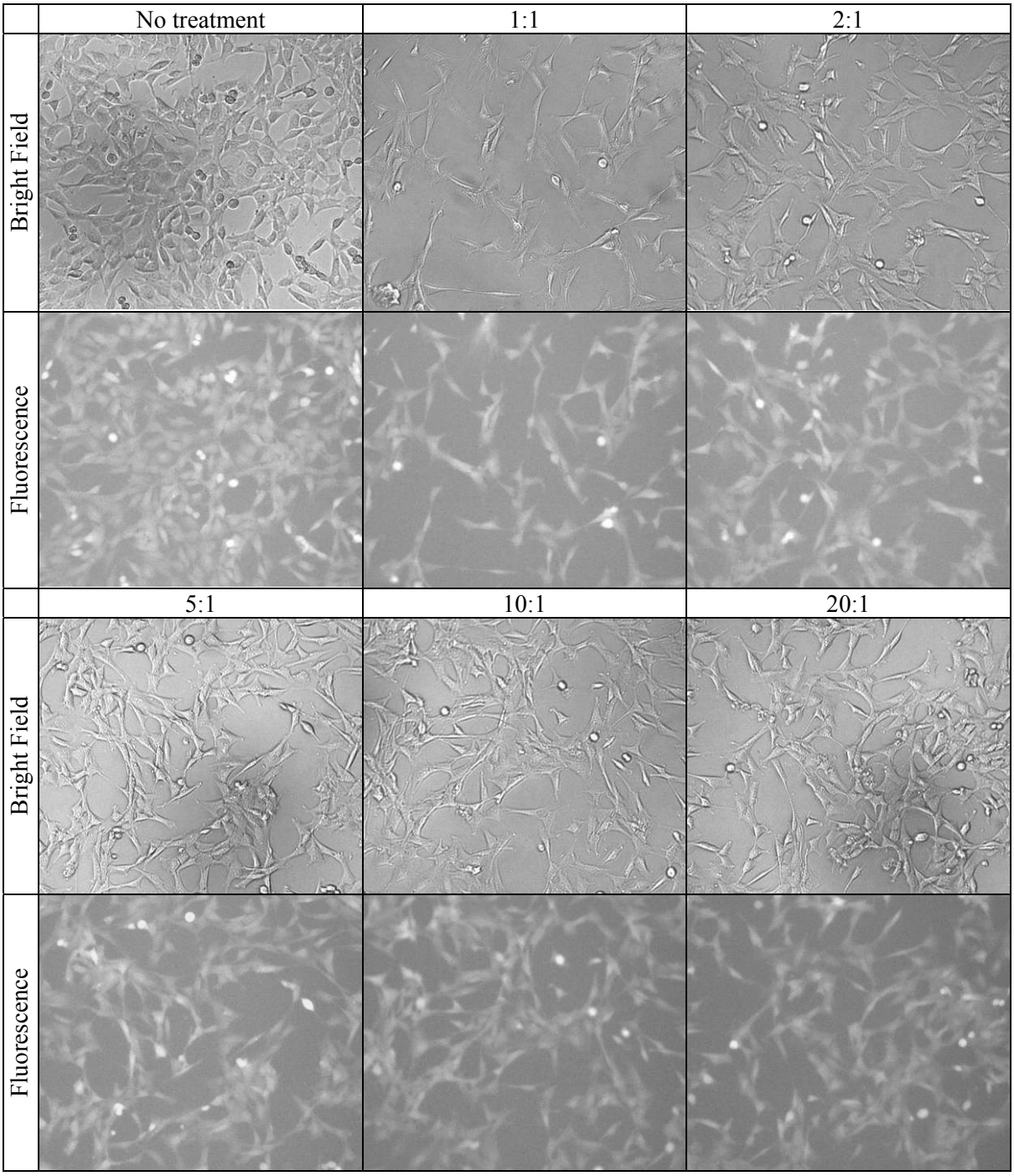

Figure 4-2. C166-GFP cells at 24 hours after eGFP siRNA transfection at specified +/- charge ratios, using R9 as transfection agent. Fluorescence and the corresponding bright field images are shown. Fluorescence images of the peptide controls are shown in the Appendix.

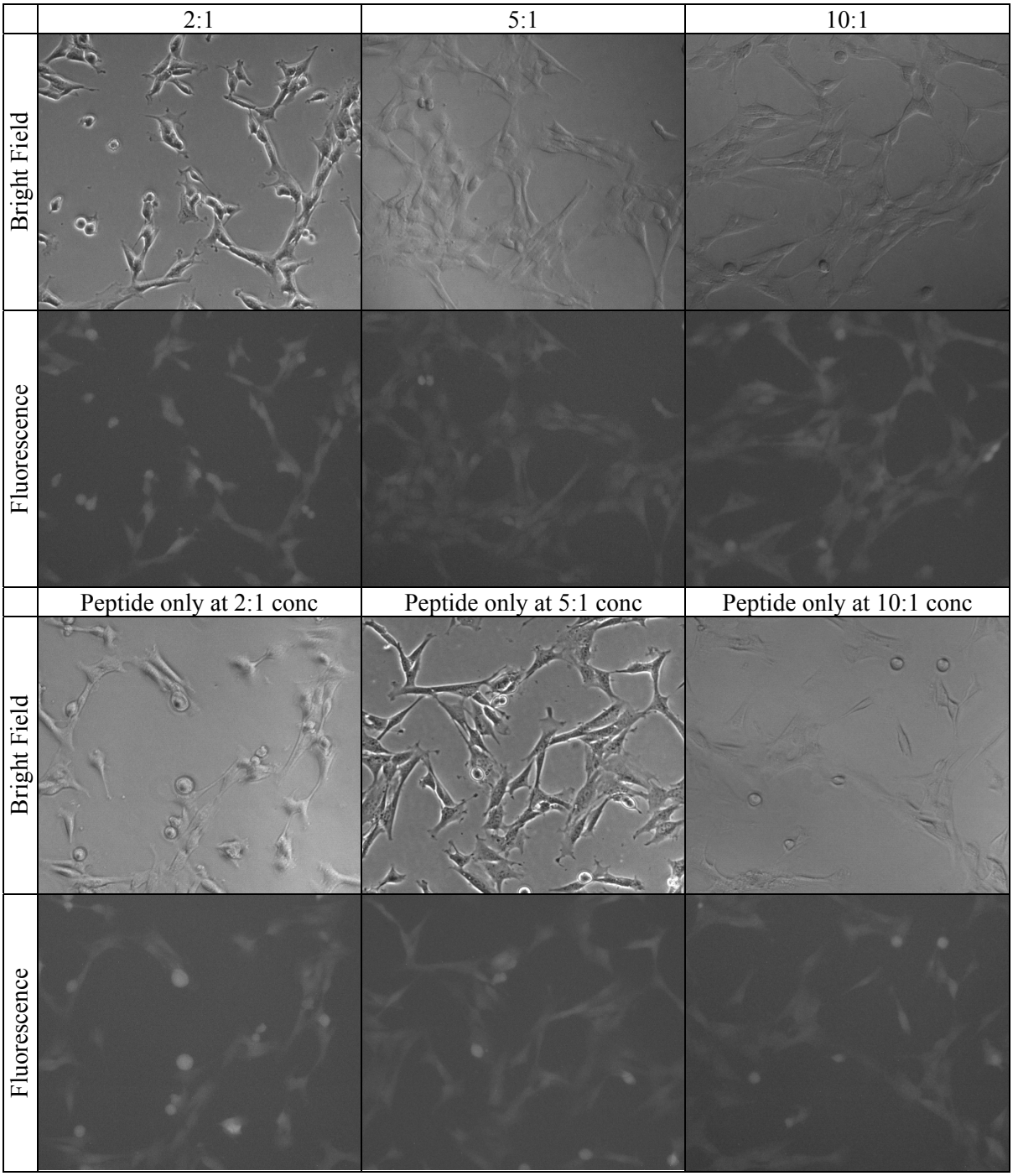

Figure 4-3. C166-GFP cells at 24 hours after eGFP siRNA transfection at specified +/- charge ratios, using EAK 16 II as transfection agent. Bottom panel shows the peptide only controls for the corresponding peptide concentration used for siRNA transfection in the top panel. Fluorescence and the corresponding bright field images are shown.

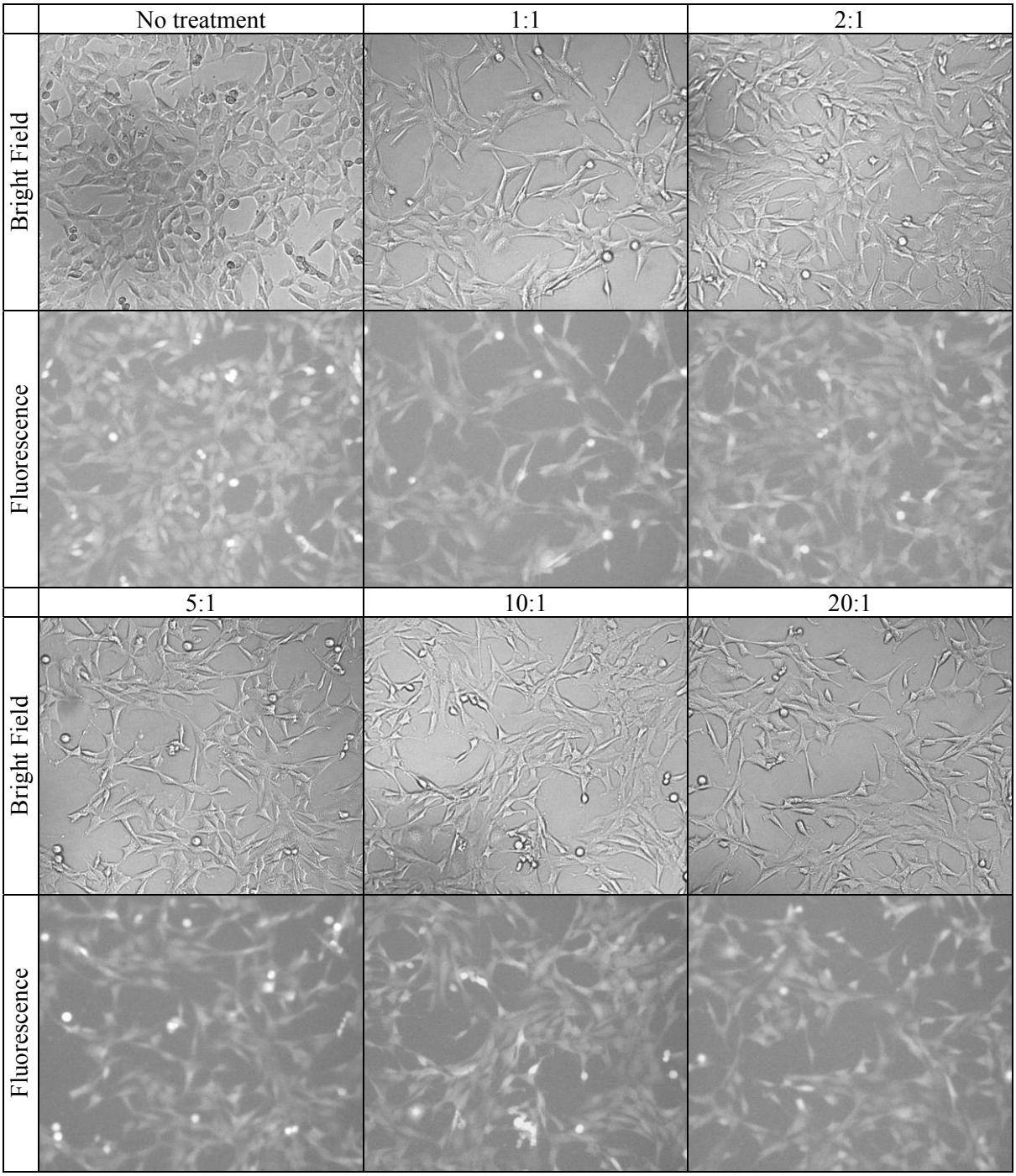

Figure 4-4. C166-GFP cells at 24 hours after eGFP siRNA transfection at specified +/- charge ratios, using EAK 16 IV as transfection agent. Fluorescence and the corresponding bright field images are shown. Fluorescence images of the peptide controls are shown in the Appendix.

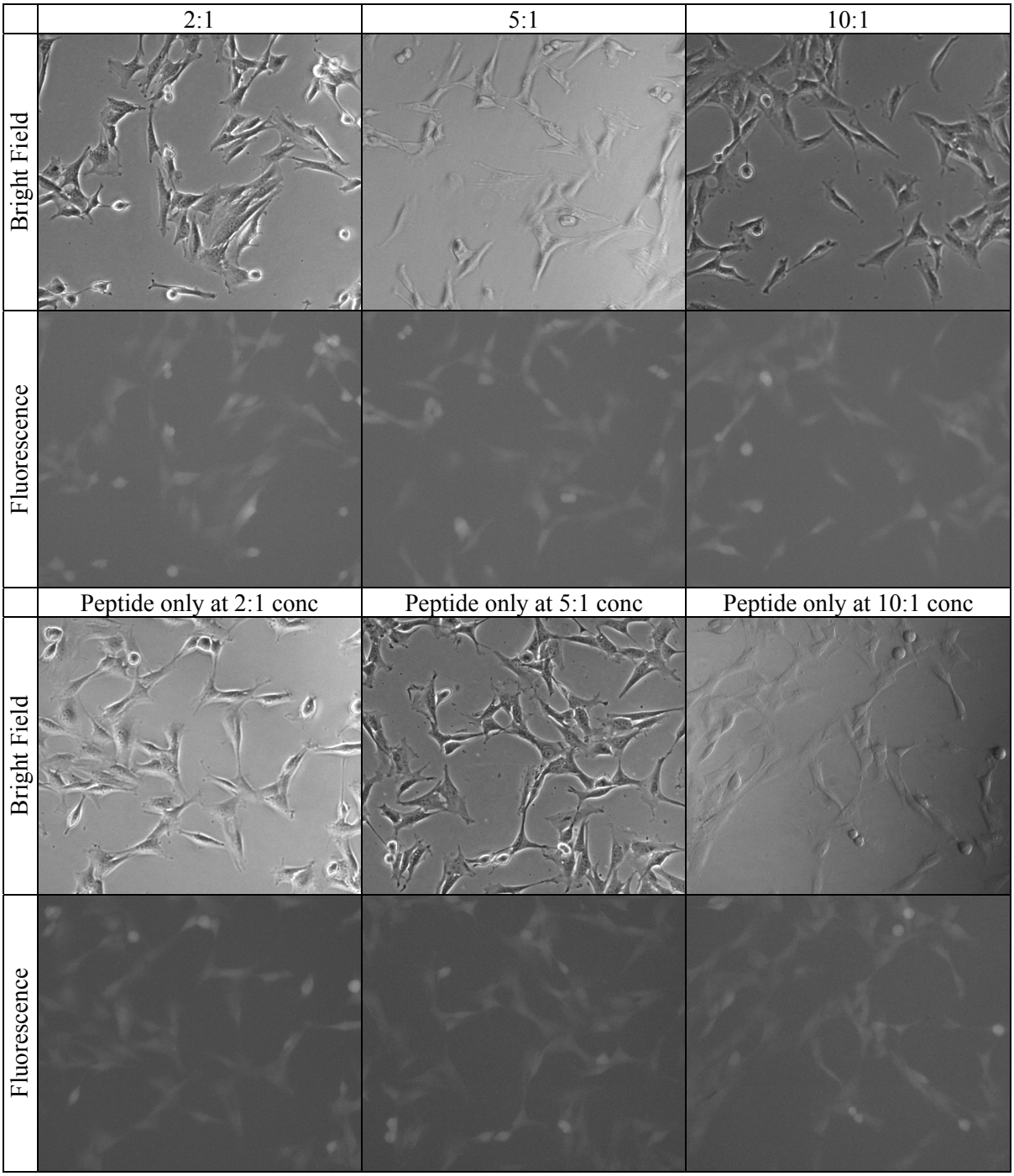

Figure 4-5. C166-GFP cells at 24 hours after eGFP siRNA transfection at specified +/- charge ratios, using ACS as transfection agent. Bottom panel shows the peptide only controls for the corresponding peptide concentration used for siRNA transfection in the top panel. Fluorescence and the corresponding bright field images are shown.

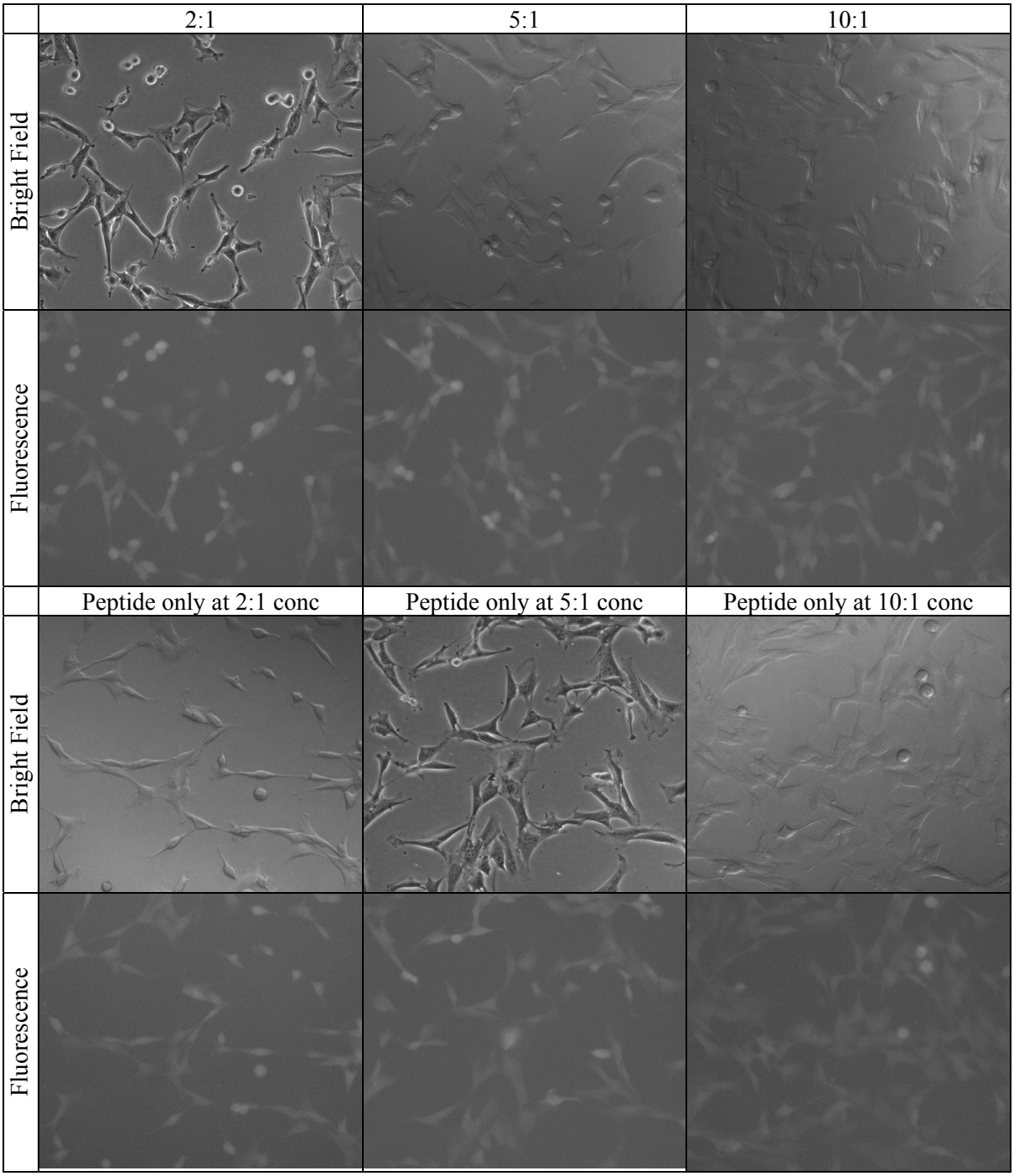

Figure 4-6. C166-GFP cells at 24 hours after eGFP siRNA transfection at specified +/- charge ratios, using ACS-R9 as transfection agent. Bottom panel shows the peptide only controls for the corresponding peptide concentration used for siRNA transfection in the top panel. Fluorescence and the corresponding bright field images are shown.

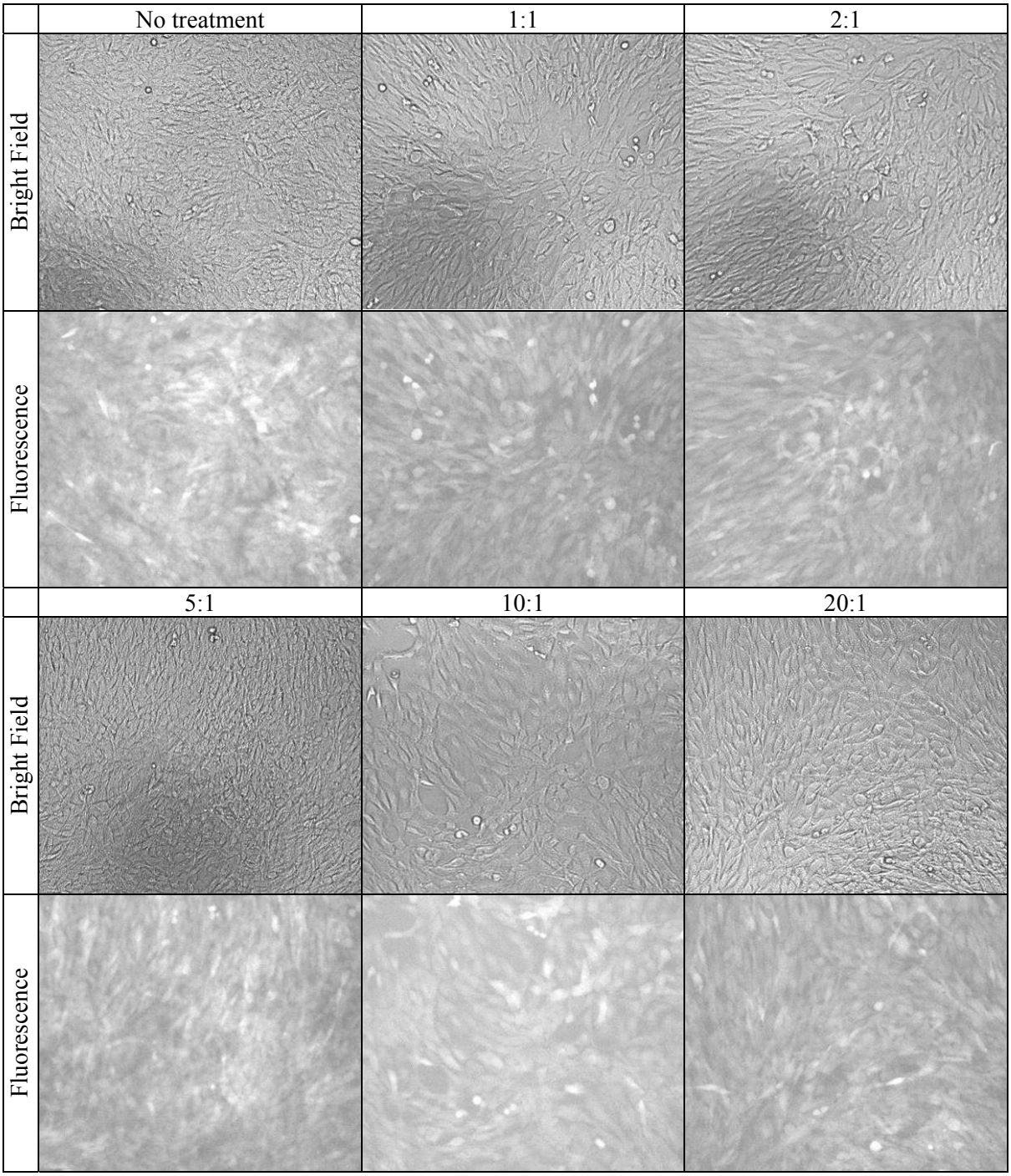

Figure 4-7. C166-GFP cells at 48 hours after eGFP siRNA transfection at specified +/- charge ratios, using R9 as transfection agent. Fluorescence and the corresponding bright field images are shown. Fluorescence images of the peptide controls are shown in the Appendix.

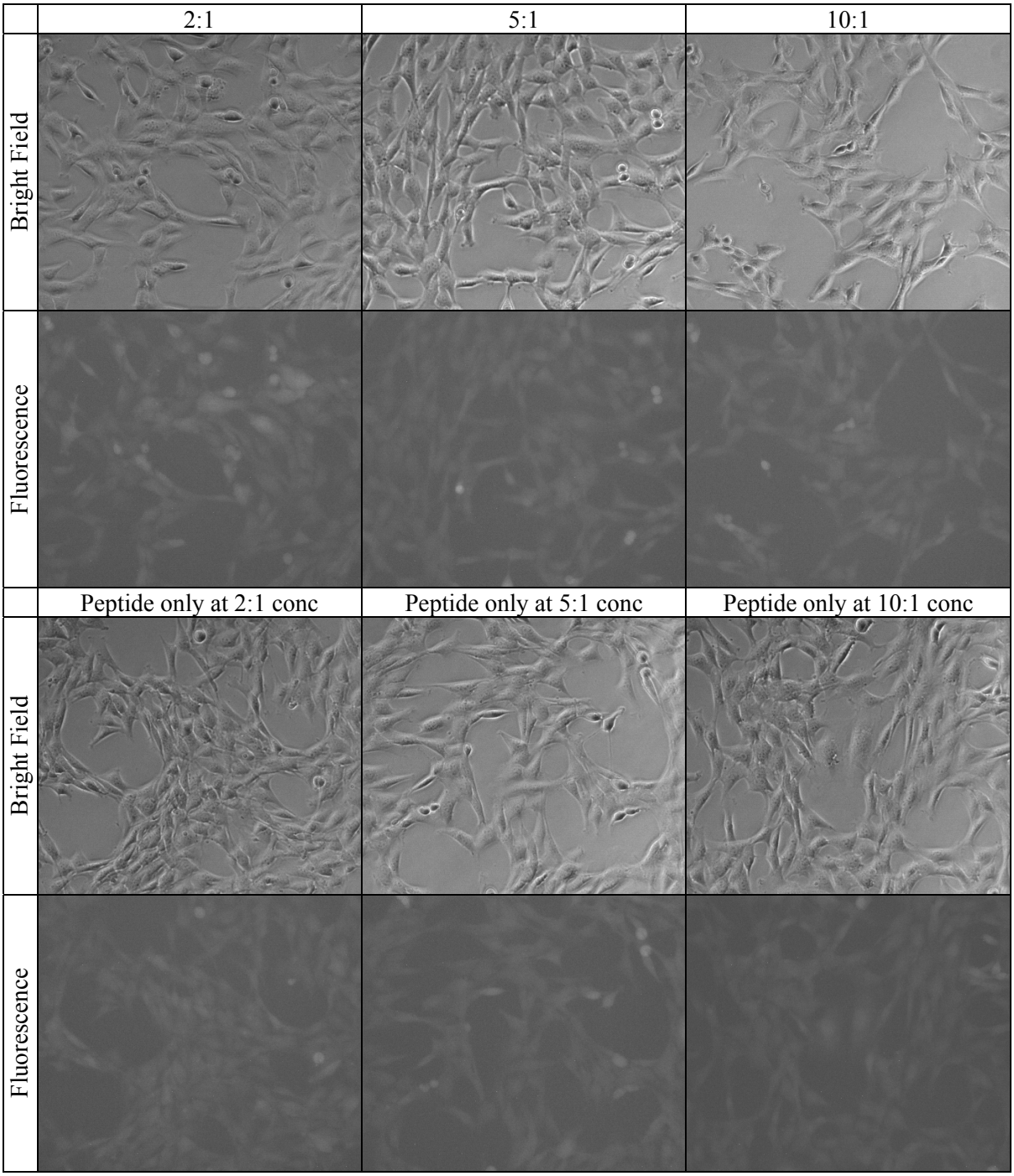

Figure 4-8. C166-GFP cells at 48 hours after eGFP siRNA transfection at specified +/- charge ratios, using EAK 16 II as transfection agent. Fluorescence and the corresponding bright field images are shown.

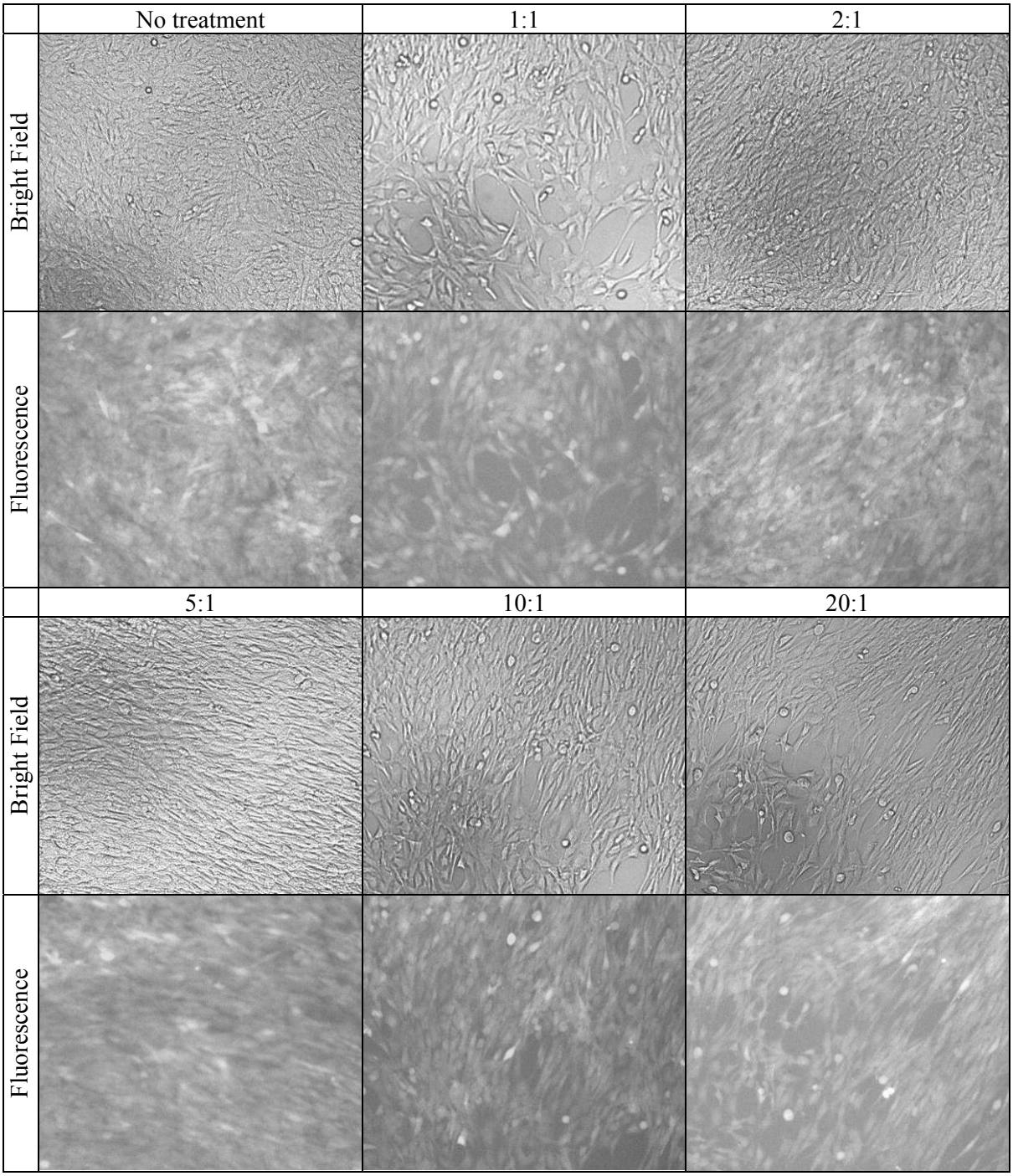

Figure 4-9. C166-GFP cells at 48 hours after eGFP siRNA transfection at specified +/- charge ratios, using EAK 16 IV as transfection agent. Fluorescence and the corresponding bright field images are shown. Fluorescence images of the peptide controls are shown in the Appendix.

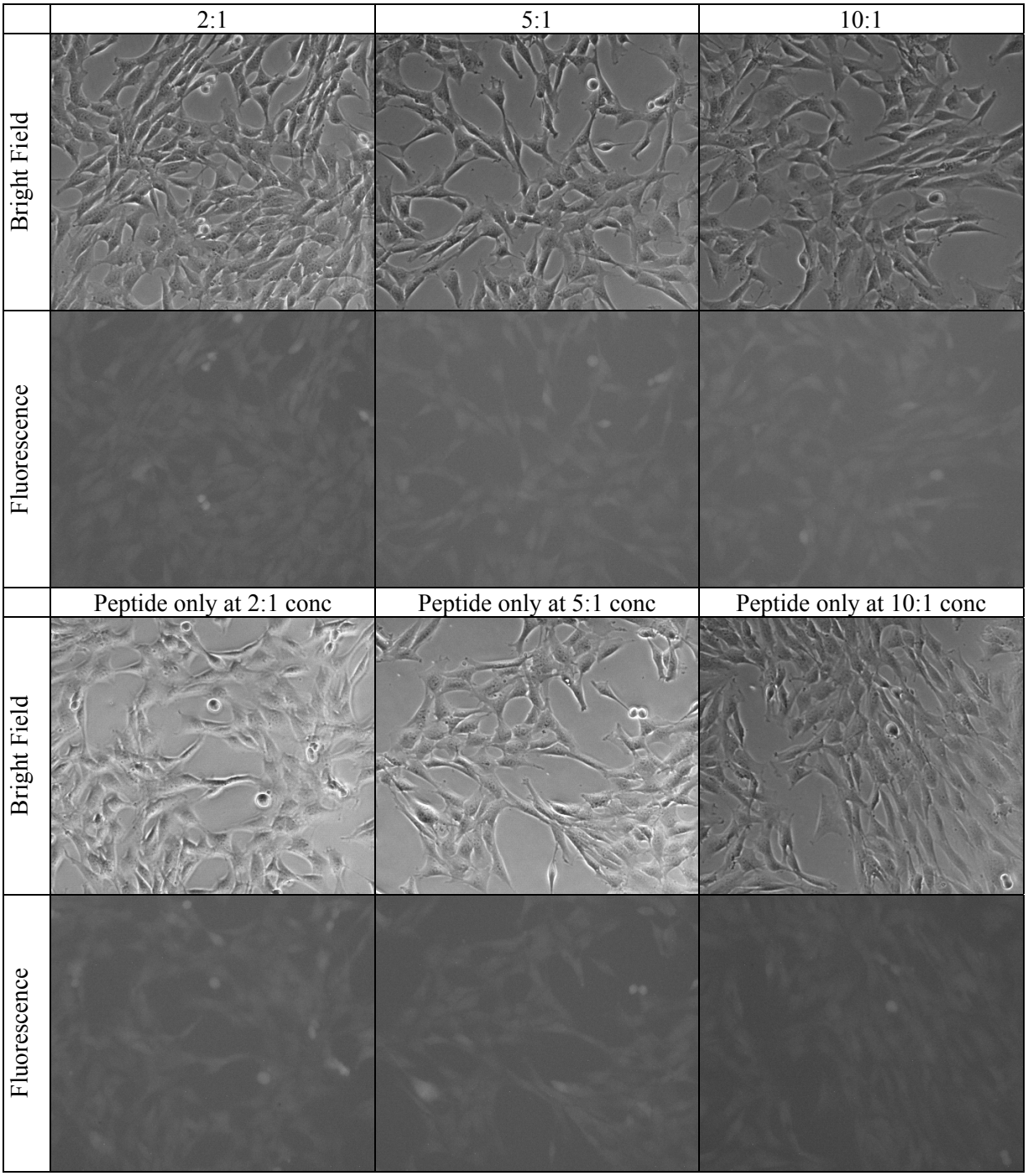

Figure 4-10. C166-GFP cells at 48 hours after eGFP siRNA transfection at specified +/- charge ratios, using ACS as transfection agent. Fluorescence and the corresponding bright field images are shown.

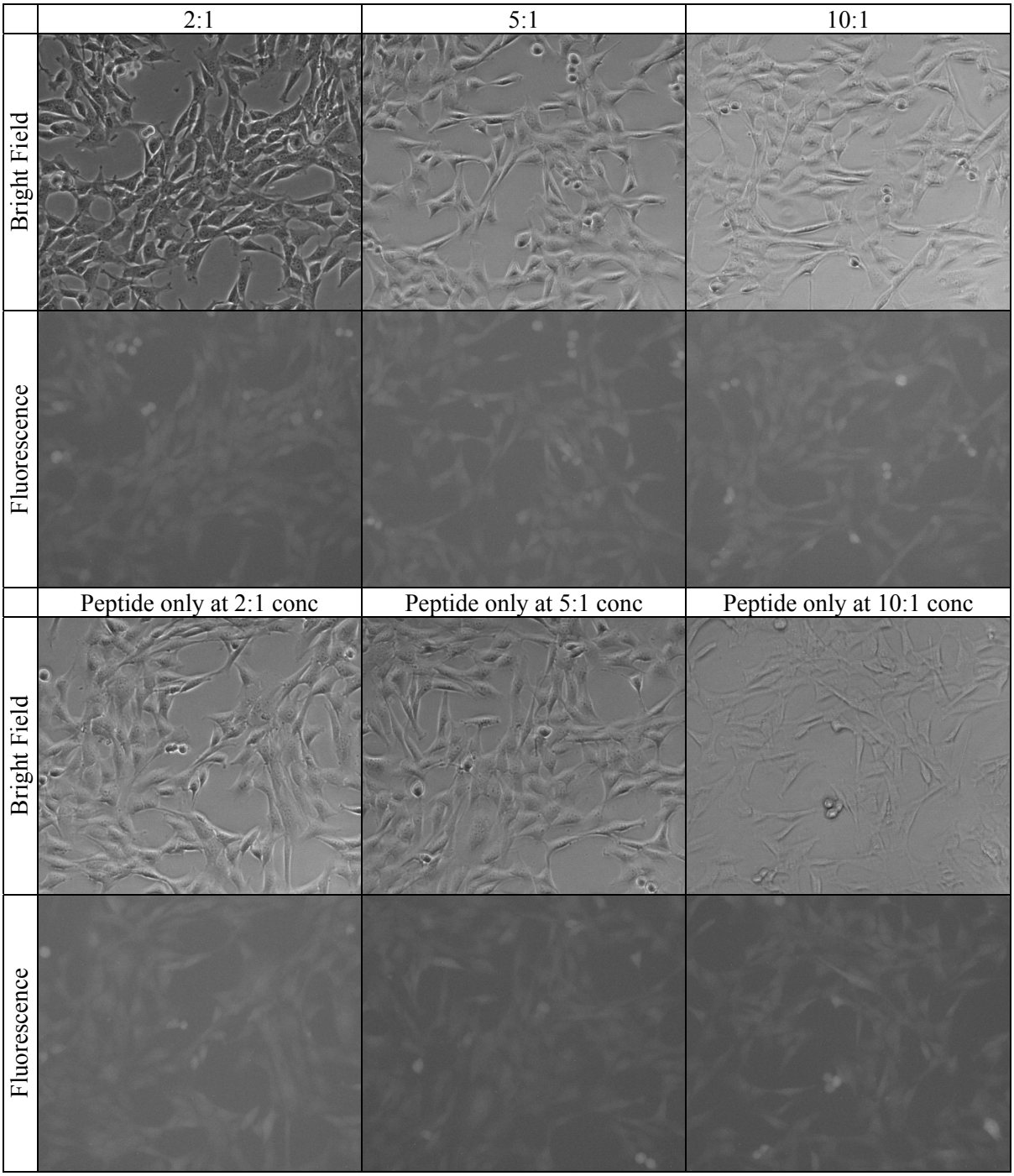

Figure 4-11. C166-GFP cells at 48 hours after eGFP siRNA transfection at specified +/- charge ratios, using ACS-R9 as transfection agent. Fluorescence and the corresponding bright field images are shown.

The GFP intensities of the C166-GFP cells treated with siRNA-peptide complexes at various charge ratios are shown in Figure 4-13 to 4-22, where Figure 4-13 to 4-17 are the images taken at 24 hours whereas Figure 4-18 to 4-22 are the images taken at 48 hours. The negative, positive, and neutral controls are shown in Figure 4-12. The positive control of using Lipofectamine 2000 as siRNA transfection agent significantly decreased the GFP intensity of C166-GFP cells. However, by comparing the GFP intensities between the non-treated cells and the siRNA-peptide complex treated cells at 24 and 48 hours, it can be seen that there is no significant decrease in fluorescence intensity from the siRNA-peptide complexes treated cells when compared to the siRNA-Lipofectamine 2000 treated cells.

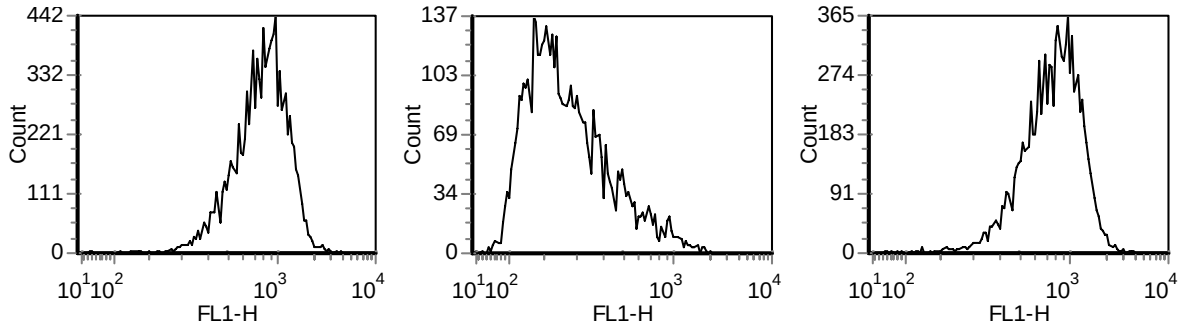

Figure 4-12. FACS results for the negative, positive, and normal controls (from left to right), which corresponds to non-treated cells, siRNA-Lipofactamine 2000 treated cells, and naked siRNA treated cells, respectively.

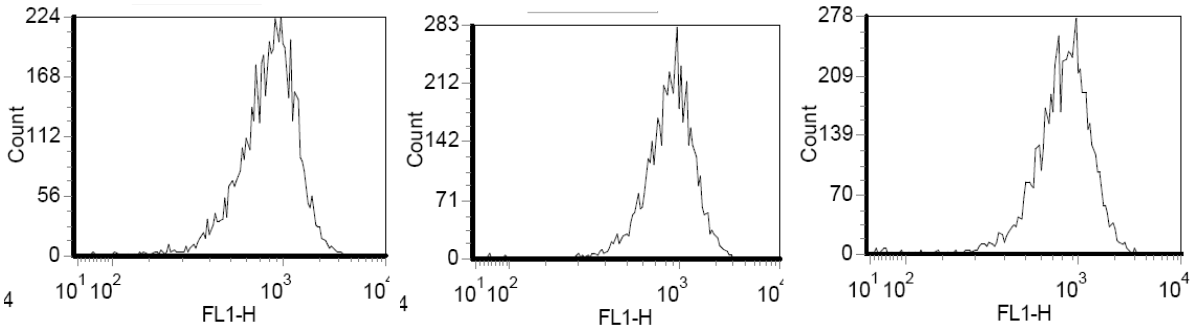

Figure 4-13. FACS results for siRNA-R9 transfected cells in 24 hours at charge ratio (+/-) of 2:1, 5:1, and 10:1 (from left to right).

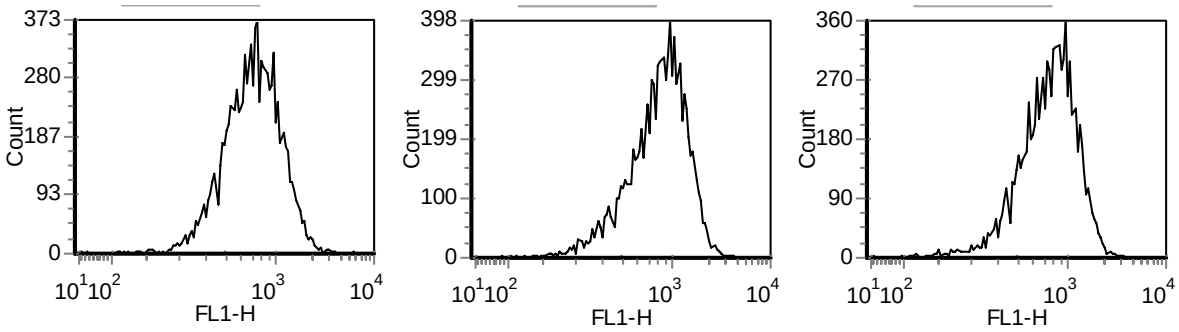

Figure 4-14. FACS results for siRNA-EAK 16 II transfected cells in 24 hours at charge ratio (+/-) of 2:1, 5:1, and 10:1 (from left to right).

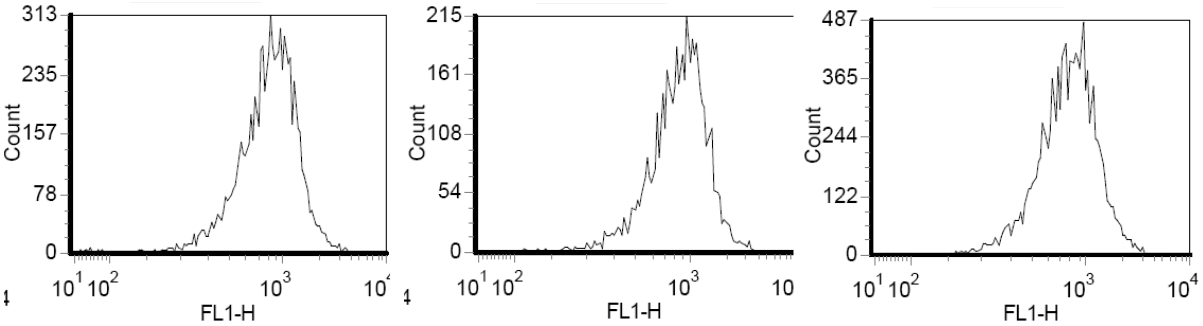

Figure 4-15. FACS results for siRNA-EAK 16 IV transfected cells in 24 hours at charge ratio (+/-) of 2:1, 5:1, and 10:1 (from left to right).

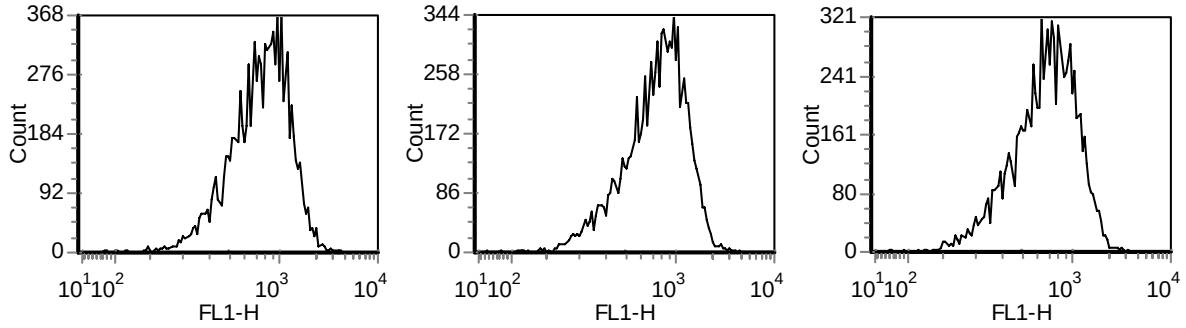

Figure 4-16. FACS results for siRNA-ACS transfected cells in 24 hours at charge ratio (+/-) of 2:1, 5:1, and 10:1 (from left to right).

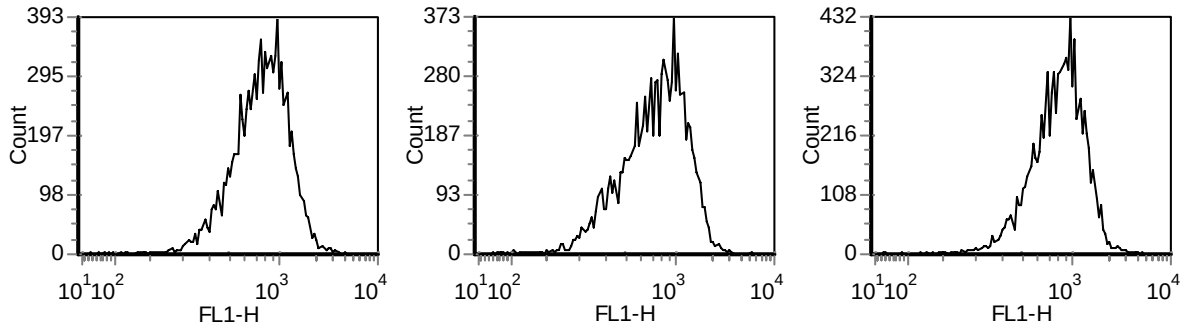

Figure 4-17. FACS results for siRNA-ACS-R9 transfected cells in 24 hours at charge ratio (+/-) of 2:1, 5:1, and 10:1 (from left to right).

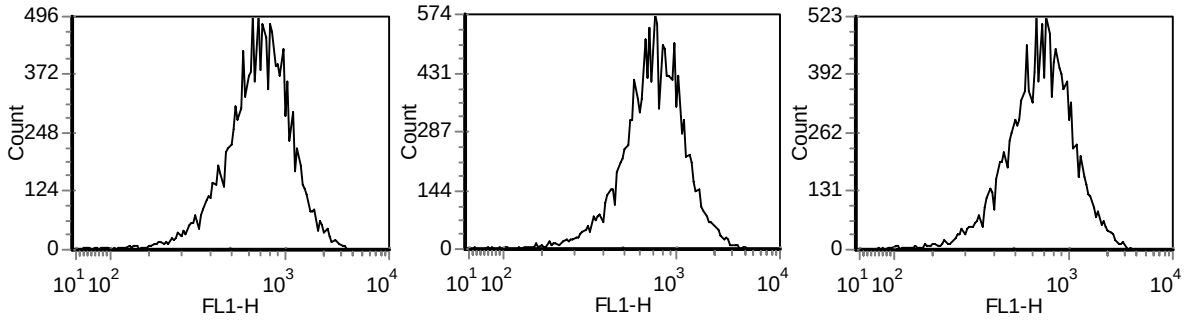

Figure 4-18. FACS results for siRNA-R9 transfected cells in 48 hours at charge ratio (+/-) of 2:1, 5:1, and 10:1 (from left to right).

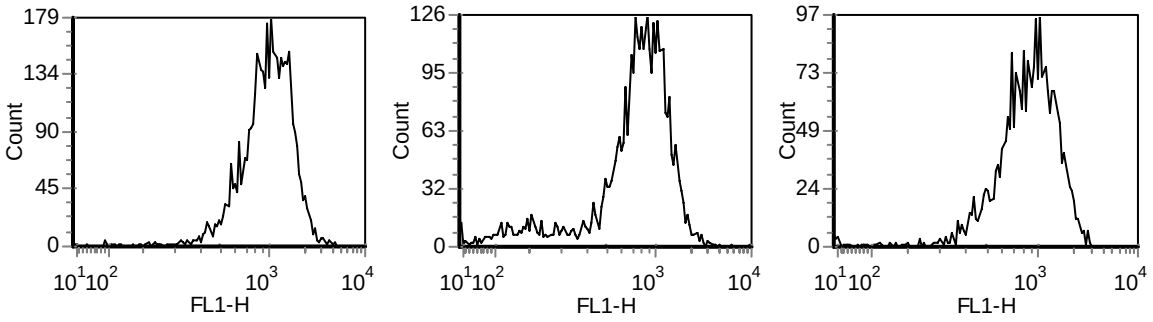

Figure 4-19. FACS results for siRNA-EAK 16 II transfected cells in 48 hours at charge ratio (+/-) of 2:1, 5:1, and 10:1 (from left to right).

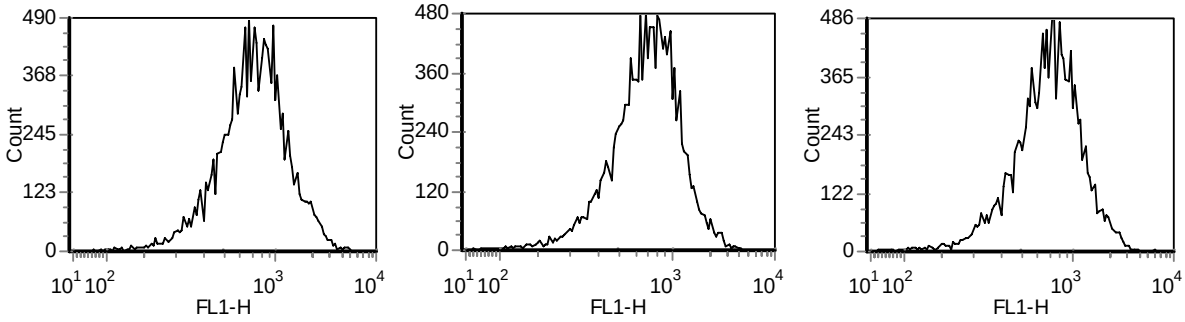

Figure 4-20. FACS results for siRNA-EAK 16 IV transfected cells in 48 hours at charge ratio (+/-) of 1:1, 5:1, and 10:1 (from left to right).

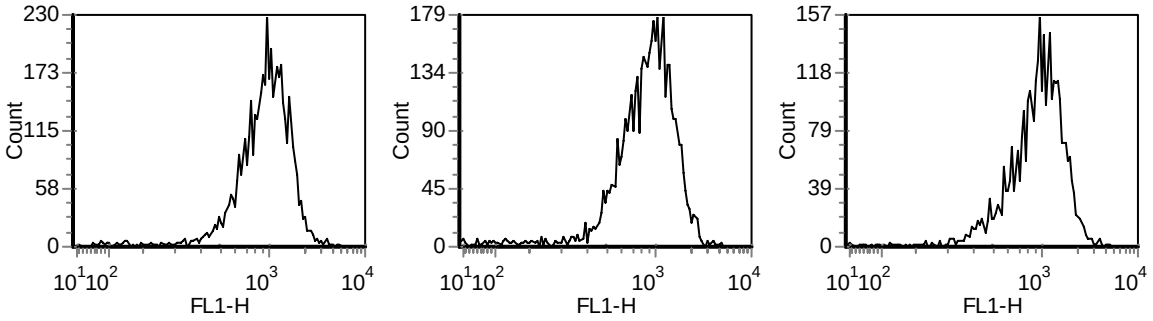

Figure 4-21. FACS results for siRNA-ACS transfected cells in 48 hours at charge ratio (+/-) of 2:1, 5:1, and 10:1 (from left to right).

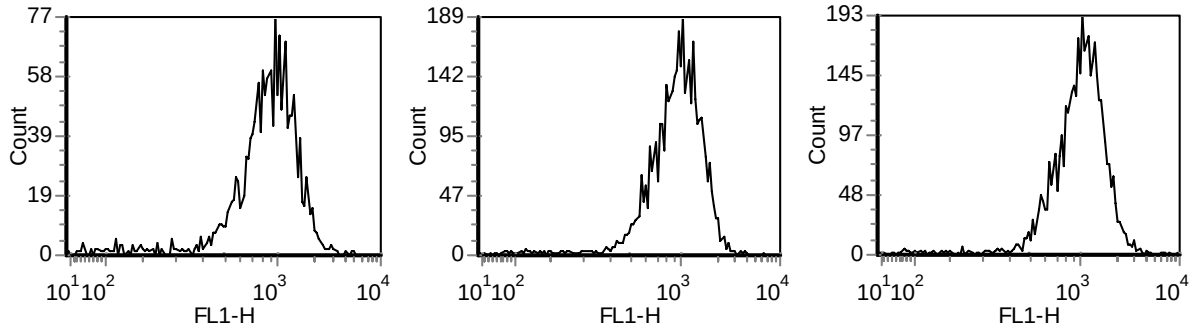

Figure 4-22. FACS results for siRNA-ACS-R9 transfected cells in 48 hours at charge ratio (+/-) of 2:1, 5:1, and 10:1 (from left to right).

This shows that at the concentration of peptide carrier used, the peptide candidates failed to promote the efficiency of siRNA transfection. The inefficient siRNA transfection is possibly due to the dissociation of siRNA-peptide complexes in the cell culture medium, or the siRNA-peptide complexes cannot be taken into the cytosol. Therefore, these peptides are deemed inefficient in promoting the efficiency of siRNA transfection within the range of experimental conditions. C166-GFP cells remained to be highly viable since their morphology observed from the scatter plots remained similar to the untreated cells (see Appendix) and they appeared to be healthy when observed under the microscope. Therefore, both the siRNA-peptide complexes and the peptide carrier are not cytotoxic within experimental conditions. In future studies, higher peptide concentrations should be used in order to verify the siRNA transfection efficiency of these peptide candidates. Unlike Lipofectamine 2000, cell viability is maintained in all cases, which indicates cytotoxicity due to peptides or siRNA peptide complexes was not observed.

Chapter 5

Conclusions

Arginine-9 and connective tissue growth factor siRNA has been used as a model for the physicochemical characterization of siRNA-peptide complexes. Further, new peptide candidates for siRNA transfection were designed. Preliminary *in vitro* investigation of peptides mediated cellular delivery of siRNA was investigated using fluorescence microscopy and flow cytometry on selected peptide sequences. The following conclusions can be drawn from the above experiments:

- The highest binding ratio for siRNA-R9 complexes was determined to be 10.3 R9 to one siRNA (corresponds to 2.2 in +/- charge ratio).
- From the CD spectra, it is suggested that the confirmation of siRNA did not undergo significant changes.
- SiRNA and R9 interact non-covalently and readily form aggregates through self association, with a maximum hydrodynamic diameter of ~1μm at siRNA saturation. Aggregation is due to the decrease in surface charge at increasing peptide concentration as demonstrated by Zeta potential measurements.
- The difference in binding ratio (UV/Vis spectra and CD is 10.3:1 and 39.1:1 from DLS) is possibly due to the difference in signal contribution between absorption and light scattering. Since the signal from absorption measurements is solely contributed by the nucleoside bases, it cannot represent the extent of the overall reaction.

- The optimal siRNA concentration for transfection is found to be 80 nM using Lipofectamine 2000.
- Selected peptide sequences, including R9, EAK 16 II, EAK 16 IV, ASC, and ASC-R9, when non-covalently bonded to eGFP siRNA, did not significantly enhance the silencing activity in C166-GFP cells.

Chapter 6

Future Work and Recommendations

In order to gain further insight in the physicochemical properties of siRNA-peptide complexes and investigate their effect on siRNA silencing, future research in this area can focus on the following:

- Complete the screening of peptide library. Since the methodology of peptide screening is developed, it should be extended to exploit the siRNA delivery capability of the remainders of the peptide library.
- A complement method of siRNA silencing detection at the protein level should be used. The focus of this research is to monitor the silencing efficiency through eGFP expression; however, complementary methods such as monitoring luciferase intensity and the concentration of a specific protein could be used as well.
- The effect of siRNA silencing should be extended to monitor at the mRNA level. Methods such as RT-PCR can be used to determine the change in mRNA concentration in various siRNA treated samples.
- Once a promising peptide candidate is identified from the library using *in vitro* methods, further experiments should be done to characterize its properties. In particular, the experiments should be directed to investigate the physicochemical properties of the siRNA-peptide complexes, as well as cytotoxicity studies using MTT/XTT assays or with fluorescent dyes in FACS.

References/Bibliography

1. S. Agrawal and R. P. Iyer, Pharmacol. & Ther., 76, 151 (1997)
2. J. Micklefield, Curr. Med. Chem., 8, 1157 (2001)
3. A. Fire, S. Q. Xu, M. K. Montgomery, S. A. Kostas, S. E. Driver, and C. C. Mello, Nature, 391, 806 (1998)
4. C. D. Novina and P. A. Sharp, Nature, 430, 161 (2004)
5. Paddison P., Caudy A., Bernstein E., Hannon G., and D. Conklin, Genes Dev., 16, 948 (2002)
6. C. Matranga, Y. Tomari, C. Shin, D. P. Bartel, and P. D. Zamore, Cell, 123, 607 (2005)
7. T. A. Rand, S. Petersen, F. Du, and X. Wang, Cell, 123, 621 (2005)
8. A. Khvorova, A. Reynolds, and S. D. Jayasena, Cell, 115, 209 (2003)
9. A. Vonarbourg, C. Passirani, P. Saulnier, and J. P. Benoit, Biomater., 27, 4356 (2006)
10. C. Passirani and J. P. Beno類, in Biomaterials for Delivery and Targeting of Proteins and Nucleic Acids edited R. I. Mahato, CRC Press, (2005), p.187
11. D. E. Owens, III and N. A. Peppas, Int. J Pharm, 307, 93 (2006)
12. A. Akinc, M. Thomas, A. M. Klibanov, and R. Langer, J. Gene Med., 7, 657 (2005)
13. H. Eliyahu, S. Siani, T. Azzam, A. J. Domb, and Y. Barenholz, Biomater., 27, 1646 (2006)
14. H. F. Liang, C. T. Chen, S. C. Chen, A. R. Kulkarni, Y. L. Chiu, M. C. Chen, and H. W. Sung, Biomater., 27, 2051 (2006)
15. M. Hashida, K. Akamatsu, M. Nishikawa, F. Yamashita, and Y. Takakura, J. Controlled Release, 62, 253 (1999)
16. Y. Matsumura and H. Maeda, Cancer Res., 46, 6387 (1986)
17. A. J. M. D'Souza and E. M. Topp, J Pharm. Sci., 93, 1962 (2004)
18. G. Oberdorster, A. Maynard, K. Donaldson, V. Castranova, J. Fitzpatrick, K. Ausman, J. Carter, B. Karn, W. Kreyling, D. Lai, S. Olin, N. Monteiro-Riviere, D. Warheit, and H. Yang, Part Fibre. Toxicol., 2, 8 (2005)

19. S. J. Douglas, S. S. Davis, and L. Illum, Crit Rev. Ther. Drug Carrier Syst., 3, 233 (1987)

20. W. N. Charman, J. Pharm. Sci., 89, 967 (2000)

21. S. K. Sahoo and V. Labhasetwar, Drug Discov. Today, 8, 1112 (2003)

22. A. Sharma and U. S. Sharma, Int. J. Pharm., 154, 123 (1997)

23. P. Sapra and T. M. Allen, Prog. Lipid Res., 42, 439 (2003)

24. D. D. Lasic and D. Papahadjopoulos, Curr. Opin. Solid St. M., 1, 392 (1996)

25. T. Gershanik and S. Benita, Eur. J. Biopharm., 50, 179 (2000)

26. E. Forssen and M. Willis, Adv. Drug Del. Rev., 29, 249 (1998)

27. S. M. Moghimi, A. C. Hunter, and J. C. Murray, Pharmacol. Rev., 53, 283 (2001)

28. S. P. Wu, A. L. Fu, Y. X. Wang, L. P. Yu, P. Y. Jia, Q. Li, G. Z. Jin, and M. J. Sun, Biochem. Biophys. Res. Commun., 346, 1 (2006)

29. A. Muratovska and M. R. Eccles, FEBS Lett., 558, 63 (2004)

30. R. S. Hotchkiss, K. W. McConnell, K. Bullok, C. G. Davis, K. C. Chang, S. J. Schwulst, J. C. Dunne, G. P. H. Dietz, M. Bahr, J. E. McDunn, I. E. Karl, T. H. Wagner, J. P. Cobb, C. M. Coopersmith, and D. Piwnica-Worms, J. Immunol., 176, 5471 (2006)

31. J. M. Bergen and S. H. Pun, MRS Bull., 30, 663 (2005)

32. M. Nichifor and G. Mocanu, ACS Sym. Ser. 934, 287, (2006)

33. D. E. Discher and A. Eisenberg, Science, 297, 967 (2002)

34. M. L. Adams, A. Lavasanifar, and G. S. Kwon, J. Pharm. Sci., 92, 1343 (2003)

35. A. Rosler, G. W. M. Vandermeulen, and H.-A. Klok, Adv. Drug Deliver. Rev., 53, 95 (2001)

36. C. Allen, D. Maysinger, and A. Eisenberg, Colloid. Surfaces B: Biointerfaces, 16, 3 (1999)

37. G. S. Kwon, M. Naito, K. kataoka, M. Yokoyama, Y. Sakurai, and T. Okano, Colloids Surf. B: Biointerfaces, 2, 429 (1994)

38. J. C. Fernandes, M. J. Tiera, and F. M. Winnik, ACS Sym. Ser. 934, 177, (2006)

39. J. M. Bergen, H. A. von Recum, T. T. Goodman, A. P. Massey, and S. H. Pun, Macromol. Biosci., 6, 506 (2006)

40. J. H. Kim and T. R. Lee, Drug Dev. Res., 67, 61 (2006)

41. I. Roy, T. Y. Ohulchanskyy, H. E. Pudavar, E. J. Bergey, A. R. Oseroff, J. Morgan, T. J. Dougherty, and P. N. Prasad, J. Am. Chem. Soc., 125, 7860 (2003)

42. P. L. Felgner, T. R. Gadek, M. Holm, R. Roman, H. W. Chan, M. Wenz, J. P. Northrop, G. M. Ringold, and M. Danielsen, Proc. Natl. Acad. Sci. USA, 84, 7413 (1987)

43. V. P. Torchilin, J. Control. Release, 73, 137 (2001)

44. K. M. Huh, S. C. Lee, Y. W. Cho, J. Lee, J. H. Jeong, and K. Park, J. Control. Release, 101, 59 (2005)

45. G. S. Kwon and T. Okano, Adv. Drug Deliv. Rev., 21, 107 (1996)

46. S. Cammas-Marion, T. Okano, and K. Kataoka, Colloid. Surfaces B: Biointerfaces, 16, 207 (1999)

47. S. C. Kim, D. W. Kim, Y. H. Shim, J. S. Bang, H. S. Oh, S. W. Kim, and M. H. Seo, J. Control. Release, 72, 191 (2001)

48. B. J. Boyd, L. M. Kaminskas, P. Karellas, G. Krippner, R. Lessene, and C. J. H. Porter, Mol. Pharm., (2006)

49. P. Kan, Z. B. Chen, C. J. Lee, and I. M. Chu, J. Control. Release, 58, 271 (1999)

50. R. Cortesi, E. Esposito, A. Maietti, E. Menagatti, and C. Nastruzzi, Int. J. Pharm., 159, 95 (1997)

51. P. Kan, Z.-B. Chen, C.-J. Lee, and I.-M. Chu, J. Control. Release, 59, 271 (1999)

52. P. J. Stevens and R. J. Lee, Anticancer Res., 23, 4927 (2003)

53. B. K. Kang, S. K. Chon, S. H. Kim, S. Y. Jeong, M. S. Kim, S. H. Cho, H. B. Lee, and G. Khang, Int. J. Pharm., 286, 147 (2004)

54. B. B. Lundberg, V. Risovic, M. Ramaswamy, and K. M. Wasan, J. Control. Release, 86, 93 (2003)

55. N. J. Meilander, G. M. Saidel, and R. V. Bellamkonda, ACS Sym. Ser.85, (2004)

56. C. Klumpp, K. Kostarelos, M. Prato, and A. Bianco, Biochim. Biophys. Acta, 1758, 404 (2006)

57. C. Fonseca, S. Simoes, and R. Gaspar, J. Control. Release, 83, 273 (2002)

58. L. Serpe, M. G. Catalano, R. Cavalli, E. Ugazio, O. Bosco, R. Canaparo, E. Muntoni, R. Frairia, M. R. Gasco, M. Eandi, and G. P. Zara, Eur. J. Pharm. Biopharm., 58, 673 (2004)

59. S.-S. Feng, L. Mu, K. Y. Win, and G. Huang, Curr. Med. Chem., 11, 413 (2004)

60. R. Savic, L. Luo, A. Eisenberg, and D. Maysinger, Science, 300, 615 (2003)

61. L. Mu and S. S. Feng, J. Control. Release, 86, 33 (2003)

62. Z. Xu, W. Gu, J. Huang, H. Sui, Z. Zhou, Y. Yang, Z. Yan, and Y. Li, Int. J. Pharm., 288, 361 (2005)

63. J. W. Lee, J. Y. Lu, P. S. Low, and P. L. Fuchs, Bioorg. Med. Chem., 10, 2397 (2002)

64. V. Guillemard and H. U. Saragovi, Cancer Res., 61, 694 (2001)

65. A. Safavy, J. A. Bonner, H. W. Waksal, D. J. Buchsbaum, G. Y. Gillespie, M. B. Khazaeli, R. Arani, D. Chen, M. Carpenter, and K. P. Raisch, Bioconjugate Chem., 14, 302 (2003)

66. C. Zhang, N. Tang, X. Liu, W. Liang, W. Xu, and V. P. Torchilin, J. Controlled Release, 112, 229 (2006)

67. D. Bhadra, S. Bhadra, and N. Jain, Pharm. Res., 23, 623 (2006)

68. J. Thongborisute, A. Tsuruta, Y. Kawabata, and H. Takeuchi, J. Drug Targeting, 14, 147 (2006)

69. N. Dinauer, S. Balthasar, C. Weber, J. Kreuter, K. Langer, and H. von Briesen, Biomater., 26, 5898 (2005)

70. C. R. Dass and P. F. Choong, Cancer Cell Int., 6, 17 (2006)

71. P. Singh, M. J. Gonzalez, and M. Manchester, Drug Dev. Res., 67, 23 (2006)

72. N. K. Green, C. W. Herbert, S. J. Hale, A. B. Hale, V. Mautner, R. Harkins, T. Hermiston, K. Ulbrich, K. D. Fisher, and L. W. Seymour, Gene Ther., 11, 1256 (2004)

73. S. Kochanek, Gene Funct. Disease, 2, 122 (2001)

74. T. Lian and R. J. Y. Ho, J. Pharm. Sci., 90, 667 (2001)

75. A. Chonn and P. R. Cullis, Curr. Opin. Biotechnol., 6, 698 (1995)

76. K. A. Edwards and A. J. Baeumner, Talanta, 68, 1432 (2006)

77. C. R. Dass and P. F. M. Choong, Journal of Controlled Release, 113, 155 (2006)

78. C. M. Lee, T. Tanaka, T. Murai, M. Kondo, J. Kimura, W. Su, T. Kitagawa, T. Ito, H. Matsuda, and M. Miyasaka, Cancer Res., 62, 4282 (2002)

79. A. Sharma and U. S. Sharma, Int. J. Pharm., 154, 123 (1997)

80. Molineux G., Cancer Treat Rev., Suppl A: 13, 6 (2002)

81. M. Whitmore, S. Li, and L. Huang, Gene Ther., 6, 1867 (1999)

82. R. Ramesh, T. Saeki, N. S. Templeton, L. Ji, L. C. Stephens, I. Ito, D. R. Wilson, Z. Wu, C. D. Branch, J. D. Minna, and J. A. Roth, Mol. Ther., 3, 337 (2001)

83. J. Yano, K. Hirabayashi, S. Nakagawa, T. Yamaguchi, M. Nogawa, I. Kashimori, H. Naito, H. Kitagawa, K. Ishiyama, T. Ohgi, and T. Irimura, Clin. Cancer Res., 10, 7721 (2004)

84. W. M. Bertling, M. Gareis, V. Paspaleeva, A. Zimmer, J. Kreuter, E. Nurnberg, and P. Harrer, Biotechnol. Appl. Biochem., 13, 390 (1991)

85. G. S. Kwon and M. L. Forrest, Drug Dev. Res., 67, 15 (2006)

86. T. Ooya and K. Park, in Biomaterials for Delivery and Targeting of Proteins and Nucleic Acids edited R. I. Mahato, CRC Press, (2005),

87. H. Arima, in Non-viral Gene Therapy: Gene Design and Delivery edited K. Taira, K. Kataoka, and T. Niidome, Springer, (2005), p.75

88. F. Fuertges and A. Abuchowski, J. Controlled Release,139 (1990)

89. K. S. Raja, Q. Wang, M. J. Gonzalez, M. Manchester, J. E. Johnson, and M. G. Finn, Biomacromol., 4, 472 (2003)

90. I. K. Oh, H. Mok, and T. G. Park, Bioconjugate Chem., 17, 721 (2006)

91. K. N. Barton, H. Stricker, A. Kolozsvary, R. Kohl, G. Heisey, T. N. Nagaraja, G. Zhu, M. Lu, J. H. Kim, S. O. Freytag, and S. L. Brown, J. of Urology, 175, 1921 (2006)

92. S. Abes, D. Williams, P. Prevot, A. Thierry, M. J. Gait, and B. Lebleu, J. Controlled Release, 110, 595 (2006)

93. M. Mannisto, S. Vanderkerken, V. Toncheva, M. Elomaa, M. Ruponen, E. Schacht, and A. Urtti, J. Controlled Release, 83, 169 (2002)

94. H. Lee, J. H. Jeong, and T. G. Park, J. Controlled Release, 79, 283 (2002)

95. S. Sundaram, S. Viriyayuthakorn, and C. M. Roth, Biomacromol., 6, 2961 (2005)

96. E. M. Barnett, B. Elangovan, K. E. Bullok, and D. Piwnica-Worms, Investigative Ophthalmol. Visual Sci., 47, 2589 (2006)

97. T. Niidome, K. Takaji, M. Urakawa, N. Ohmori, A. Wada, T. Hirayama, and H. Aoyagi, Bioconjugate Chem., 10, 773 (1999)

98. Q. L. Lu, G. Bou-Gharios, and T. A. Partridge, Gene Ther., 10, 131 (2003)

99. M. A. Lindsay, Curr. Opin. Pharmacol., 2, 587 (2002)

100. P. M. Fischer, E. Krausz, and D. P. Lane, Bioconjugate Chem., 12, 825 (2001)

101. P. A. Wender, D. J. Mitchell, K. Pattabiraman, E. T. Pelkey, L. Steinman, and J. B. Rothbard, Proc. Natl. Acad. Sci. USA, 97, 13003 (2000)

102. T. B. Potocky, A. K. Menon, and S. H. Gellman, J. Biol. Chem., 278, 50188 (2003)

103. P. A. Wender, J. B. Rothbard, T. C. Jessop, E. L. Kreider, and B. L. Wylie, J. Am. Chem. Soc., 124, 13382 (2002)

104. J. E. Summerton, Ann. N. Y. Acad. Sci., 1058, 62 (2005)

105. S. Deshayes, S. Gerbal-Chaloin, M. C. Morris, G. drian-Herrada, P. Charnet, G. Divita, and F. Heitz, Biochim. Biophys. Acta, 1667, 141 (2004)

106. L. A. Kueltzo, N. Normand, P. O'Hare, and C. R. Middaugh, J. Biol. Chem., 275, 33213 (2000)

107. L. Chaloin, P. Vidal, A. Heitz, N. Van Mau, J. Mery, G. Divita, and F. Heitz, Biochem., 36, 11179 (1997)

108. S. Deshayes, T. Plenat, G. drian-Herrada, G. Divita, C. LeGrimellec, and F. Heitz, Biochem., 43, 7698 (2004)

109. B. J. Calnan, S. Biancalana, D. Hudson, and A. D. Frankel, Genes Dev., 5, 201 (1991)

110. Z. Wei, C. H. Tung, T. Zhu, W. A. Dickerhof, K. J. Breslauer, D. E. Georgopoulos, M. J. Leibowitz, and S. Stein, Nucleic Acids Res., 24, 655 (1996)

111. S. D. Conner and S. L. Schmid, Nat., 422, 37 (2003)

112. M. E. Herbig, K. Weller, U. Krauss, A. G. Beck-Sickinger, H. P. Merkle, and O. Zerbe, Biophys. J ., 89, 4056 (2005)

113. S. Futaki, T. Suzuki, W. Ohashi, T. Yagami, S. Tanaka, K. Ueda, and Y. Sugiura, J. Biol. Chem., 276, 5836 (2001)

114. T. Letoha, S. Gaal, C. Somlai, Z. Venkei, H. Glavinas, E. Kusz, E. Duda, A. Czajlik, F. Petak, and B. Penke, J. Pep. Sci., 11, 805 (2005)

115. C. Rudolph, C. Plank, J. Lausier, U. Schillinger, R. H. Muller, and J. Rosenecker, J. Biol. Chem., 278, 11411 (2003)

116. J. Fernandez-Carneado, M. J. Kogan, S. Pujals, and E. Giralt, Biopoly., 76, 196 (2003)

117. M. Silhol, M. Tyagi, M. Giacca, B. Lebleu, and E. Vives, Eur. J. Biochem., 269, 494 (2002)

118. M. Keller, T. Tagawa, M. Preuss, and A. D. Miller, Biochem., 41, 652 (2002)

119. M. Weber, I. Andreou, and N. Bezay, Eur. Pat. Appl., C12N15/11; C12N15/11, (2006)

120. M. Murata, S. Kagiwada, S. Takahashi, and S. Ohnishi, J. Biol. Chem., 266, 14353 (1991)

121. P. Midoux, R. Mayer, and M. Monsigny, Biochim. Biophys. Acta, 1239, 249 (1995)

122. I. Freulon, M. Monsigny, P. Midoux, and R. Mayer, Bioscience Reports, 20, 383 (2000)

123. P. Midoux, A. Kichler, V. Boutin, J. C. Maurizot, and M. Monsigny, Bioconjugate Chem., 9, 260 (1998)

124. J. D. Lear and W. F. DeGrado, J. Biol. Chem., 262, 6500 (1987)

125. J. A. Hughes, A. I. Aronsohn, A. V. Avrutskaya, and R. L. Juliano, Pharm. Res., 13, 404 (2006)

126. S. Oess and E. Hildt, Gene Ther., 7, 750 (2000)

127. U. Krauss, M. Muller, M. Stahl, and A. G. Beck-Sickinger, Bioorg. Med. Chem. Lett., 14, 51 (2004)

128. C. Plank, B. Oberhauser, K. Mechtler, C. Koch, and E. Wagner, J. Biol. Chem., 269, 12918 (1994)

129. Y. Z. Lin, S. Y. Yao, R. A. Veach, T. R. Torgerson, and J. Hawiger, J. Biol. Chem., 270, 14255 (1995)

130. S. Dokka, D. Toledo-Velasquez, X. Shi, L. Wang, and Y. Rojanasakul, Pharmaceutical Research, 14, 1759 (1997)

131. H. Noguchi, H. Kaneto, G. C. Weir, and S. Bonner-Weir, Diabetes, 52, 1732 (2003)

132. G. Dom, C. Shaw-Jackson, C. Matis, O. Bouffioux, J. J. Picard, A. Prochiantz, M. P. Mingeot-Leclercq, R. Brasseur, and R. Rezsohazy, Nucleic Acids Res., 31, 556 (2003)

133. P. Lundberg, M. Magzoub, M. Lindberg, M. Hallbrink, J. Jarvet, L. E. G. Eriksson, U. Langel, and A. Graslund, Biochem. Biophys. Res. Commun., 299, 85 (2002)

134. A. Elmquist, M. Lindgren, T. Bartfai, and U. Langel, Exp. Cell Res., 269, 237 (2001)

135. C. Rousselle, P. Clair, J. M. Lefauconnier, M. Kaczorek, J. M. Scherrmann, and J. Temsamani, Mol. Pharmacol., 57, 679 (2000)

136. S. Li, S. P. Wu, M. Whitmore, E. J. Loeffert, L. Wang, S. C. Watkins, B. R. Pitt, and L. Huang, Am. J. Physiol., 276, L796 (1999)

137. E. P. Loret, E. Vives, P. S. Ho, H. Rochat, J. Van Rietschoten, and W. C. Johnson, Jr., Biochem., 30, 6013 (1991)

138. S. Fawell, J. Seery, Y. Daikh, C. Moore, L. L. Chen, B. Pepinsky, and J. Barsoum, Proc. Natl. Acad. Sci. USA, 91, 664 (1994)

139. A. Astriab-Fisher, D. S. Sergueev, M. Fisher, B. Ramsay Shaw, and R. L. Juliano, Biochem. Pharm., 60, 83 (2000)

140. K. Melikov and L. Chernomordik, Cell. Mol. Life Sci., 62, 2739 (2005)

141. J. P. Richard, K. Melikov, H. Brooks, P. Prevot, B. Lebleu, and L. V. Chernomordik, J. Biol. Chem., 280, 15300 (2005)

142. J. S. Wadia, R. V. Stan, and S. F. Dowdy, Nat. Med., 10, 310 (2004)

143. D. Derossi, A. H. Joliot, G. Chassaing, and A. Prochiantz, J. Biol. Chem., 269, 10444 (1994)

144. G. Drin, M. Mazel, P. Clair, D. Mathieu, M. Kaczorek, and J. Temsamani, Eur. J Biochem., 268, 1304 (2001)

145. E. Barany-Wallje, S. Keller, S. Serowy, S. Geibel, P. Pohl, M. Bienert, and M. Dathe, Biophys. J ., 89, 2513 (2005)

146. G. Drin, S. Cottin, E. Blanc, A. R. Rees, and J. Temsamani, J. Biol. Chem., 278, 31192 (2003)

147. D. J. Mitchell, L. Steinman, D. T. Kim, C. G. Fathman, and J. B. Rothbard, J. Pep. Res., 56, 318 (2000)

148. R. C. Adami and K. G. Rice, J Pharm. Sci., 88, 739 (1999)

149. D. L. McKenzie, K. Y. Kwok, and K. G. Rice, J. Biol. Chem., 275, 9970 (2000)

150. R. I. Mahato, J. Drug Targeting, 7, 249 (1997)

151. M. C. Morris, L. Chaloin, F. Heitz, and G. Divita, Curr. Opin. Biotechnol., 11, 461 (2000)

152. J. Gariepy and K. Kawamura, Trends Biotechnol., 19, 21 (2000)

153. W. Yu, K. F. Pirollo, B. Yu, A. Rait, L. Xiang, W. Huang, Q. Zhou, G. Ertem, and E. H. Chang, Nucleic Acids Res., 16, 32 (2004)

154. S. Futaki, T. Suzuki, W. Ohashi, T. Yagami, S. Tanaka, K. Ueda, and Y. Sugiura, J. Biol. Chem., 276, 5836 (2001)

155. J. B. Rothbard, E. Kreider, C. L. VanDeusen, L. Wright, B. L. Wylie, and P. A. Wender, J. Med. Chem., 45, 3612 (2002)

156. L. Chaloin, P. Vidal, P. Lory, J. Mery, N. Lautredou, G. Divita, and F. Heitz, Biochem. Biophys. Res. Commun., 243, 601 (1998)

157. F. Heitz, C. Le Grimellec, J. Mery, G. Divita, and N. Van Mau,Proc. 2nd Int. 7th Am. Pep. Sym.,830 (2001)

158. N. Van Mau, V. Vie, G. Divita, C. Le Grimellec, and F. Heitz,Proc. Eu. Pep. Sym, 26th,65 (2001)

159. L. Chaloin, M. C. Morris, N. Van Mau, J. Mery, G. Divita, and F. Heitz, Curr. Top. Peptide Protein Res., 3, 153 (1999)

160. F. Simeoni, M. C. Morris, F. Heitz, and G. Divita, Nucleic Acids Res., 31, 2717 (2003)

161. L. Chaloin, E. De, P. Charnet, G. Molle, and F. Heitz, Biochim. Biophys. Acta, 1375, 52 (1998)

162. Parente RA, Nir S, and Szoka FC Jr., J. Biol. Chem., 263, 4724 (1988)

163. Gottschalk S, Sparrow JT, Hauer J, Mims MP, Leland FE, Woo SL, and Smith LC., Gene Ther., 3, 48 (1996)

164. J. Oehlke, A. Scheller, B. Wiesner, E. Krause, M. Beyermann, E. Klauschenz, M. Melzig, and M. Bienert, Biochim. Biophys. Acta, 1414, 127 (1998)

165. X. Y. Liu, S. L. Timmons, Y. Z. Lin, and J. Hawiger, Proc. Natl. Acad. Sci. USA, 93, 11819 (1996)

166. M. Peitz, K. Pfannkuche, K. Rajewsky, and F. Edenhofer, Proc. Natl. Acad. Sci. USA, 99, 4489 (2002)

167. M. C. Morris, J. Depollier, J. Mery, F. Heitz, and G. Divita, Nat. Biotechnol., 19, 1173 (2001)

168. E. D? L. Chaloin, A. Heitz, J. M閞y, G. Molle, and F. Heitz, J. Pep. Sci., 7, 41 (2001)

169. M. Pooga, M. Hallbrink, M. Zorko, and U. Langel, FASEB J., 12, 67 (1998)

170. N. Ohmori, T. Niidome, T. Kiyota, S. Lee, G. Sugihara, A. Wada, T. Hirayama, and H. Aoyagi, Biochem. Biophys. Res. Commun.,245 (1998)

171. C. Keyes-Baig, J. Duhamel, S. Y. Fung, J. Bezaire, and P. Chen, J. Am. Chem. Soc., 126, 7522 (2004)

172. T. Niidome, M. Wakamatsu, A. Wada, T. Hirayama, and H. Aoyagi, J. Pep. Sci., 6, 271 (2000)

173. W. Li, F. Nicol, and F. C. Szoka Jr., Adv. Drug Deliv. Rev., 56, 967 (2004)

174. T. B. Wyman, F. Nicol, O. Zelphati, P. V. Scaria, C. Plank, and F. C. Szoka Jr., Biochem., 36, 3008 (1997)

175. J. G. Michael, Cell. Mol. Life Sci., 60, 844 (2003)

176. M. K. Ghosh, K. Ghosh, O. Dahl, and J. S. Cohen, Nucleic Acids Res., 21, 5761 (1993)

177. V. A. Bloomfield, Crothers, D. M., and Tinoco, I., Nucleic acids : structures, properties, and functions, University Science Books, Sausalito, Calif., (2000)

178. W. Bujalowski and T. M. Lohman, Biochem., 26, 3099 (1987)

179. M. Wang, M. Law, J. Duhamel, and P. Chen, Biophysical Journal, 93, 2477 (2007)

180. K. G. Wagner, Eur. J. Biochem., 10, 261 (1969)

181. H. Lodish, Berk, A., Zipursky, S. L., Matsudaira, P., Baltimore, D., and Darnell, J. E., Molecular Cell Biology, W. H. Freeman & Co., New York, (1999)

182. R. J. Hunter, Zeta potential in colloid science: principles and applications, Academic Press, London, (1981)

183. S. Futaki, T. Suzuki, W. Ohashi, T. Yagami, S. Tanaka, K. Ueda, and Y. Sugiura, J. Biol. Chem., 276, 5836 (2001)

184. D. Kneller. 1996. NNPREDICT Protein Secondary Structure Prediction [Webpage] <http://alexander.compbio.ucsf.edu/ñomi/nnpredict.html>

185. S. P. Persengiev, X. I. A. O. ZHU, and M. R. Green, RNA, 10, 12 (2004)

186. K. Taira, Kataoka, K., and Niidome, T., Non-viral gene therapy : gene design and delivery, Springer, New York, (2005)

187. C. Foged, H. M. Nielsen, and Frokjaer.S, Int. J. Pharm., 331, 160 (2007)

188. A. Muratovska and M. R. Eccles, FEBS Lett., 558, 63 (2004)

Appendix A

Equilibrium Binding Isotherm Determination

SiRNA has 42 negative charges per molecule and R9 has 9 positive charges per molecule. Therefore, it is expected that siRNA molecules can interact with multiple R9 molecules through columbic forces. (Figure A1a) Furthermore, two hydrogen atoms from the guanidino group of each arginine can hydrogen bond with the oxygen and nitrogen at the purine base of guanine within the major groove of the GC base pair. (Figure A1b) It is anticipated that electrostatic interaction and hydrogen bonding are the major driving forces for the interaction between siRNA and R9. (This is verified by salt dissociation experiment.) In other words, siRNA is present as a macromolecule that can interact with multiple R9 ligands in a non-sequence-specific and non-covalent manner. In order to characterize the complexation reaction quantitatively, it is essential to obtain an accurate equilibrium binding isotherm.

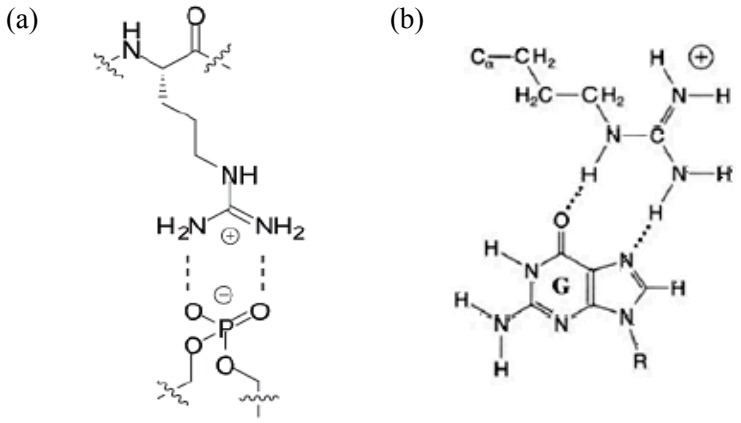

Figure A1 (a) Columbic interactions between positively charged guanidino group of arginine and negatively charged phosphated group of siRNA. (b) Hydrogen bonds between guanidino group of arginine and guanine of siRNA in the major groove. [1]

Hypochromic effect of siRNA absorbance at 260 nm is observed upon its interaction with R9. By increasing peptide concentrations at a fixed siRNA concentration, three titration curves expressed in terms of hypochromicity were obtained at siRNA concentrations of 1.5 uM, 3.0 uM, and 4.5 uM.

According to thermodynamics, the interaction between siRNA and R9 would establish equilibrium between the free siRNA sites, free peptide and bound siRNA sites. A siRNA molecule consists of 21 base pairs and it forms a double helical structure with two 3' overhangs. It can be viewed as a linear lattice with N repeating units. It is assumed that each R9 covers the same number of phosphate groups (*n*) on a siRNA. Since hypochromicity is observed upon R9-siRNA complexation, it follows that the extinction coefficients of the complexes is lower than that of the free siRNA. If there are *r* binding state and each binding

state *i* has a distinct extinction coefficient, then according to the Beer's Law, the optical density of a R9-siRNA complex solution, OD_{obs}, can be expressed as

$$OD_{obs} = \varepsilon_f \mathrm{lM}_f + \sum_{i=1}^{r} \varepsilon_{bi} \mathrm{lM}_{bi} \quad (1)$$

where respectively ε_f and M_f are the extinction coefficient and molar concentrations of phosphate groups of unbound siRNA, ε_{bi} and M_{bi} are extinction coefficient and molar concentrations of phosphate groups of bound siRNA in state *i*, *l* is the light path length of cuvette.

On the other hand, the mass conservation equation between M_f, M_b and M_t, which represents the free, bound and total siRNA phosphate concentrations, is

$$M_t = M_f + \sum_i M_{bi} \quad (2)$$

Furthermore, the binding density of the siRNA at state *i*, ν_i, is defined as the number of peptide molecules bound per siRNA phosphate group

$$\nu_i = \frac{L_{bi}}{M_t} = \frac{1/n M_{bi}}{M_t} \quad (3)$$

where, L_{bi} is the bound peptide concentration for complexes in stage *i*.

Substitute Equations 2 and 3 into Equation 1,

$$OD_{obs} = \varepsilon_f \mathrm{lM}_t + nlM_t \sum_{i=1}^{r} \nu_i (\varepsilon_{bi} - \varepsilon_f) \tag{4}$$

Given that the absorbance of the free siRNA, OD_i is simply $\varepsilon_f l M_t$, the relative change in absorbance expressed in terms of hypochromicity (H), can be related to the extent of binding by

$$H = \frac{OD_i - OD_{obs}}{OD_i} = n \sum \nu_i \Delta\varepsilon_{ri} \tag{5}$$

where $\Delta\varepsilon_{ri}$ is the relative change in extinction coefficient at state *i*. Therefore, the experimentally observed hyprochromicity is only a function of binding density ν_i. Further, to show that the fraction of siRNA bound is only a function of the free peptide concentration L_f, consider the equilibrium between the free siRNA sites, free peptide and bound siRNA sites:

$$siRNA\ \ free\ \ sites + \frac{1}{n} Peptide \underset{}{\overset{K}{\rightleftharpoons}} siRNA\ occupied\ \ sites$$

where K represents the equilibrium binding constant, which is related to the equilibrium quantities through

$$K = \frac{M_b}{L_f^{1/n} \cdot M_f} \tag{6}$$

where M_b is the sum siRNA phosphate concentrations for all binding states, and it is equal to ΣM_{bi}.

Substitute reaction site conservation equation (Equation 2) into Equation 6 and express in terms of binding density (Equation 3), one obtains

$$K = \frac{1}{L_f^{1/n} \cdot \left(\frac{1}{\sum_i \nu_i n} - 1 \right)} \tag{7}$$

From Equation 7, it is shown that the overall binding density is only a function of free peptide concentration. Equation 5 illustrated that the experimental observed hypochromicity is a unique function of the binding density, whereas Equation 7 demonstrated that the binding density is a unique function of the free peptide concentration. In other words, hypochromicity is also a unique function to the free peptide concentration, related through the binding density. As a result, the free peptide concentration and binding density will be constant for a number of different combinations of total peptide and total siRNA concentrations (L_{t_x}, M_{t_x})

taken at a constant hypochromicity value, given that it follows the peptide mass conservation equation

$$L_t = L_f + M_t \sum_i \nu_i \tag{8}$$

When two siRNA titration curves were obtained, the binding density and free peptide concentration at each hypochromicity can be obtained with a set of two simultaneous equations of Equation 8. When three or more siRNA titration curves were obtained, the above quantities can be obtained through linear regression of Equation 8. Through the use of the above analysis technique by Lohman and Bujalowski [2], a model independent binding isotherm can be obtained without applying any assumptions.

Fitted values of total peptide concentration are calculated at chosen hypochromicity values for siRNA concentrations of 1.5uM, 3.0uM, and 4.5uM. Linear regression is performed according to Equation 8 to obtain binding densities and free peptide concentrations at each hypochromicity value. However, the calculated free peptide concentration is negative in the experimental relevant range, which means that this analysis is not applicable to this experimental system. Figure A 2 is a plot of binding densities versus free peptide concentrations. Since the signal contributed by the siRNA is solely from the nucleoside bases and it is possible that the decrease in absorbance cannot reflect the interactions that undergo other modes of interaction, such as electrostatic interaction with the phosphate backbone and

charge dipole interaction with the sugar ring. Furthermore, aggregation of complexes also affects the applicability of this method.

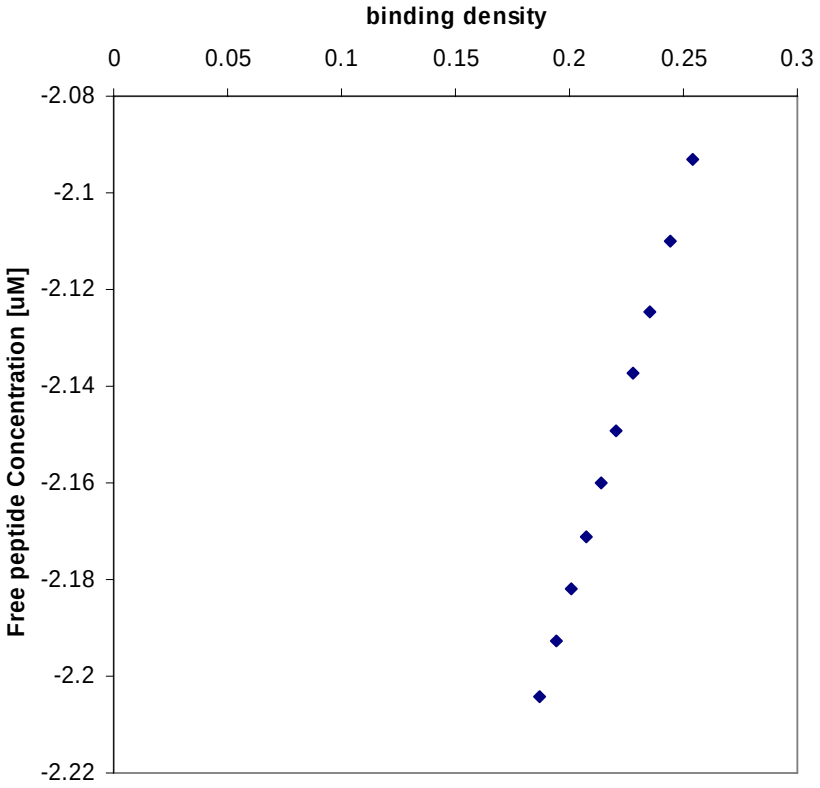

Figure A 2. Calculated binding isotherm for CTGF siRNA-R9 complexes. Following the analysis developed by Bujalowski and Lohman, the calculated free peptide concentrations were infeasible.

References

1. J. B. Rothbard, E. Kreider, C. L. VanDeusen, L. Wright, B. L. Wylie, and P. A. Wender, J. Med. Chem., 45, 3612 (2002)

2. T. M. Lohman and W. Bujalowski, Methods Enzymol. edited T. S. Robert, Academic Press, 208, 258, (1991)

Appendix B

Auxiliary Data/Graphs

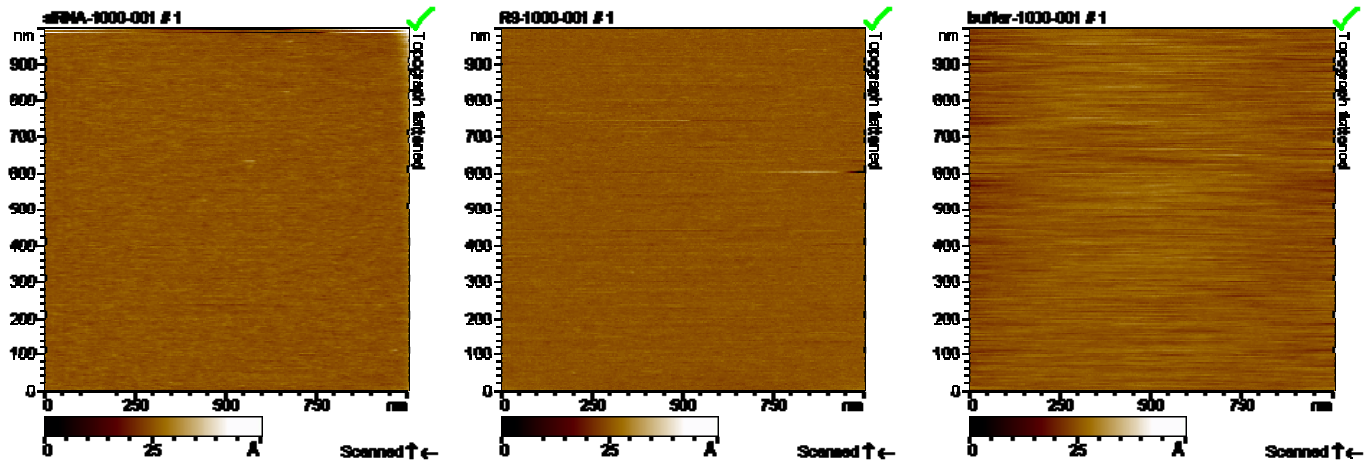

Figure A 3. AFM Images for the experimental controls: siRNA at 1000 nM (left), R9 at 100 uM (middle), and HEPES buffer only (right).

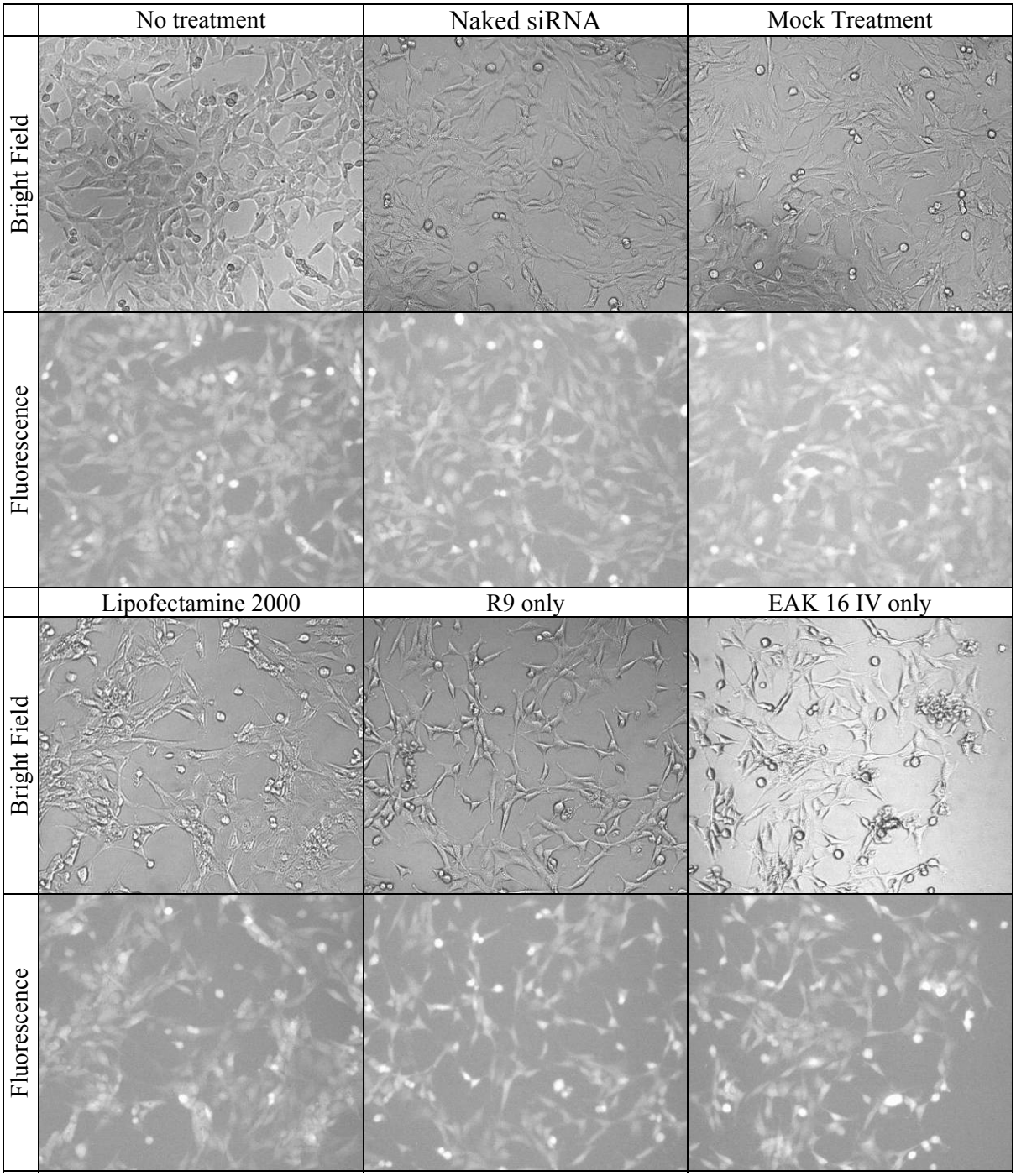

Figure A 4. Controls for the C166-GFP transfection experiments, taken at 24 hours after eGFP siRNA transfection. Negative and positive controls are cells with no treatment and cells treated with Lipofectamine 2000-siRNA complexes, respectively. Normal controls include cells treated with naked siRNA, mock treatment, and peptide carrier only. Fluorescence and the corresponding bright field images are shown.

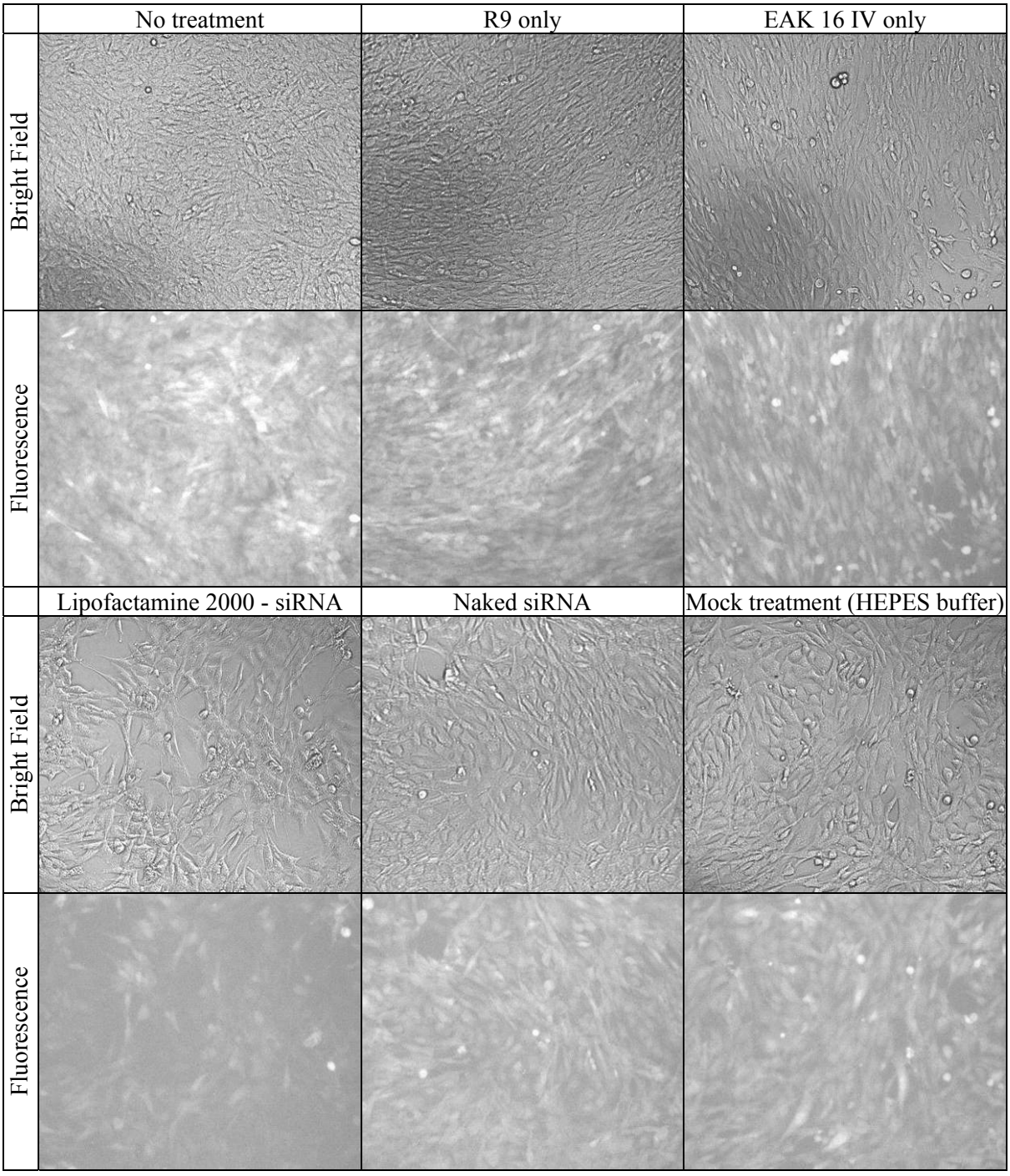

Figure A 5**.** Controls for the C166-GFP transfection experiments, taken at 48 hours after eGFP siRNA transfection. Negative and positive controls are cells with no treatment and cells treated with Lipofectamine 2000-siRNA complexes, respectively. Normal controls include cells treated with naked siRNA, mock treatment, and peptide carrier only. Fluorescence and the corresponding bright field images are shown.

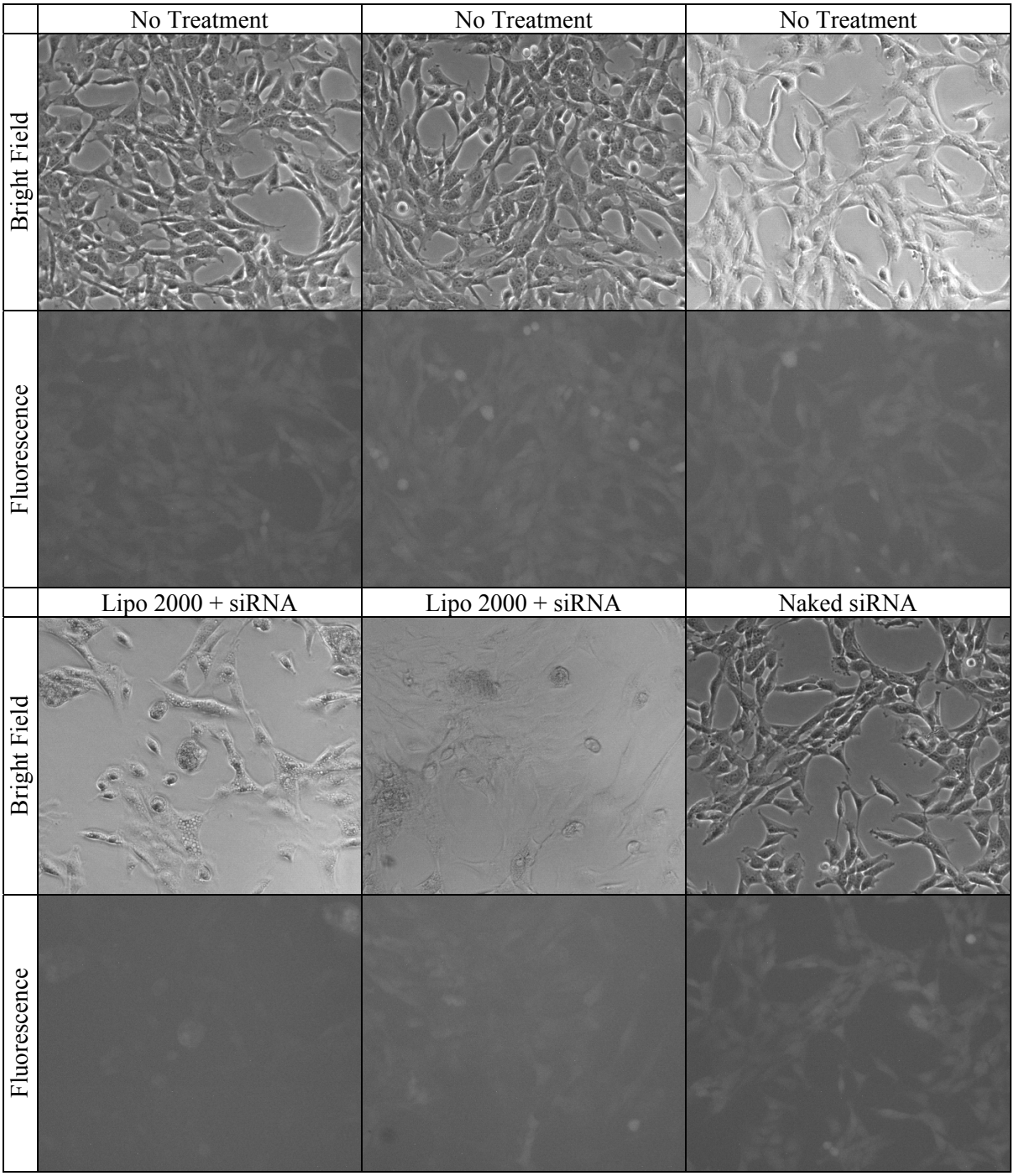

Figure A 6**.** Controls for the C166-GFP transfection experiments, taken at 48 hours after eGFP siRNA transfection. Negative and positive controls are cells with no treatment and cells treated with Lipofectamine 2000-siRNA complexes, respectively. Normal controls include cells treated with naked siRNA. Fluorescence and the corresponding bright field images are shown.

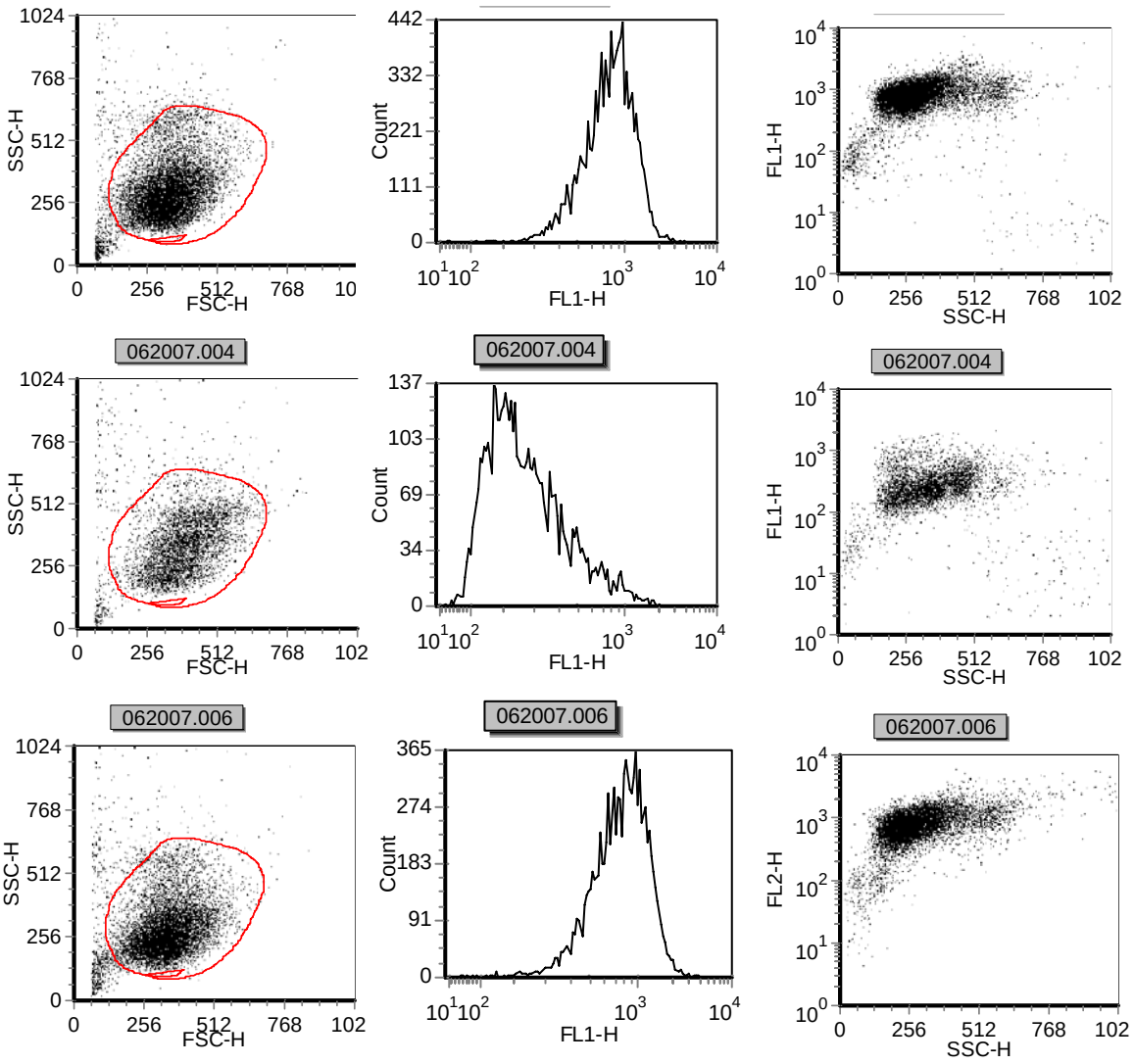

Figure A 7. FACS results for the negative (Top), positive (Middle), and normal (Bottom) controls shown in three plots: forward versus side scatter (left column), GFP intensity plots (middle column), and GFP fluorescence versus side scatter (right column). The gate applied for the analysis of result is shown in the forward scatter versus side scatter plot.

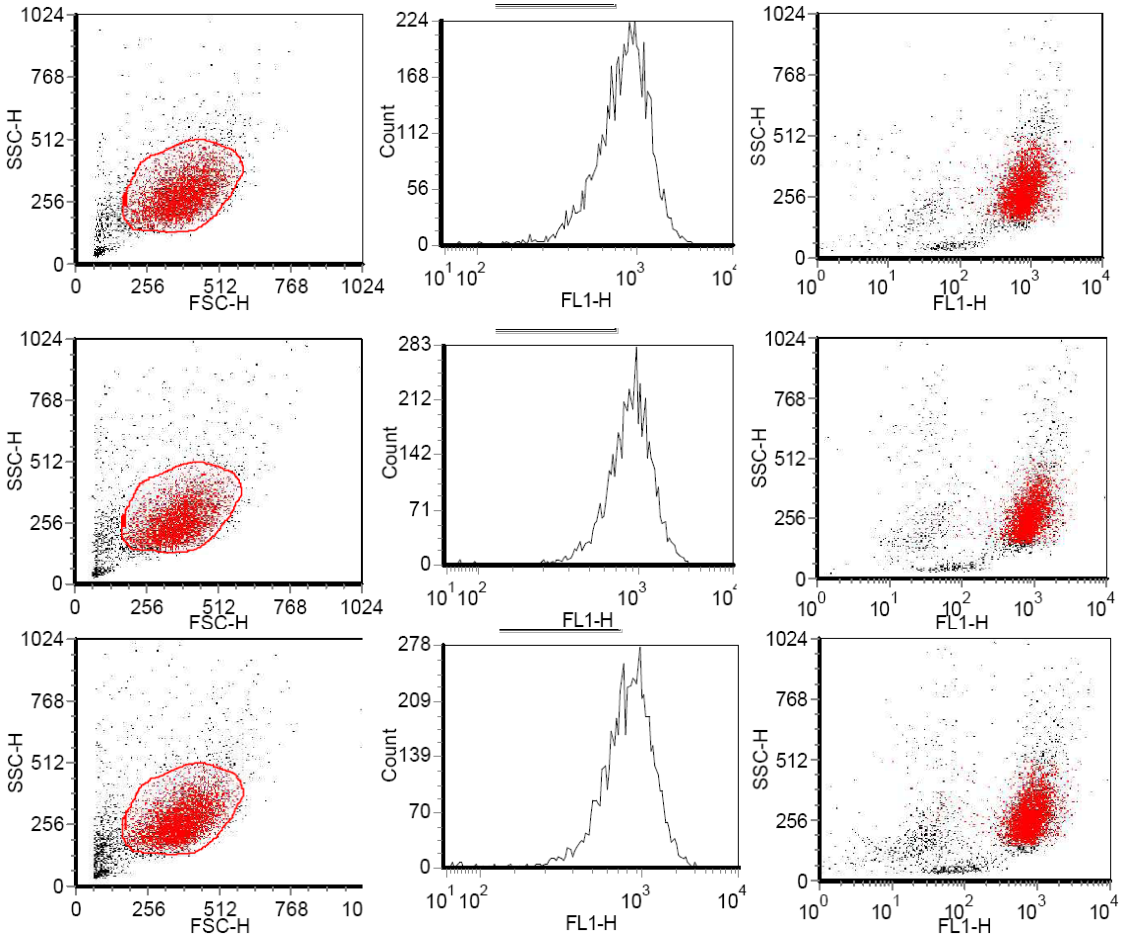

Figure A 8. FACS results in terms of scatter plot (left), histogram of fluorescence (middle), and side scatter versus fluorescence intensity (right), for siRNA-R9 transfected cells in 24 hours at charge ratio (+/-) of 2:1 (Top), 5:1 (Middle), and 10:1 (Bottom).

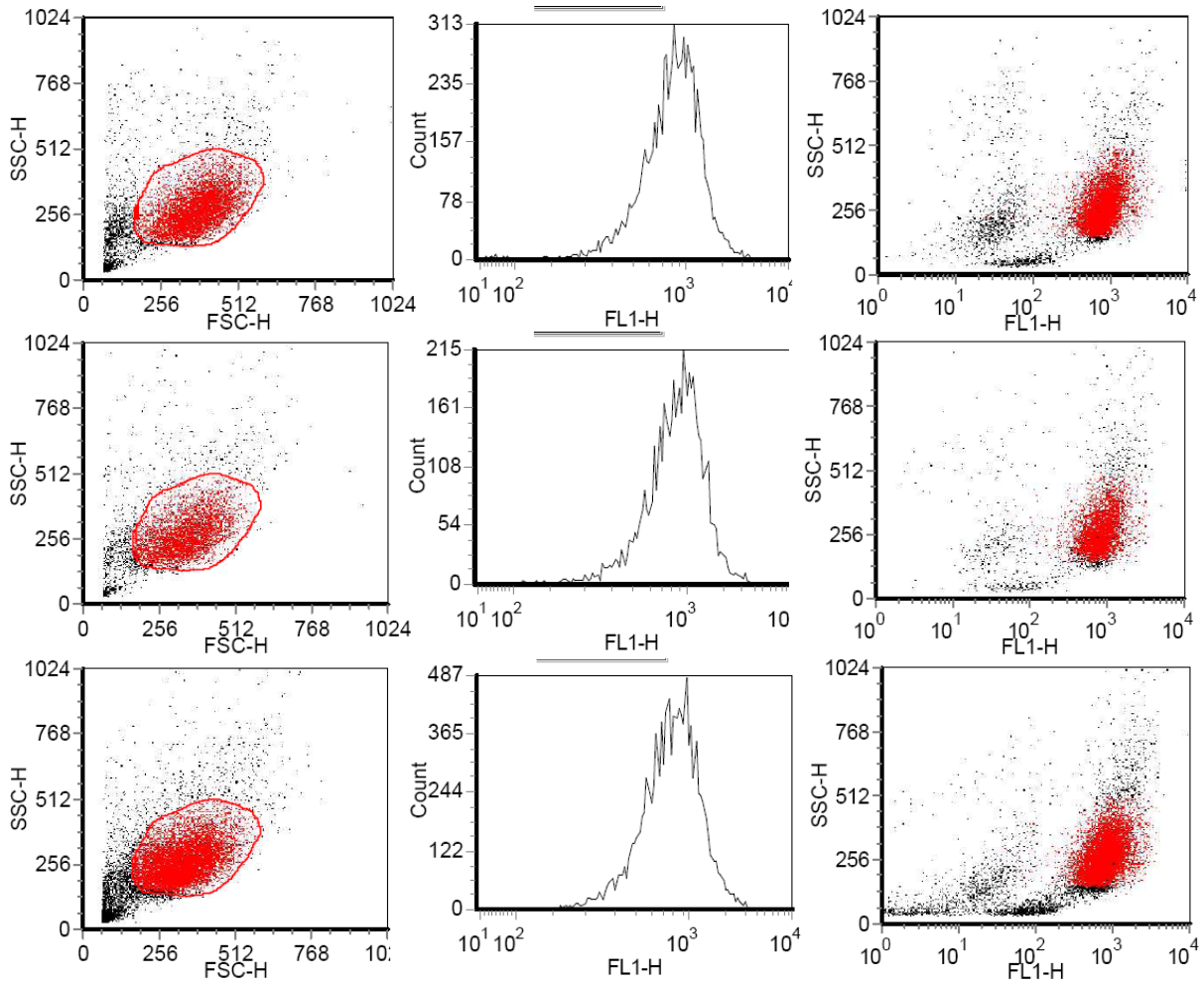

Figure A 9. FACS results for siRNA-EAK 16 IV transfected cells in 24 hours at charge ratio (+/-) of 2:1 (Top), 5:1 (Middle), and 10:1 (Bottom).

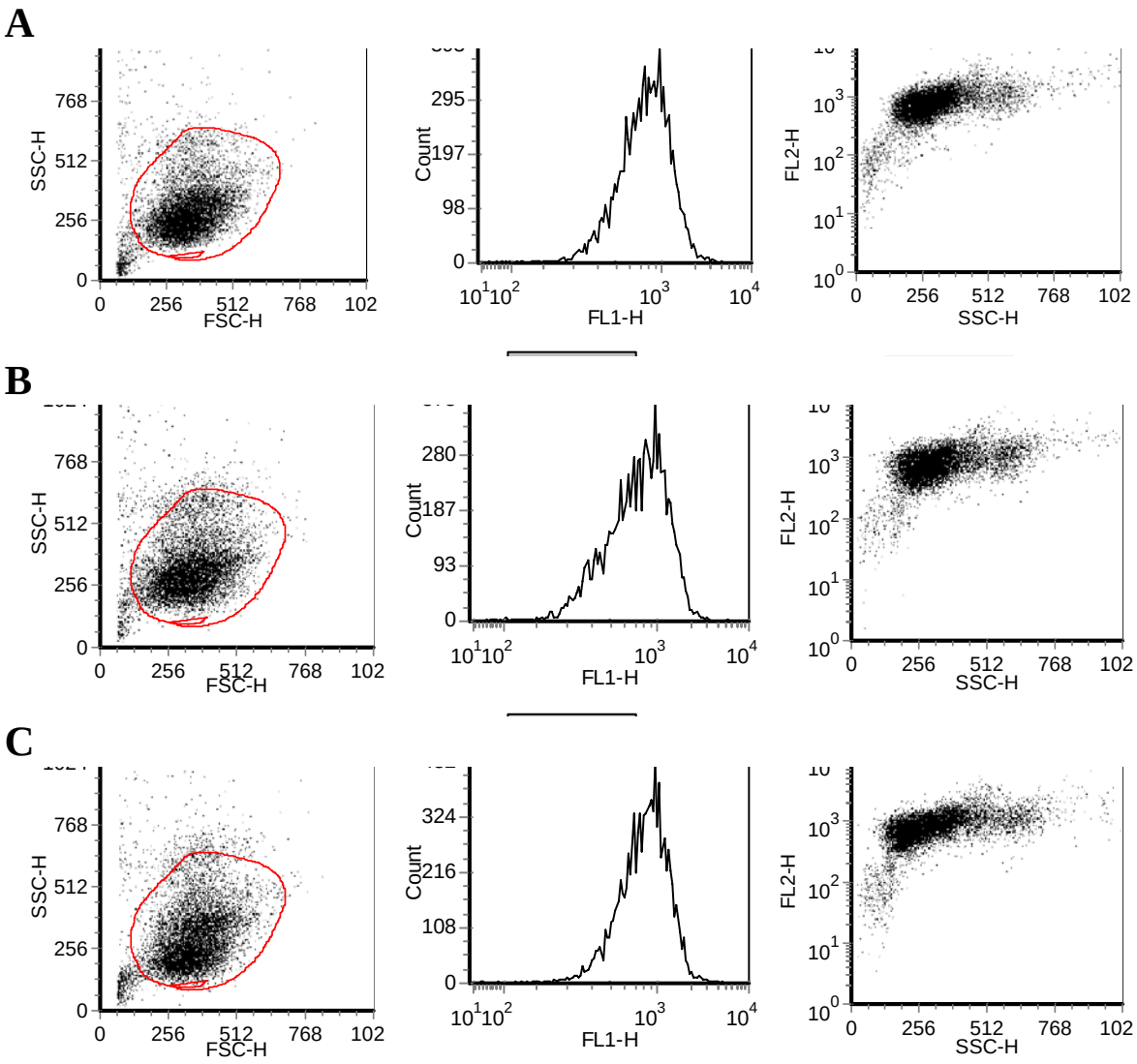

Figure A 10. FACS results for siRNA-ACS-R9 transfected cells in 24 hours at charge ratio (+/-) of 2:1 (Top), 5:1 (Middle), and 10:1 (Bottom).

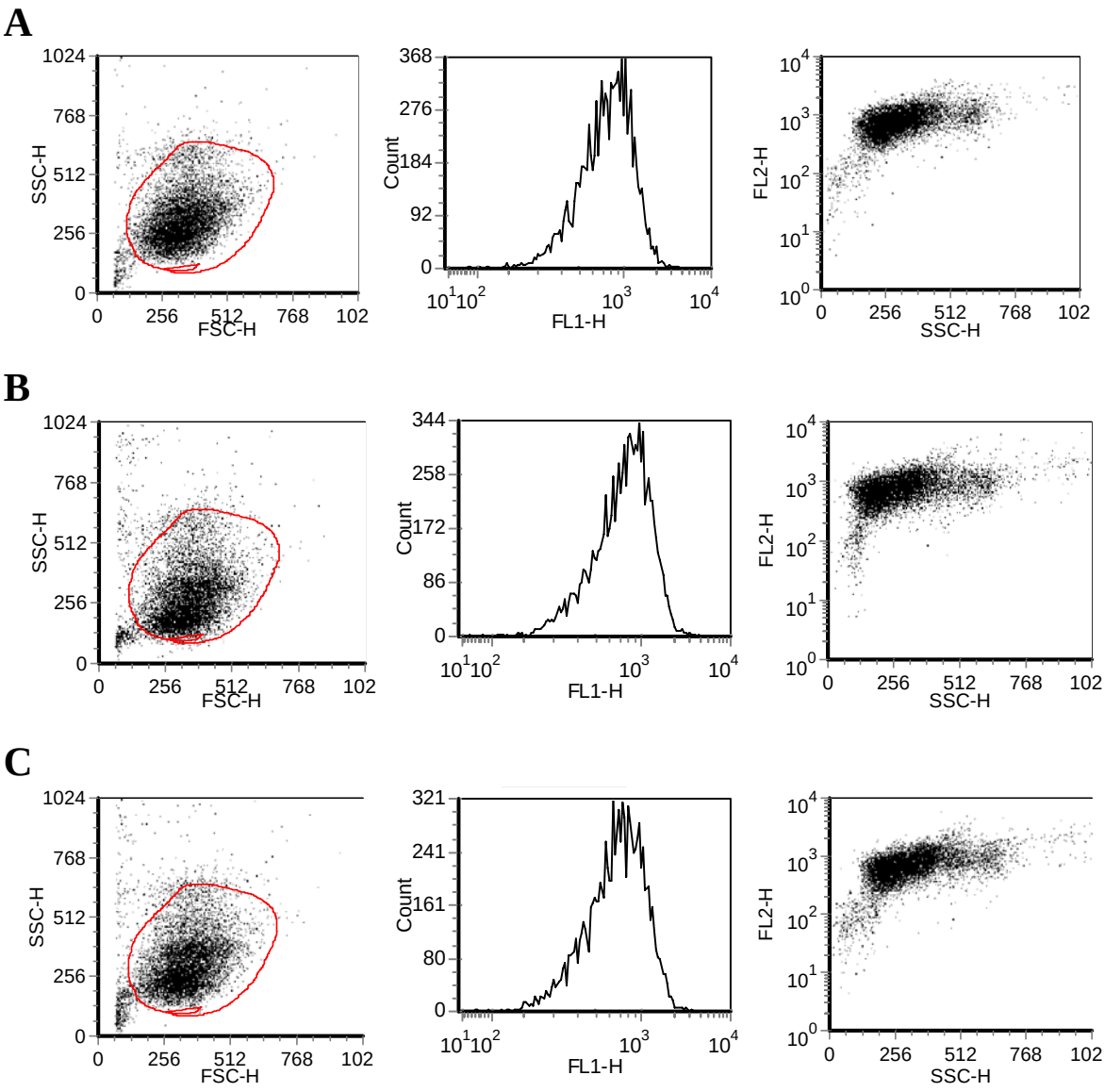

Figure A 11. FACS results for siRNA-ACS transfected cells in 24 hours at charge ratio (+/-) of 2:1 (Top), 5:1 (Middle), and 10:1 (Bottom).

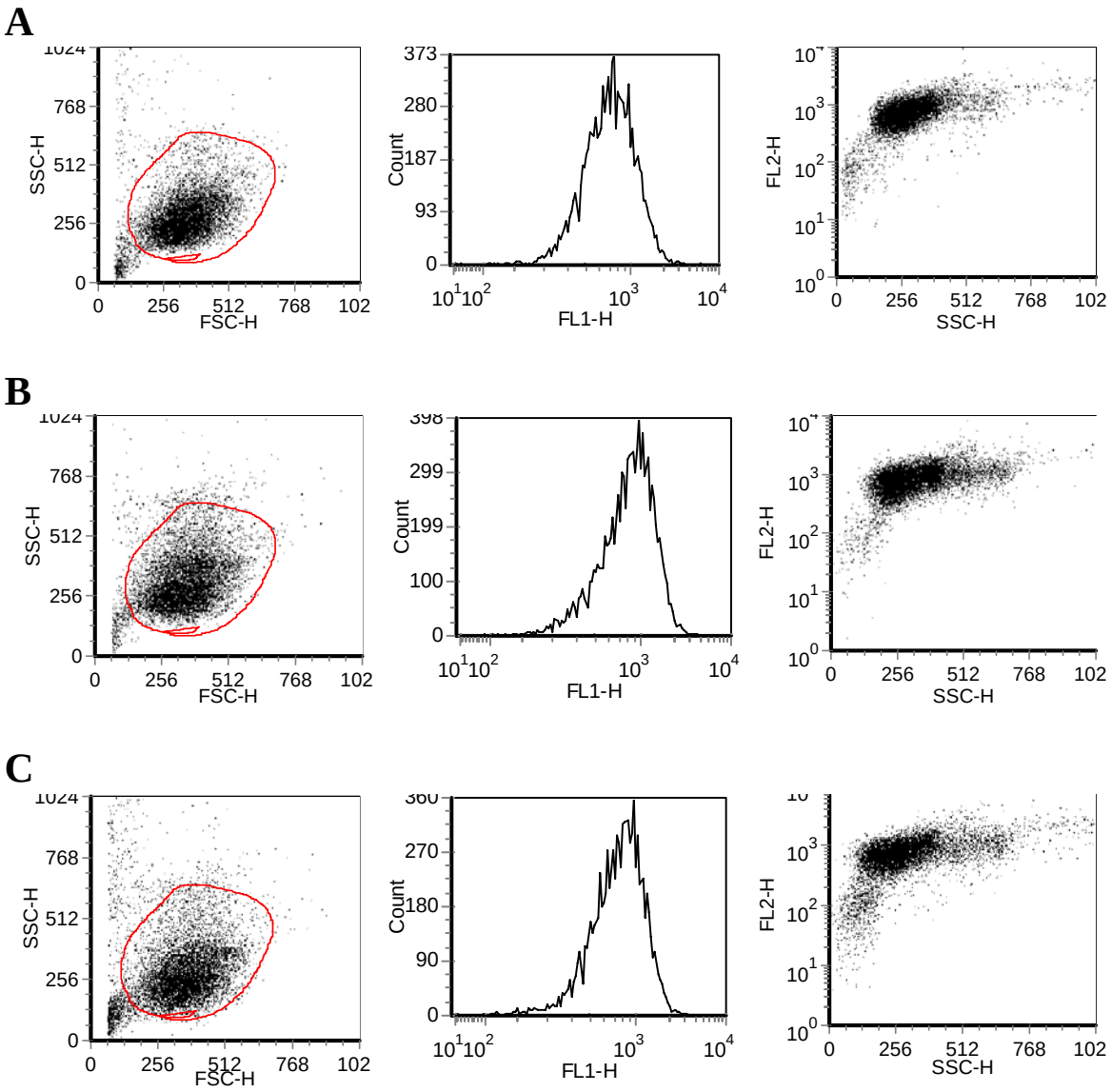

Figure A 12. FACS results for siRNA-EAK 16 II transfected cells in 24 hours at charge ratio (+/-) of 2:1 (Top), 5:1 (Middle), and 10:1 (Bottom).

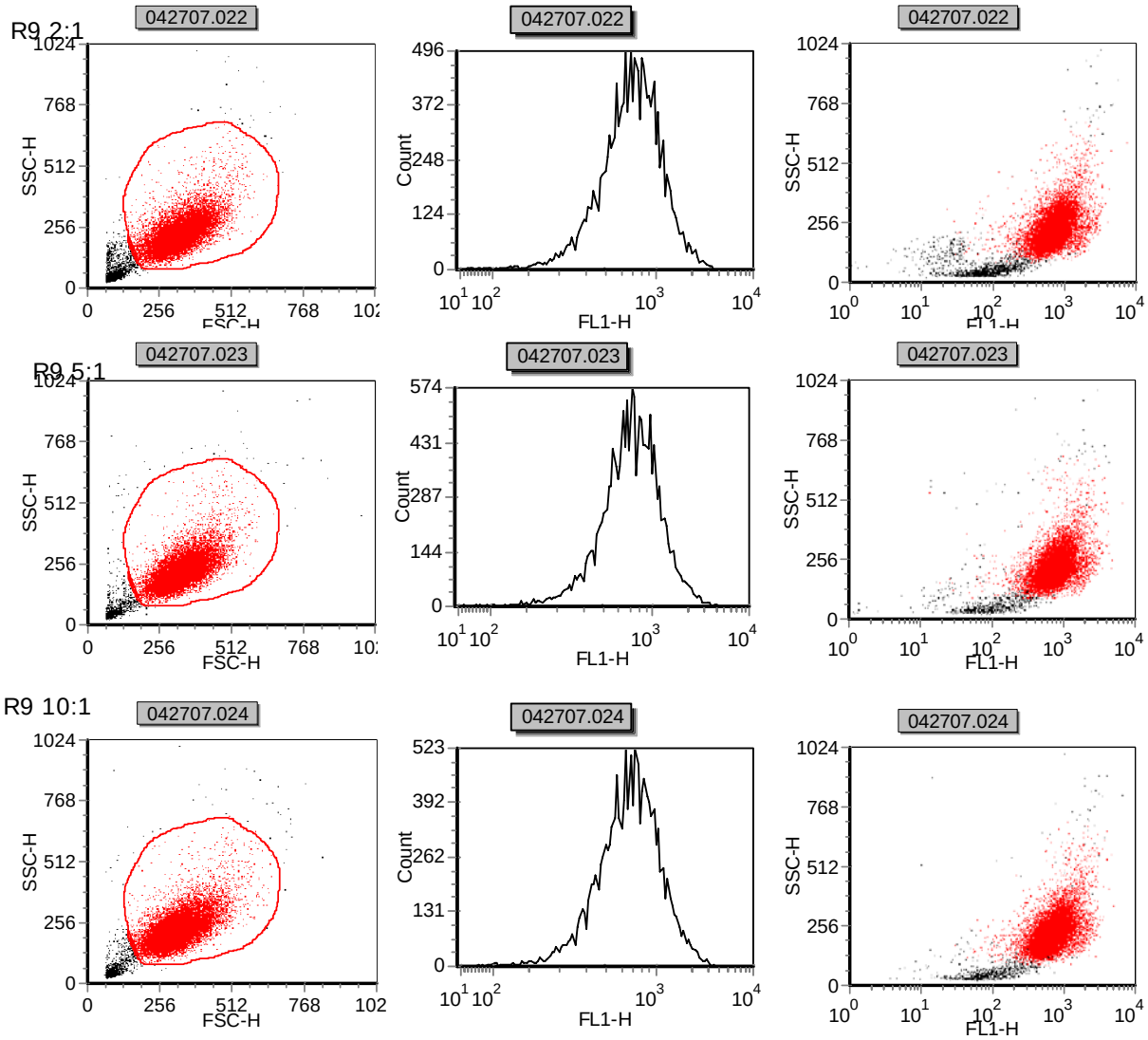

Figure A 13. FACS results for siRNA-R9 transfected cells in 48 hours at charge ratio (+/-) of 2:1 (Top), 5:1 (Middle), and 10:1 (Bottom).

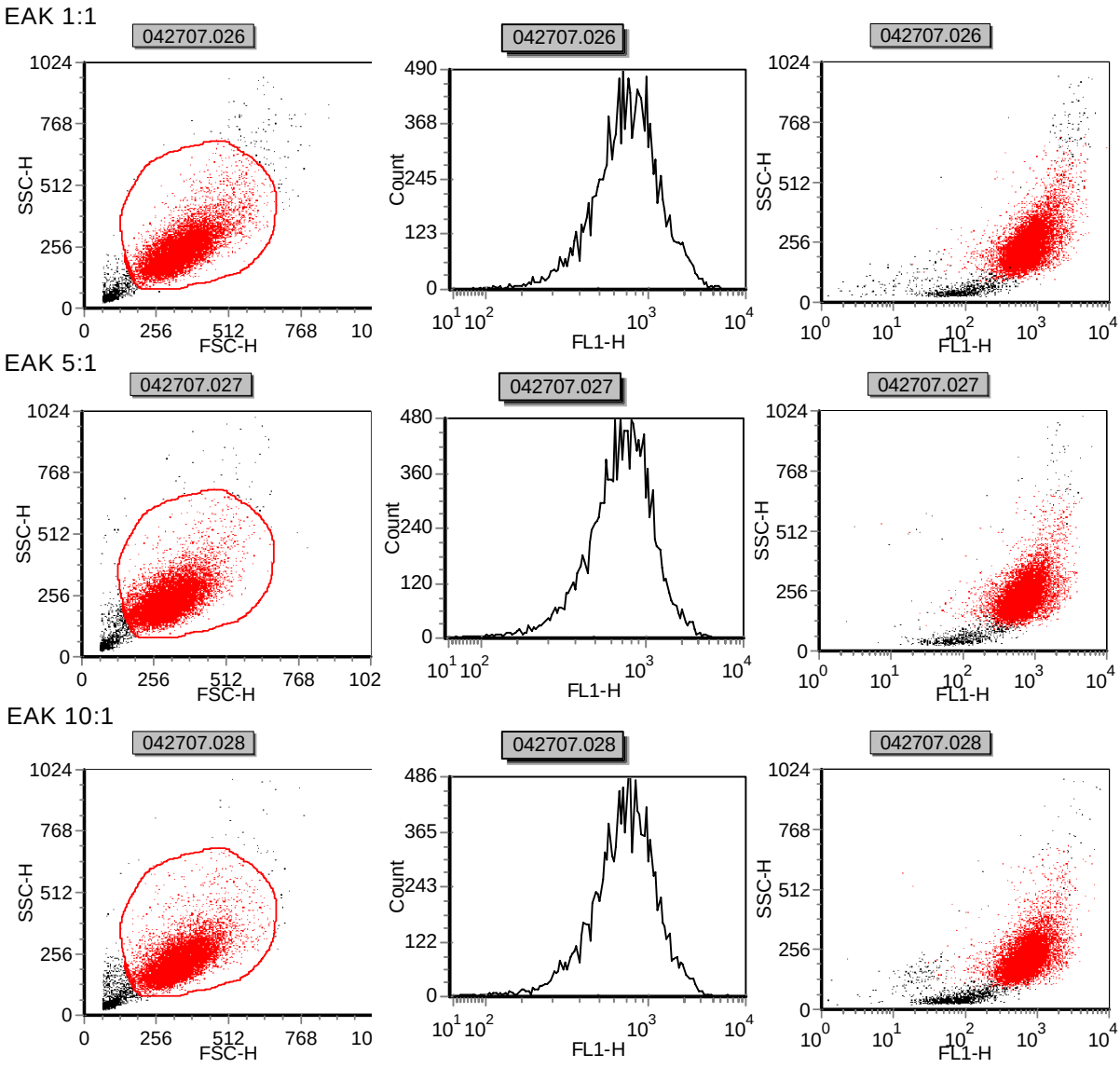

Figure A 14. FACS results for siRNA-EAK 16 IV transfected cells in 48 hours at charge ratio (+/-) of 1:1 (Top), 5:1 (Middle), and 10:1 (Bottom).

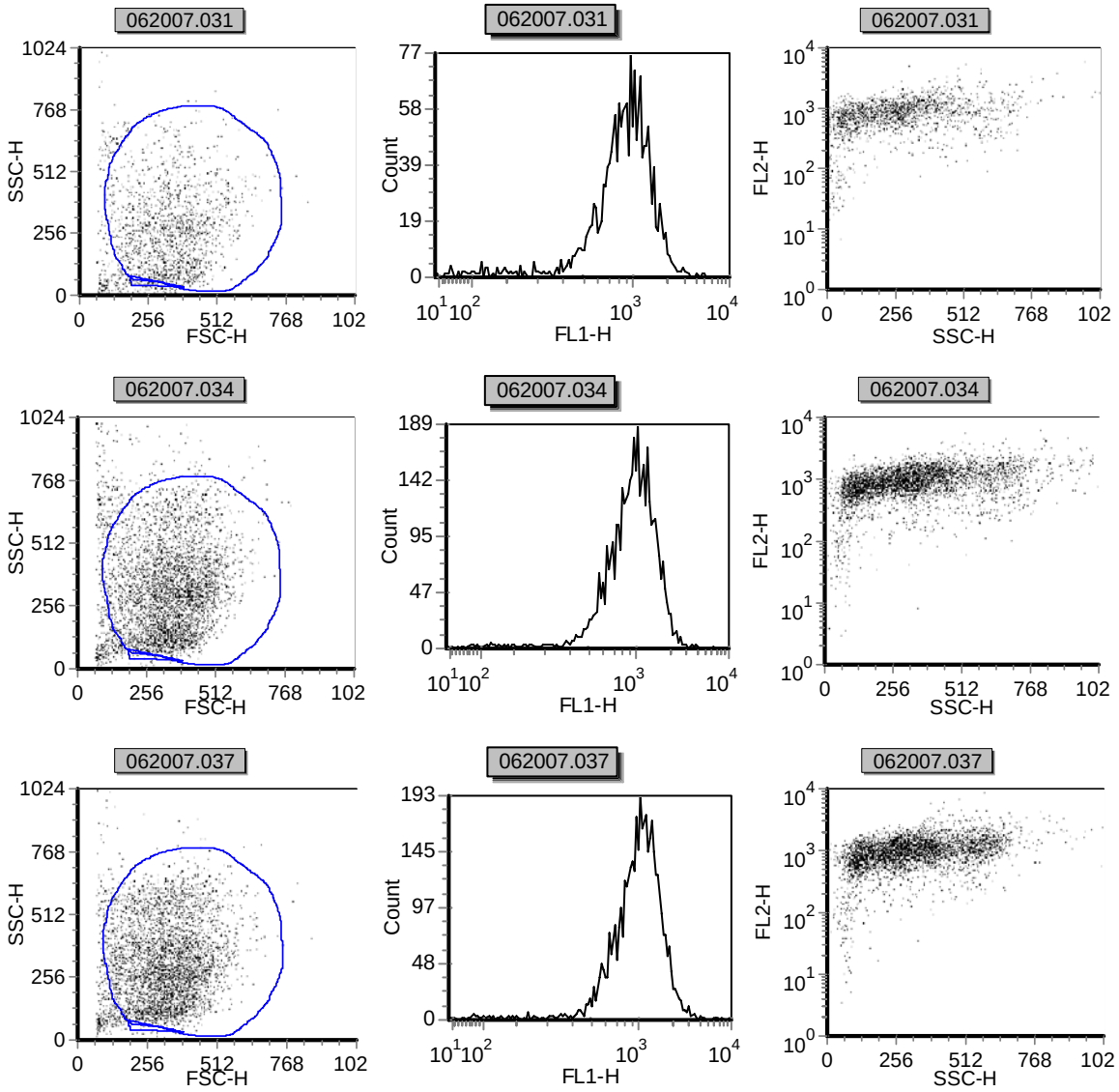

Figure A 15. FACS results for siRNA-ACS-R9 transfected cells in 48 hours at charge ratio (+/-) of 2:1 (Top), 5:1 (Middle), and 10:1 (Bottom).

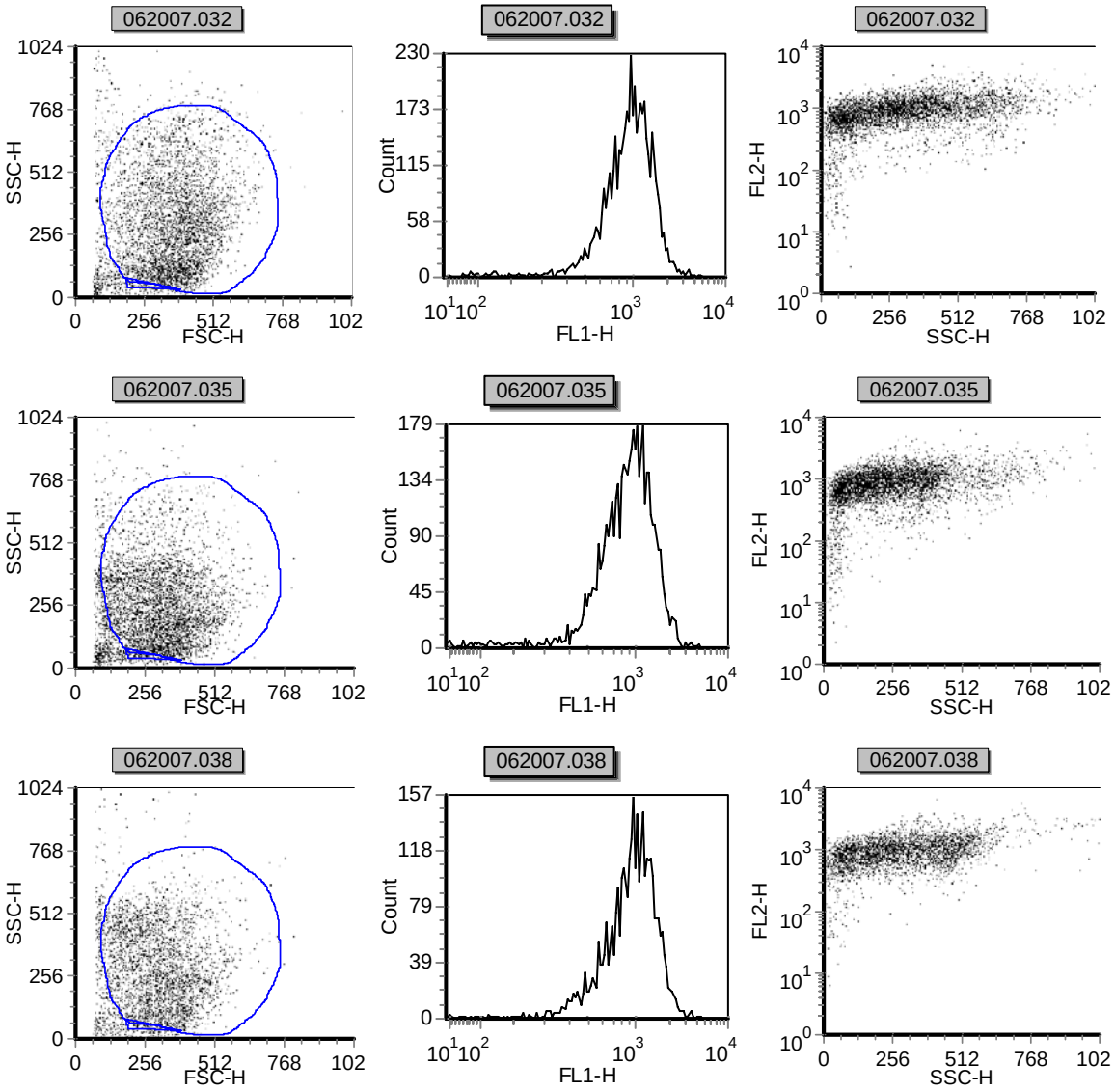

Figure A 16. FACS results for siRNA-ACS transfected cells in 48 hours at charge ratio (+/-) of 2:1 (Top), 5:1 (Middle), and 10:1 (Bottom).

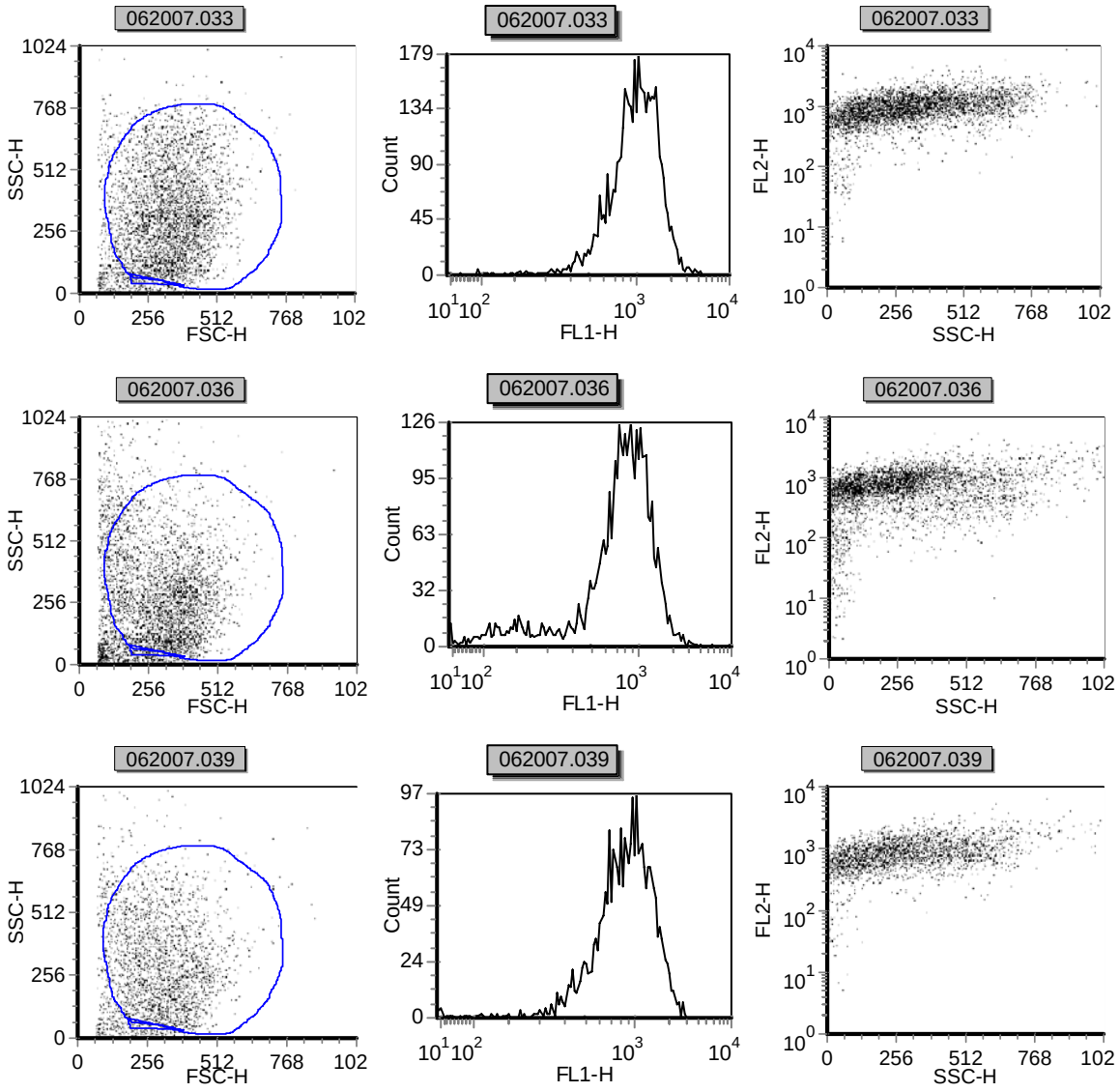

Figure A 17. FACS results for siRNA-EAK 16 II transfected cells in 48 hours at charge ratio (+/-) of 2:1 (Top), 5:1 (Middle), and 10:1 (Bottom).

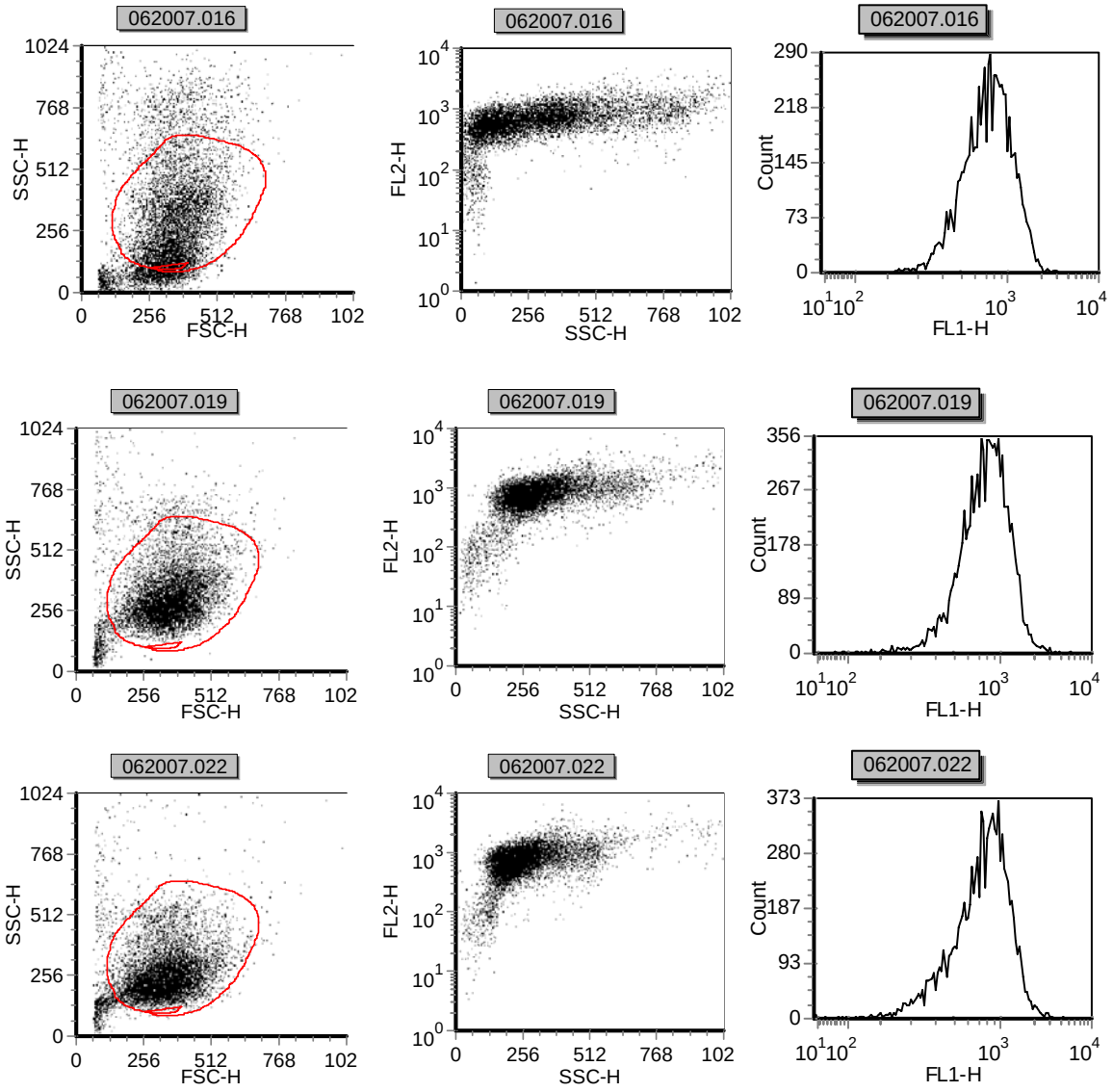

Figure A 18. FACS results for ACS-R9 only controls in 24 hours at charge ratio (+/-) of 2:1 (Top), 5:1 (Middle), and 10:1 (Bottom).

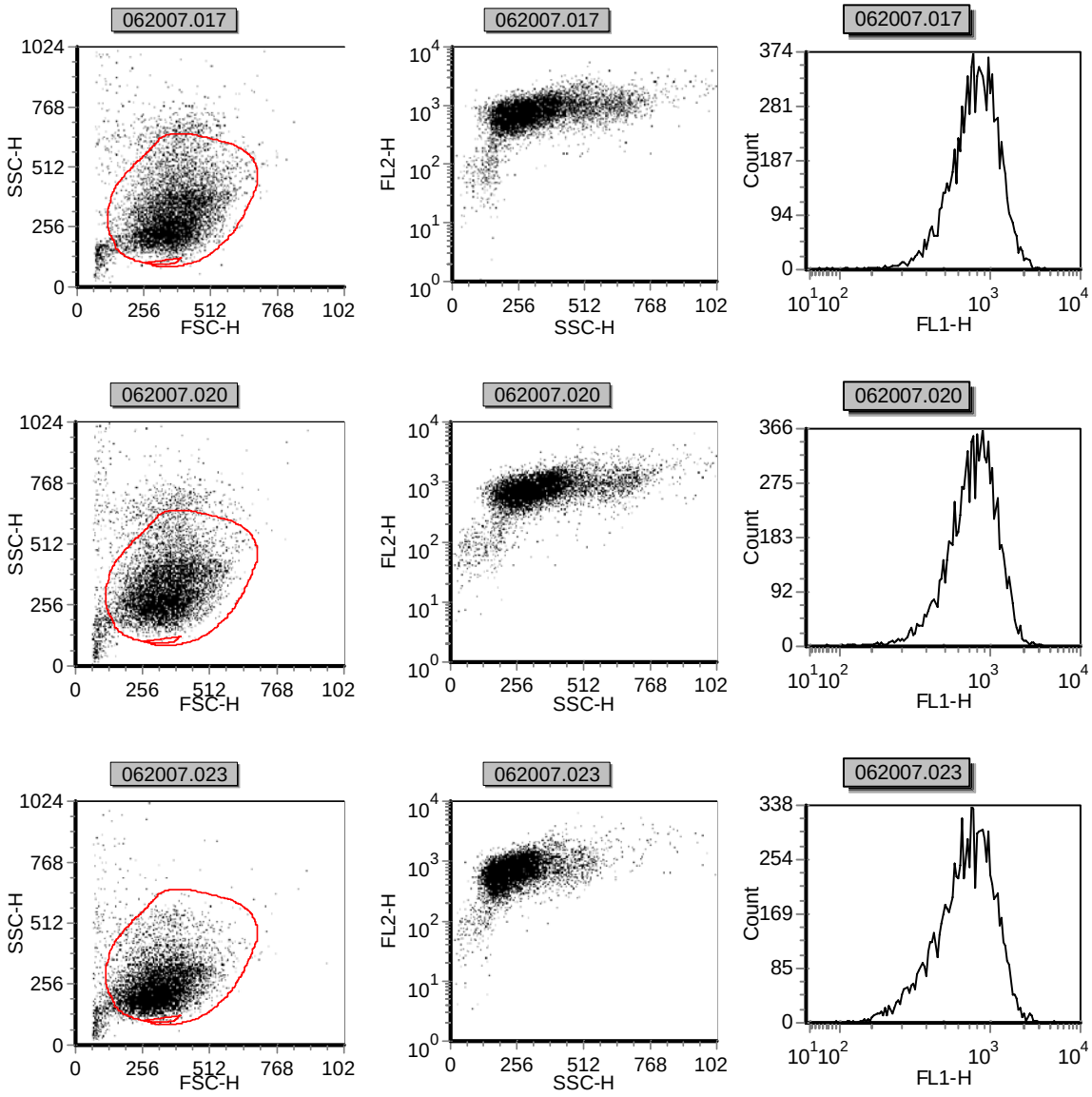

Figure A 19. FACS results for EAK 16 II only controls in 24 hours at charge ratio (+/-) of 2:1 (Top), 5:1 (Middle), and 10:1 (Bottom).

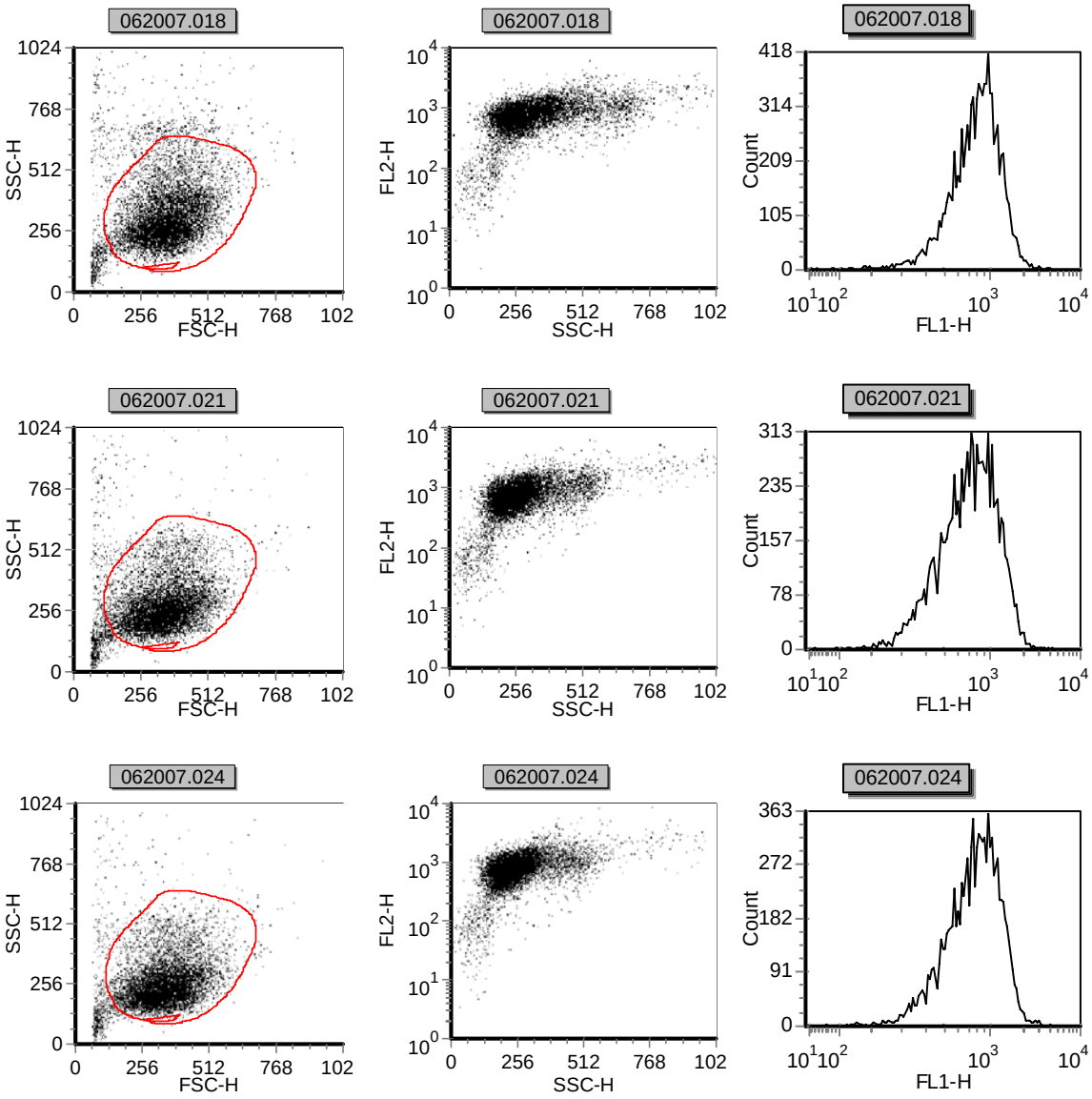

Figure A 20. FACS results for ACS only controls in 24 hours at charge ratio (+/-) of 2:1 (Top), 5:1 (Middle), and 10:1 (Bottom).

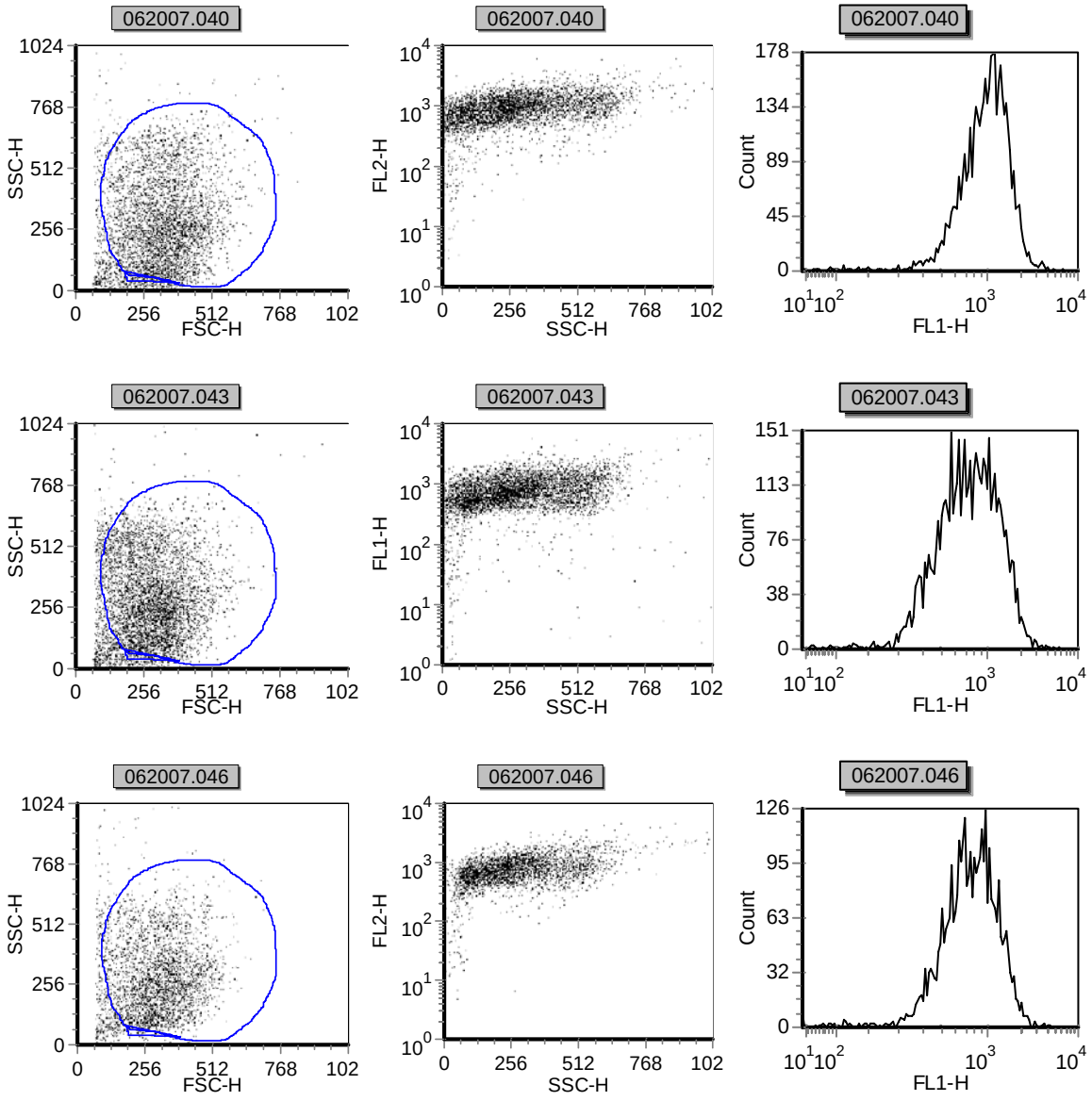

Figure A 21. FACS results for ACS-R9 only controls in 24 hours at charge ratio (+/-) of 2:1 (Top), 5:1 (Middle), and 10:1 (Bottom).

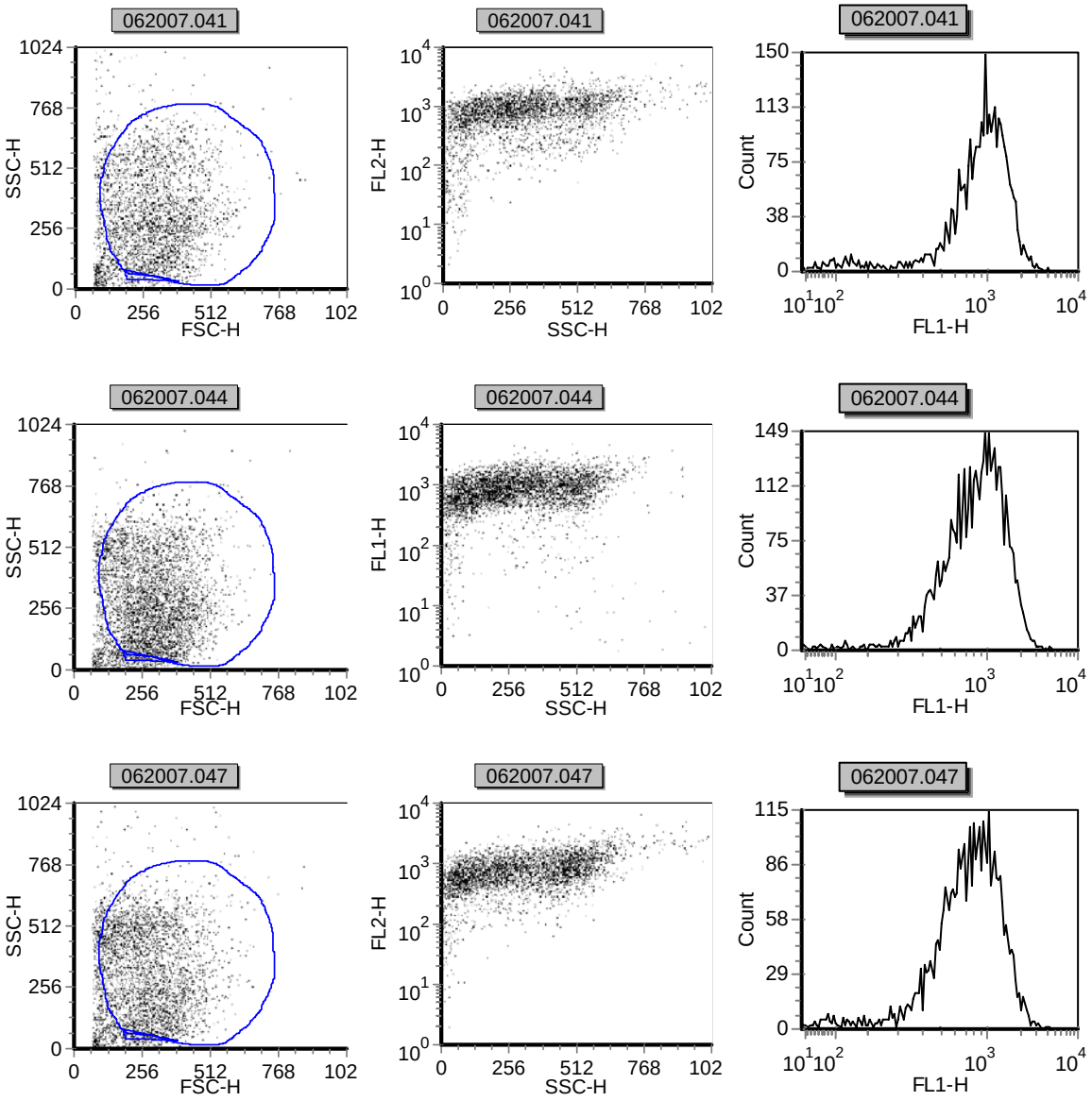

Figure A 22. FACS results for EAK 16 II only controls in 24 hours at charge ratio (+/-) of 2:1 (Top), 5:1 (Middle), and 10:1 (Bottom).

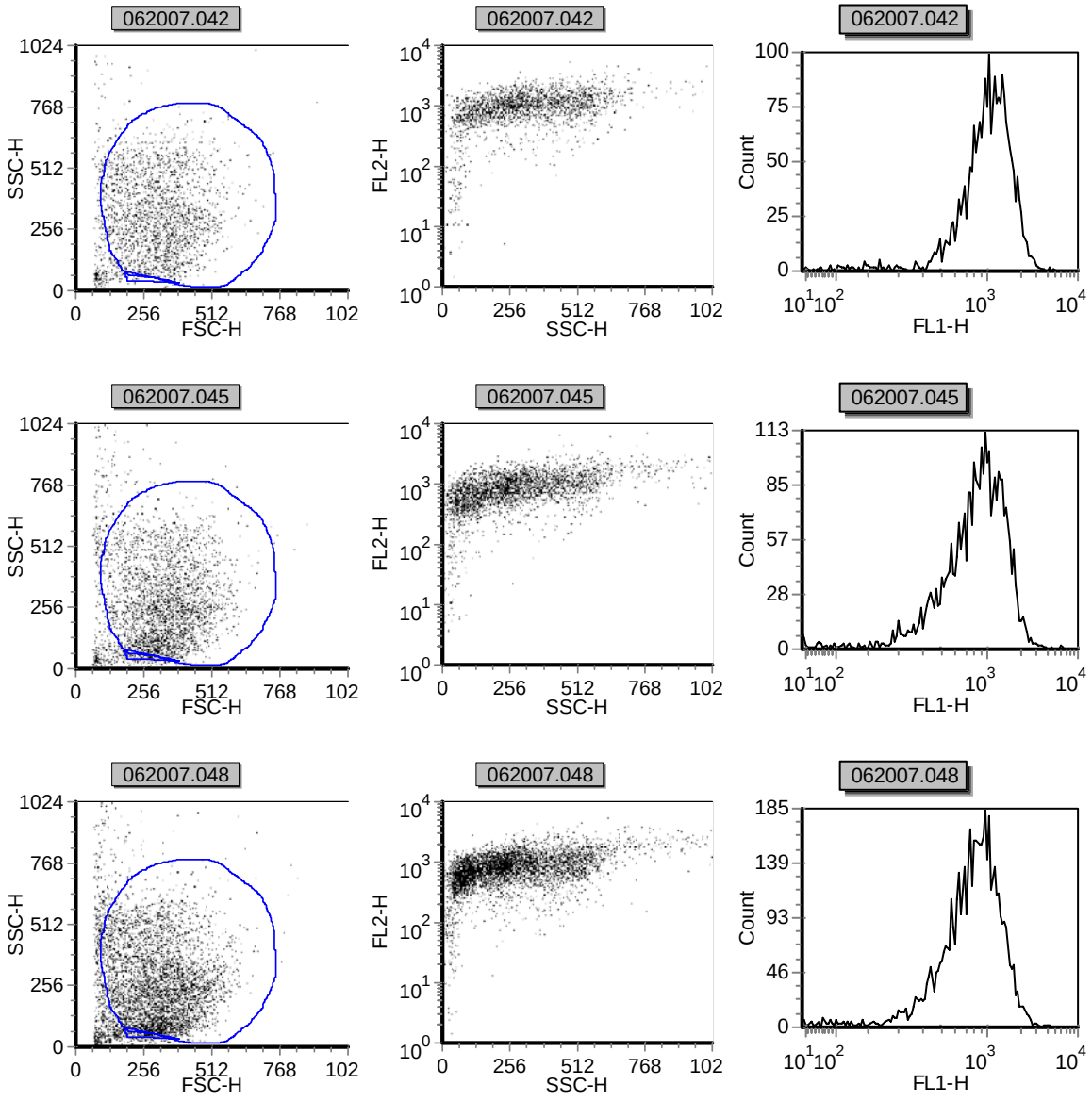

Figure A 23. FACS results for ACS only controls in 24 hours at charge ratio (+/-) of 2:1 (Top), 5:1 (Middle), and 10:1 (Bottom).

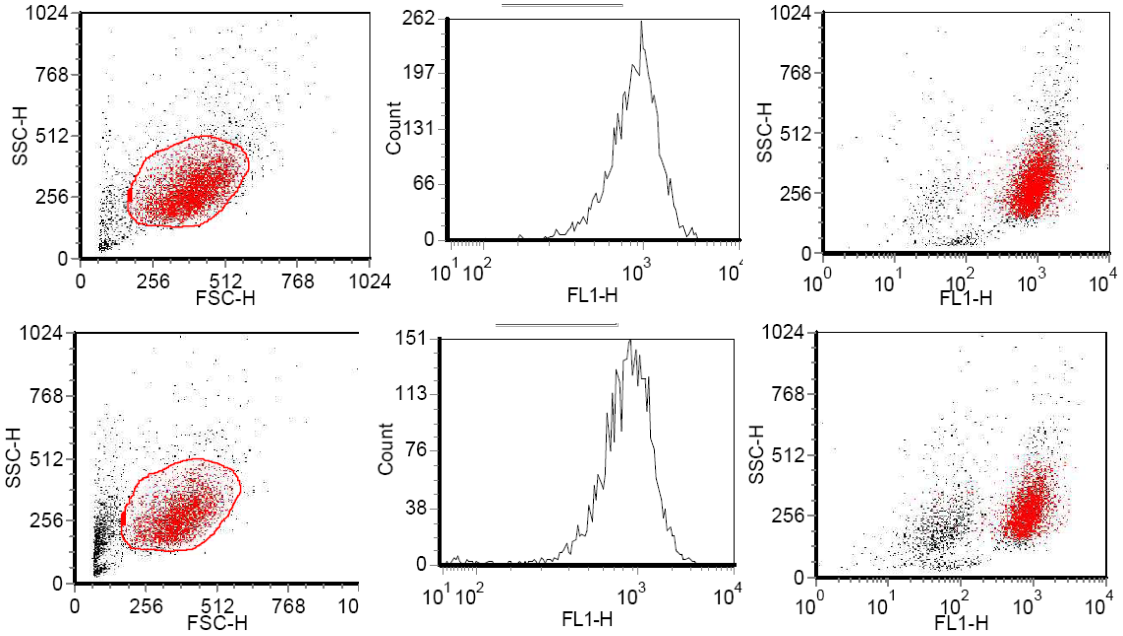

Figure A 24. FACS results for siRNA- R9 transfected cells in 24 hours at charge ratio (+/-) of 1:1 (Top) and 20:1 (Bottom).

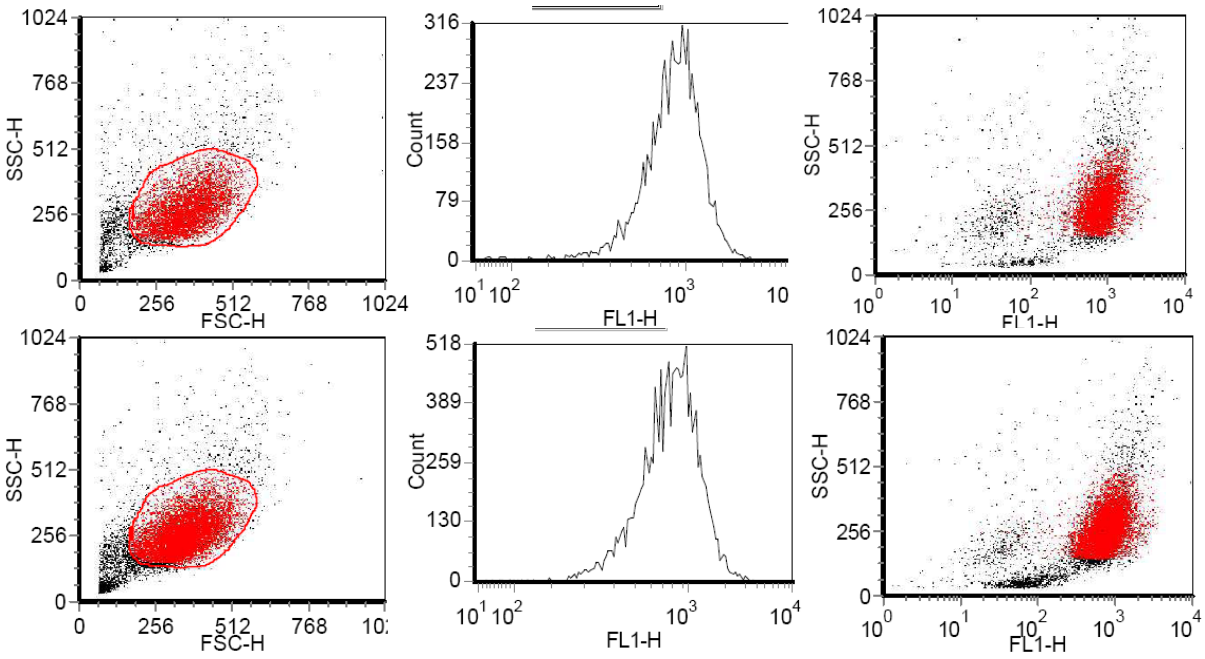

Figure A 25. FACS results for siRNA- EAK 16 IV transfected cells in 24 hours at charge ratio (+/-) of 1:1 (Top) and 20:1 (Bottom).

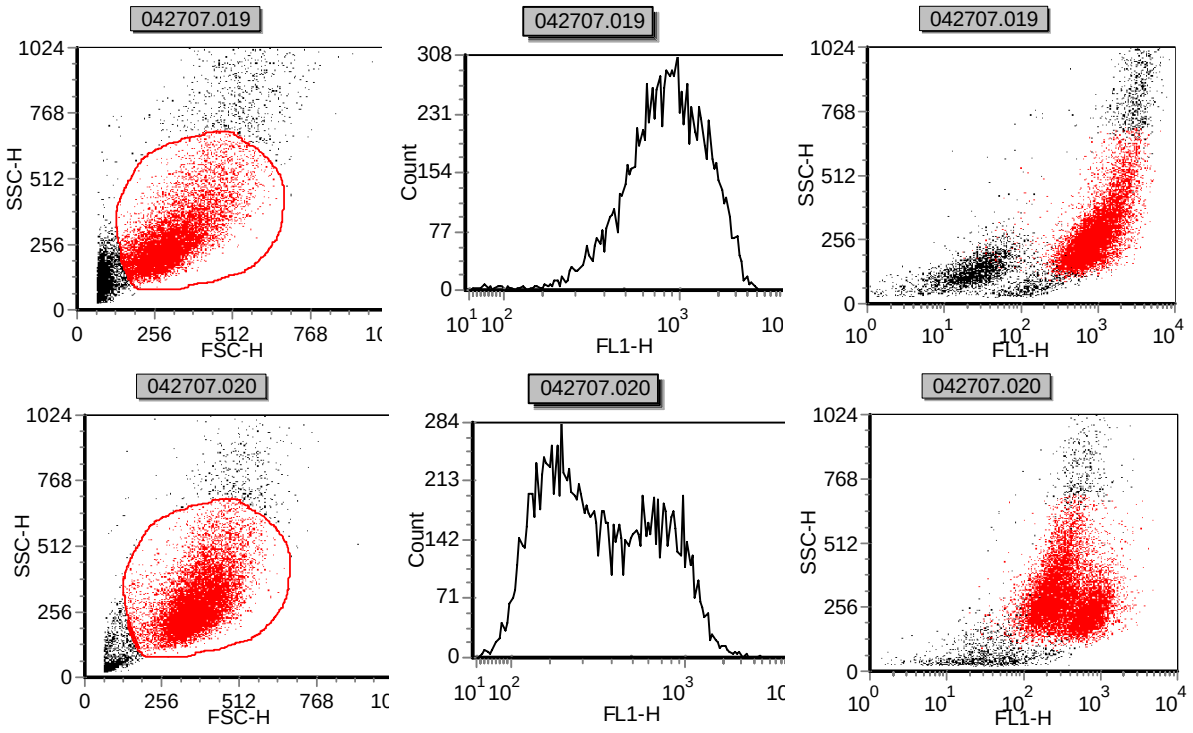

Figure A 26. FACS results for the negative (Top) and positive (Bottom) controls shown in three plots: forward versus side scatter (left column), GFP intensity plots (middle column), and GFP fluorescence versus side scatter (right column). The gate applied for the analysis of result is shown in the forward scatter versus side scatter plot.

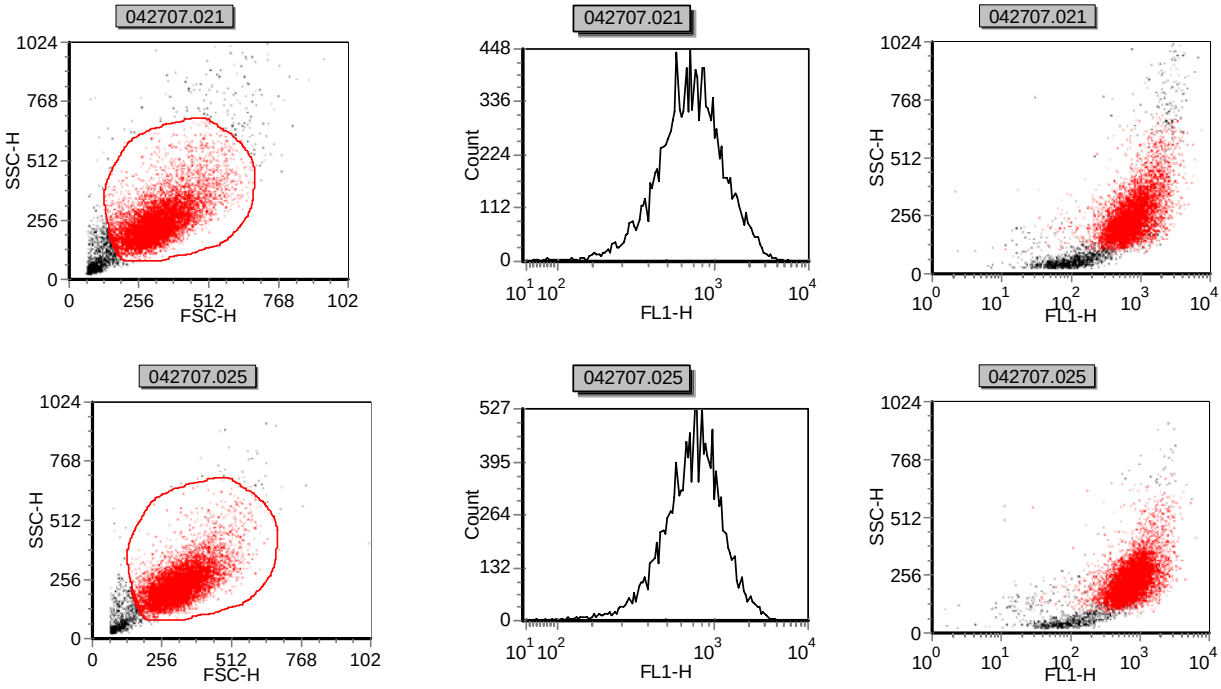

Figure A 27. FACS results for siRNA- R9 transfected cells in 48 hours at charge ratio (+/-) of 1:1 (Top) and 20:1 (Bottom).

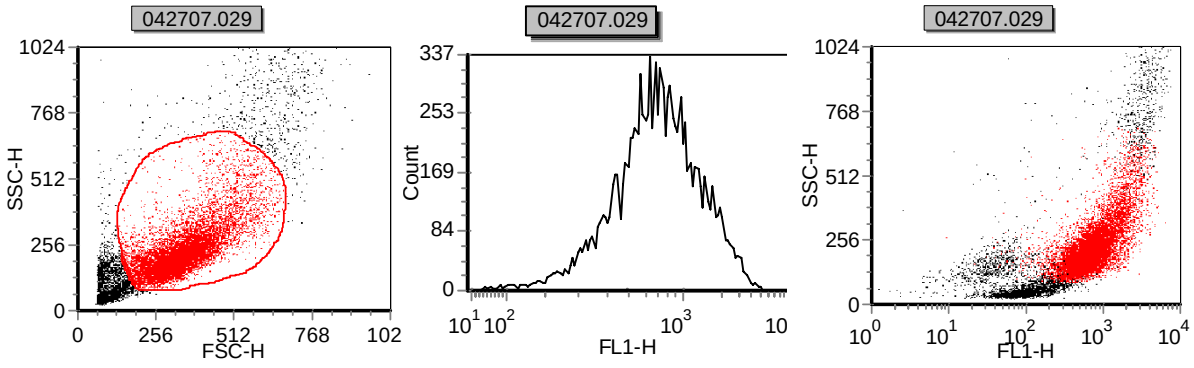

Figure A 28. FACS results for siRNA- EAK 16 IV transfected cells in 48 hours at charge ratio (+/-) of 20:1.

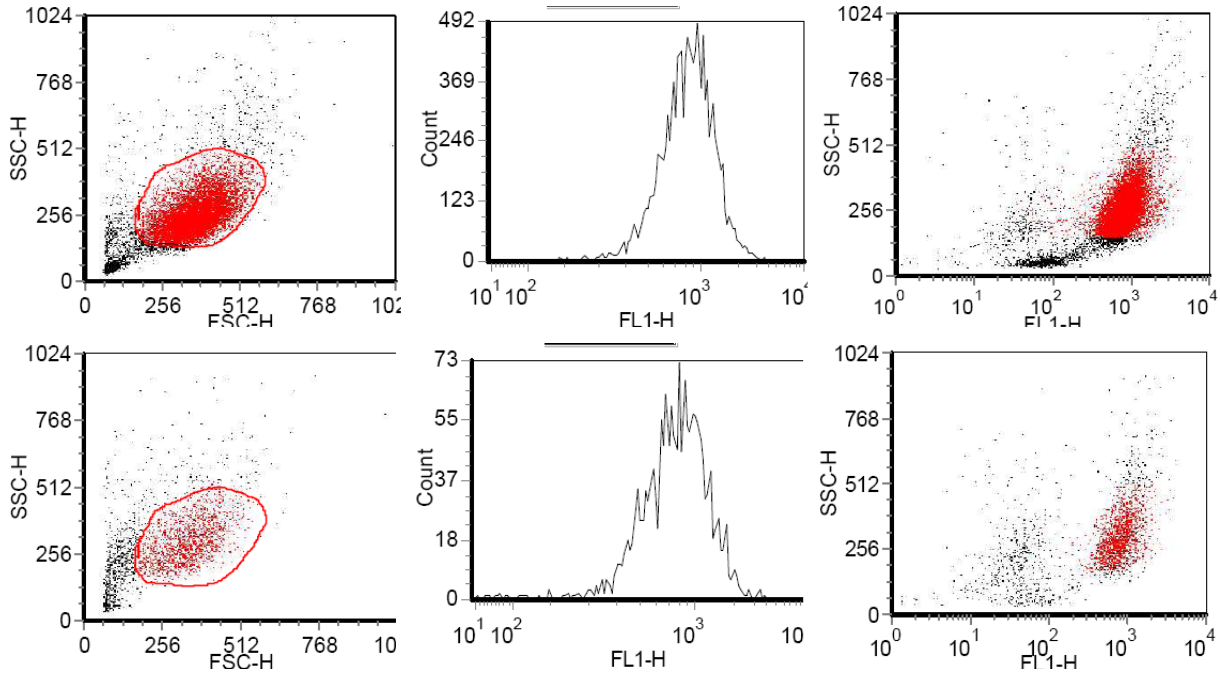

Figure A 29. FACS results for peptide only controls in 24 hours at charge ratio (+/-) of 20:1 for R9 (Top) and EAK 16 IV (Bottom).

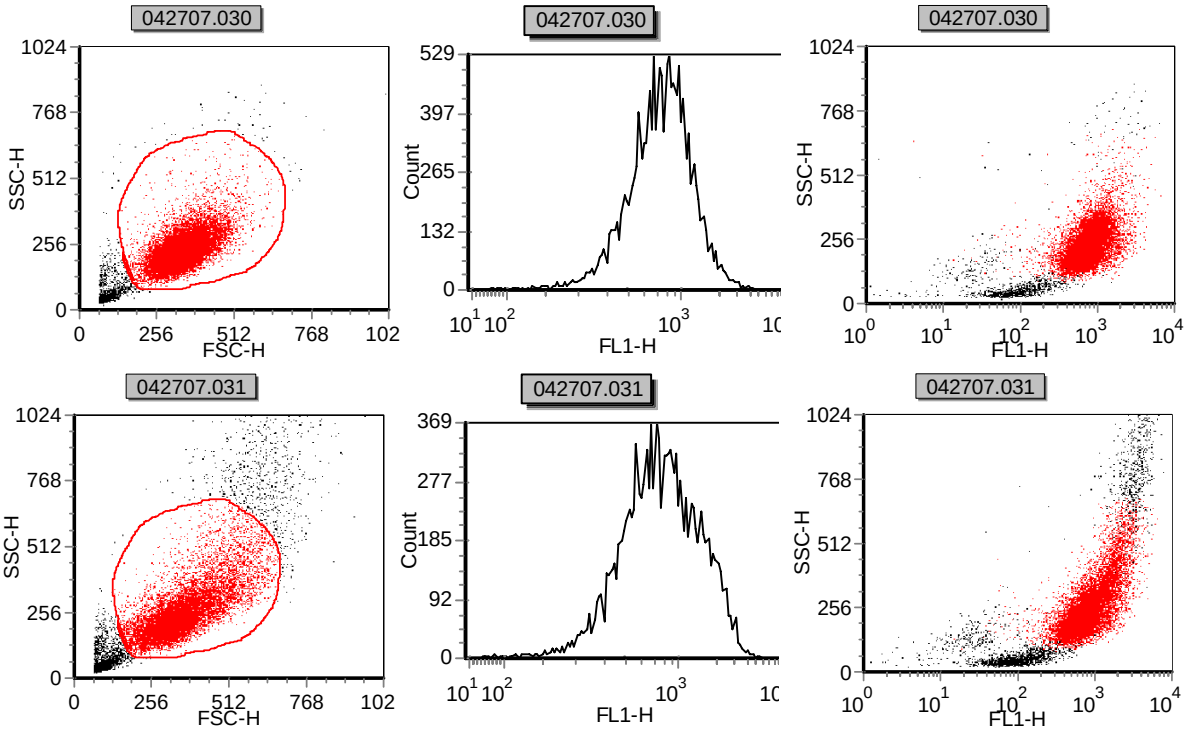

Figure A 30. FACS results for peptide only controls in 48 hours at charge ratio (+/-) of 20:1 for R9 (Top) and EAK 16 IV (Bottom).